Understanding the Relationship between Aerosols and Clouds: Field Investigations and Instrument Development

Thesis by

Timothy M. VanReken

In Partial Fulfillment of the Requirements

for the Degree of

Doctor of Philosophy

California Institute of Technology

Pasadena, California

2004

(Defended October 31, 2003)

Acknowledgements

When I decided to come to Caltech, I didn't know what I was getting myself into; I'm not sure anybody really does. But it appears that I've made it through the long rough stretches and the occasional smooth spot. Countless friends and colleagues helped me to this point, and they all deserve to be recognized. However, that would make the rest of the thesis look a little thin, so I'll stick to the big ones.

I was privileged to have two excellent advisors to show me what it is to be a good scientist. John Seinfeld and Rick Flagan are each extraordinary individuals, but as collaborators they provide their students with enormous advantages over what any single advisor could provide. John has always maintained the perfect sense of perspective; whether it's a scientific problem or a bureaucratic one, he's always recognized what is important and what is merely required for completeness, and has made sure I understood the difference. He's treated me with the same balanced view; things did not always go according to plan, but he made sure that I didn't lose sight of the larger goals that motivated my work. I thank him for that.

While John was always involved, it was Rick Flagan who was most helpful in the laboratory on a day-to-day basis. No detail was ever too small to raise with Rick, and there were few topics on which he didn't add valuable insight. My skills in the laboratory were almost nonexistent when I began my work at Caltech, but after working with Rick for so long, there are few tasks that would intimidate me. I'm not sure to what degree I'll use the specific knowledge I've gained during my years here, but thanks to him I'll always know the value of taking something apart just to put it back together again.

While my two advisors have had the largest impact on my professional development, my friends and colleagues in the Seinfeld and Flagan research groups are what have made the good days great and the bad days manageable. Patrick Chuang and Don Collins spent countless hours teaching me what it takes to make good aerosol measurements, including knowing how and when to take a break. Rob Griffin and Peter Adams made me like part of the gang, and decided to hike

too fast at just the right time. Thanos Nenes has been my cohort through more all-night parties and all-night homework sessions than was probably good for us. Roya Bahreini, David Cocker, Bill Conant Dean Holunga, Brian Mader, Adam Olsen, Michelle Ostraat, Denis Phares, Tracey Rissman, Mohan Sankaran, Jim Smith, Tomtor Varutbangkul, and Jian Wang all made the lab as fun a workplace as it could possibly be. I wouldn't have made it through without them.

Beyond my advisors and colleagues, there were many people who helped me during my years as a graduate student. The secretarial staff, especially Ann Hilgenfeldt, have been incredibly helpful in making administrative hoops just go away; I didn't thank them often enough. I'd also like to thank Marty Gould for all the fantastic work he's done for me over the years; he saved me from missing deadlines more than once. And of course the staff at CIRPAS: Haf Jonsson, Nava Roy, Mike Hubbell, Roy Woods, Bob Bluth, Bob Rogell, and Reggie Burch made field work as easy and fun as it could ever be, and even managed to occasionally forget that I was a scientist.

I also want to thank the people who have believed in me the most and the longest. My family never doubted my abilities, even when I did. They've always had my desires first in their hearts, and made sure that my life was more than just my work. It's been hard living so far from my parents and Mike and Sara for so long, with so little time together. I want to thank them for believing in me and for reminding me that no matter how bad things got, I always had them on my side.

Finally, I want to thank Serena. If I'd gained nothing from my time at Caltech except for your heart, these years would still be the best-spent of my life. It took some time for us to get to where we are now, but it's been worth it, even when it seemed like the everyone but you knew how I felt. Thank you so much for giving me a chance.

Abstract

The research presented in this thesis is part of the ongoing effort to better understand the role of atmospheric aerosols in the development of clouds. Cloud condensation nuclei (CCN) are the subset of the aerosol population that can activate and grow into cloud droplets under suitable atmospheric conditions. The supersaturation at which a given CCN will activate is dependent on the particle's size and composition, but the details of the relationship are not completely understood. CCN observations from the CRYSTAL-FACE (Cirrus Regional Study of Tropical Anvils and Cirrus Layers- Florida Area Cirrus Experiment) field campaign are presented in Chapter 2. These measurements are compared to predictions based on measured aerosol size distributions with an assumed chemical composition to determine whether activation theory is sufficient to describe what is observed. The analysis indicates that, in cases like those included in the study, CCN concentrations can be accurately predicted from the size distribution even in the absence of detailed chemical compositional data.

A case study is described in Chapter 3 to demonstrate the potential importance of anthropogenic aerosols in the development of clouds. During a CRYSTAL-FACE flight, an aerosol plume was encountered in the boundary layer near the base of a large mixed-phase convective cloud. Evidence suggests that an oil-burning power plant south of Miami was the likely source of the plume. The convective cloud was probed at higher altitudes, and a spatial gradient was observed in the ice particle concentrations. The evidence linking the plume in the boundary layer to the upper-level trends is inconclusive, but worthy of further study.

The measurement of CCN in the atmosphere is difficult, and improved instrumentation would significantly improve our ability to obtain the detailed information necessary to understand the relationship between aerosols and clouds. The concept for an improved CCN spectrometer is outlined in Chapter 4; this new design would expand the resolvable range of supersaturations for which data can be obtained. The dependence of the instrument's performance on various design

parameters is evaluated, and a configuration is proposed that would be a significant improvement over currently available instrumentation.

Contents

List of Figures

List of Tables

1 Introduction

The role of airborne particulate matter, or aerosols, in the formation and propagation of clouds has been a field of active research for several decades. Clouds play a vital role in Earth's climate, both in the hydrological cycle and in maintaining the planetary radiative balance. Aerosols are known to affect cloud processes in numerous ways; for example, they are intentionally employed to initiate precipitation in cloud seeding activities [*Silverman,* 2001] and they account for the occurrence of cirrus contrails behind aircraft [*Changnon*, 1981] and "ship tracks" in marine stratocumulus layers [*Durkee et al.,* 2000]. The subset of the aerosol populations that have the potential to form cloud droplets are known as cloud condensation nuclei, or CCN. In general terms, clouds form when a warm, moist air mass cools below its dew point; when this occurs, the excess water vapor will condense on the available CCN. This process is well understood in general terms, but the complexity of both the initial aerosol populations and the numerous interdependent cloud microphysical processes make the details of the system very difficult to isolate.

Increasing our knowledge base in this field is vital to the larger goal of ascertaining the impact of anthropogenic activities on global climate. More than 20% of incoming solar radiation is reflected back to space before reaching the Earth's surface, most of it by clouds [*Seinfeld and Pandis,* 1998]. Changing this fraction by even a small amount could have significant climatic effects, both regionally and globally. There is extensive ongoing research focused on determining to what extent anthropogenic aerosol emissions affect the reflectivity of clouds, and on predicting the importance of these effects on global climate change. This field of study is much less advanced than most others that play a role in the Earth's climate. The most recent report of the Intergovernmental Panel on Climate Change (IPCC) [*Intergovernmental Panel on Climate Change,* 2001] classifies the level of scientific understanding of the cloud-related aerosol effects, collectively known as the "indirect aerosol effects," as "very low"; in comparison, the level of scientific understanding for greenhouse gases was labeled "high" by the IPCC. Better

understanding of cloud processes in general, and of the role of aerosols in said processes in particular, will allow significant progress in ascertaining the overall anthropogenic influence on climate.

The slow progress towards a detailed understanding of cloud processes is largely a result of the considerable inconvenience inherent in making direct measurements of their microphysical properties. Clouds are transitory in time and space, and usually located well above ground level; their complexity cannot be simulated in a laboratory setting. In situ measurements require an airborne platform, a complication that inevitably leads to sacrifices in data quantity and/or quality. Ground-based measurements in and below clouds are possible, but only at times and in places where the clouds are near to the surface. Ground and satellite-based remote measurements allow for extensive spatial and/or temporal coverage, but require the interpretation of bulk properties to obtain an approximation of microphysical details. As a consequence of these limitations to current measurement capabilities, advances in our understanding of aerosol/cloud interactions generally requires drawing conclusions from an incomplete data set, and revisiting those conclusions as additional tools become available.

The goal of this thesis is to increase the understanding of atmospheric CCN and the role they play in cloud development. Chapter 2 details the results of extensive CCN observations made during the CRYSTAL-FACE campaign in south Florida during the summer of 2002 and presents a simplified closure analysis to determine whether it is possible to predict CCN concentrations from other aerosol measurements. Chapter 3 is a case study from CRYSTAL-FACE; during one flight late in the campaign, atypically large spatial variations in the boundary layer aerosol were observed. The chapter examines whether these variations have an observable impact on the upper-level microphysics of a convective cloud in the vicinity. Chapter 4 presents the theoretical development of a new CCN spectrometer that would be a significant improvement over currently available instrumentation. Finally, Chapter 5 summarizes the thesis and presents some general goals for future work.

2 Toward Aerosol/Cloud Condensation Nuclei (CCN) Closure during CRYSTAL-FACE

2.1 Abstract

During July 2002, measurements of cloud condensation nuclei (CCN) were made in the vicinity of southwest Florida as part of the CRYSTAL-FACE (Cirrus Regional Study of Tropical Anvils and Cirrus Layers- Florida Area Cirrus Experiment) field campaign. These observations, at supersaturations of 0.2% and 0.85%, are presented here. The performance of each of the two CCN counters was validated through laboratory calibration and an *in situ* intercomparison. The measurements indicate that the aerosol sampled during the campaign was predominantly marine in character: the median concentrations were 233 cm^{-3} (at $S = 0.2\%$) and 371 cm^{-3} (at $S = 0.85\%$). Three flights during the experiment differed from this general trend; the aerosol sampled during the two flights on July 18 was more continental in character, and the observations on July 28 indicate high spatial variability and periods of very high aerosol concentrations. This study also includes a simplified aerosol/CCN closure analysis. Aerosol size distributions were measured simultaneously with the CCN observations, and these data are used to predict a CCN concentration using Köhler theory. For the purpose of this analysis, an idealized composition of pure ammonium sulfate was assumed. The analysis indicates that in this case, there was good general agreement between the predicted and observed CCN concentrations: at $S = 0.2\%$, $N_{predicted}/N_{observed} = 1.047$ ($R^2 = 0.911$); at $S = 0.85\%$, $N_{predicted}/N_{observed} = 1.201$ ($R^2 = 0.835$). The impacts of the compositional assumption and of including in-cloud data in the analysis are addressed. The effect of removing the data from the July 28 flight is also examined; doing so improves the result of the closure analysis at $S = 0.85\%$. When omitting that atypical flight, $N_{predicted}/N_{observed} = 1.085$ ($R^2 = 0.770$), at $S = 0.85\%$.

---

*This chapter is reproduced by permission from "Toward aerosol/cloud condensation nuclei (CCN) closure during CRYSTAL-FACE," by T. M. VanReken, T. A. Rissman, G. C. Roberts, V. Varutbangkul, H. H. Jonsson, R. C. Flagan, and J. H. Seinfeld; *Journal of Geophysical Research (Atmospheres), 108*(D20), 4633, doi:10.1029/2003JD003582, 2003.

2.2 Introduction

The importance of clouds in the climate system is well established; clouds play a vital role in the global radiation budget and hydrological cycle. Clouds form when a parcel of air becomes supersaturated with respect to water vapor, and the excess water condenses rapidly on ambient particles to form droplets. For this rapid condensation (termed activation) to occur at a given supersaturation, the particle must have sufficient soluble mass; this subset of the aerosol population is called cloud condensation nuclei, denoted CCN. The atmospheric concentration of CCN is often substantially enhanced by human activities, and the various ways that this enhancement affects the radiative properties of clouds are collectively known as indirect aerosol forcing (the inclusion of the word "indirect" differentiates these effects from the direct aerosol effect, which describes the radiative interactions of the particles themselves). Cloud processes are complex by nature and heavily dependent on purely dynamical factors, but in general terms indirect aerosol effects can be split into two categories. For a given supersaturation, an air mass with a higher CCN concentration would produce a cloud with a higher droplet concentration, but a smaller mean droplet diameter; this often results in a more reflective cloud, and is known as the first indirect effect, or Twomey effect [*Twomey*, 1977]. The second indirect effect, identified by *Albrecht* [1989], also stems from the smaller average droplet diameter in polluted clouds; a smaller mean droplet size inhibits the processes that lead to precipitation, thereby increasing cloud lifetime and, therefore, cloud coverage.

While observations support the existence of indirect aerosol effects on a local scale [*Johnson et al.*, 1996; *Rosenfeld*, 1999; *Durkee et al.*, 2000; *Rosenfeld*, 2000; *Garrett et al.*, 2002], current understanding of the processes involved is insufficient to accurately predict the global importance of indirect aerosol forcing. The *Intergovernmental Panel on Climate Change* [2001] estimates that the first indirect effect results in a global mean forcing of between 0 and -2 W/m^2, and does not give an estimate for the second indirect effect, which is also expected to be one of cooling. Reliable predictions regarding climate forcing await more detailed understanding of the dependence of cloud properties on aerosol properties.

The first step in understanding the relationship between the ambient aerosol and the cloud that forms therefrom is to know the activation properties of the atmospheric aerosol. In theory, if a particle's size and chemical composition were precisely known, the supersaturation at which

activation occurs could be calculated using Köhler theory [*Seinfeld and Pandis*, 1998]. However, ambient aerosol populations can contain myriad chemical species, the activation properties of most of which have not been established. Furthermore, recent studies have demonstrated that simply categorizing aerosol species into soluble and insoluble fractions is sometimes insufficient [*Cruz and Pandis*, 1998; *Hegg et al.*, 2001; *Raymond and Pandis*, 2002]; slightly soluble species, surfactants, and soluble gases can affect activation either thermodynamically or kinetically [*Charlson et al.*, 2001; *Nenes et al.*, 2002]. To establish the connection between theory and the actual atmosphere, it is desirable to directly measure the portion of the aerosol population that activates at a given supersaturation. Such a measurement generally involves exposing an aerosol sample to a known supersaturation; the CCN active at that supersaturation rapidly grow to a size at which they can be counted by standard techniques. In the laboratory, instruments using such measurement strategies can be tested using aerosols whose size and chemical properties are carefully controlled. Then, the activation behavior of an ambient aerosol can be measured, giving rise to a so-called closure experiment, whereby measured CCN concentrations are compared against predictions based on simultaneously measured aerosol size and composition data. A successful closure study serves to validate both the performance of the CCN instrument itself and the theoretical basis for the prediction of the activation properties of the aerosol.

The CRYSTAL-FACE (Cirrus Regional Study of Tropical Anvils and Cirrus Layers- Florida Area Cirrus Experiment) field campaign in the Florida Keys during July 2002 had as its goal to investigate the properties of tropical convective systems and the resultant cirrus layers. These cirrus layers, known as anvils, affect the radiative balance [*Ramanathan et al.*, 1989], and a detailed understanding of the physical processes involved in their formation would enhance the ability to predict their occurrence and lifetime. As part of the CRYSTAL-FACE campaign, the CIRPAS Twin Otter aircraft flew twenty research missions, focused on characterizing the ambient aerosol in the vicinity of the convective systems, measuring cloud properties, and on making radiation measurements below the cirrus anvils. Data were collected both over land and water along the southwest coast of Florida; Figure 2.1 shows the flight tracks for the missions for which CCN data are available. Table 2.1 provides details on each research flight, and Table 2.2 lists the aerosol and gas-phase instrumentation onboard the Twin Otter.

This study presents the airborne CCN measurements from CRYSTAL-FACE and examines the extent to which it is possible to predict CCN concentrations from size distribution data in the absence of a detailed knowledge of the aerosol composition. Two CCN counters were onboard

the Twin Otter (Table 2.2). One instrument, operating at a supersaturation of approximately 0.85%, provided useful data for all but three flights, when electrical noise from another instrument caused the CCN counter to malfunction. The second CCN counter, with an effective supersaturation of approximately 0.2%, was operated for all but one flight from CF-8 through the end of the campaign; no data are available from CF-16 due to an instrument malfunction. The reliability of these measurements is verified by laboratory experiments, by a field inter-comparison of the two instruments, and by comparison with other instruments measuring aerosol concentration. After establishing the validity of the data, the observations are described in more detail, in order to provide a comprehensive picture of the typical summertime CCN population over southwest Florida. A simplified closure analysis follows, comparing the CCN dataset at both measured supersaturations to size spectral data from the Caltech Differential Mobility Analyzer (DMA, described by *Wang et al.* [2003]), assuming an idealized (ammonium sulfate) composition. The study concludes by discussing the sensitivity of the results to assumptions made in the analysis.

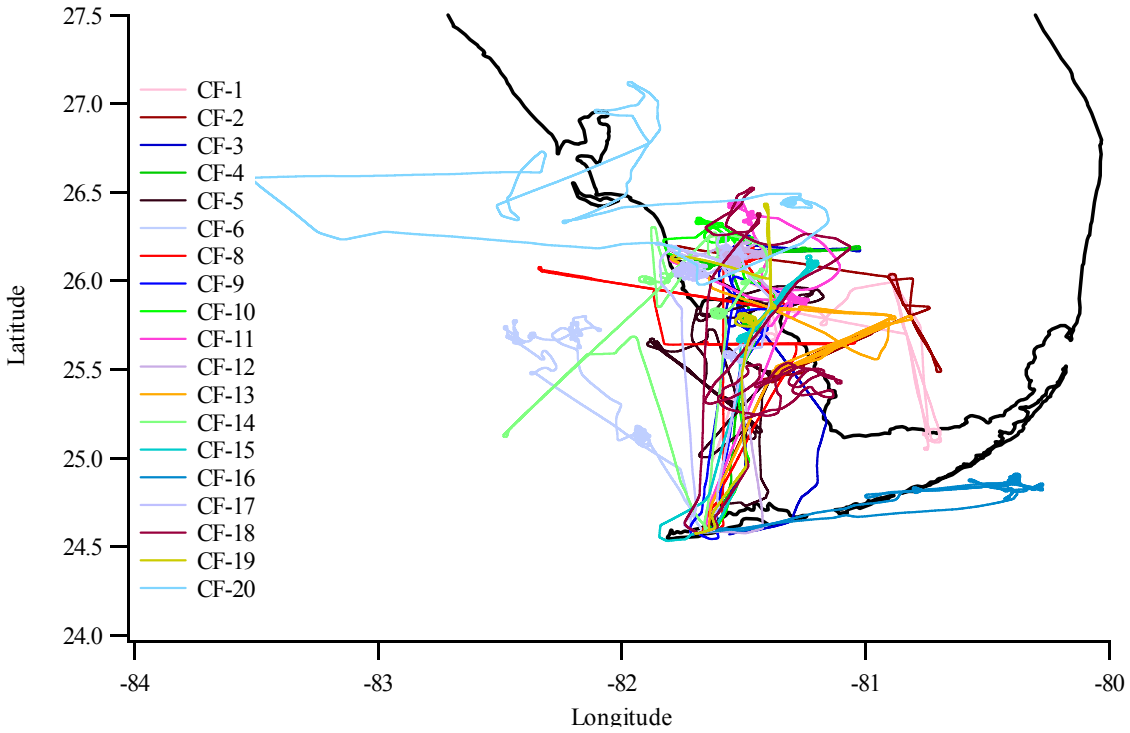

Figure 2.1: Flight tracks for the CRYSTAL-FACE flights for which CCN data are available.

Table 2.1: Summary of Twin Otter missions for the CRYSTAL-FACE campaign.

Flight Number	Date	Launch Time (GMT)	Flight Duration	Mission Type	CCN Data	
					0.2%	0.85%
CF-1	July 3	11:59	4:01	Radiation	No	Yes
CF-2	July 3	17:50	3:03	Radiation	No	Yes
CF-3	July 6	12:34	3:13	Radiation	No	Yes
CF-4	July 7	12:23	3:14	Cloud	No	Yes
CF-5	July 7	17:23	4:44	Radiation	No	Yes
CF-6	July 10	14:04	3:41	Cloud	No	Yes
CF-7	July 11	15:25	4:44	Radiation	No	No
CF-8	July 13	17:25	4:54	Cloud, Rad.	Yes	No
CF-9	July 16	17:52	2:16	Clear Air	Yes	No
CF-10	July 18	14:24	2:30	Cloud	Yes	Yes
CF-11	July 18	18:00	2:59	Radiation	Yes	Yes
CF-12	July 19	14:58	2:50	Cloud	Yes	Yes
CF-13	July 19	19:01	4:06	Radiation	Yes	Yes
CF-14	July 21	17:13	4:21	Radiation	Yes	Yes
CF-15	July 23	19:29	4:24	Radiation	Yes	Yes
CF-16	July 25	14:00	2:09	Cloud	No	Yes
CF-17	July 26	15:56	4:03	Cloud	Yes	Yes
CF-18	July 28	18:31	4:03	Radiation	Yes	Yes
CF-19	July 29	13:28	1:27	Clear Air	Yes	Yes
CF-20	July 29	17:00	4:10	Radiation	Yes	Yes

Table 2.2: Twin Otter aerosol and trace gas payload during CRYSTAL-FACE.

Instrument	**Measurement**	**Sampling Interval**
Aerosol Mass Spectrometer (AMS)	Particle size and composition: 50nm-1.0μm	60s
Aerodynamic Particle Sizer (APS)	Size distribution: 0.37-2.0μm	27s
Carbon Monoxide (CO)	Carbon Monoxide Concentration	1s
Cloud Condensation Nucleus Counter (Caltech)	CCN at S_c=0.85%	2s
Cloud Condensation Nucleus Counter (Scripps)	CCN at S_c=0.2%	1s
Condensation Particle Counters (CPCs)	Particle concentration: cut sizes at 3, 7, and 12 nm	1s
Differential Mobility Analyzer (DMA)	Aerosol size distribution: 10-900 nm	103s
Multi-sample Aerosol Collection System (MACS)	Aerosol samples for TEM analysis	Variable (Minutes)
Water Vapor (NOAA)	Water Vapor Concentration	1s
Cloud, Aerosol, Precipitation Spectrometer (CAPS)	Size distribution: 0.3μm-1.6mm	1s
Forward Scattering Spectrometer Probe (FSSP-100)	Size distribution: 0.5-47μm	1s
Passive Cavity Aerosol Spectrometer Probe (PCASP)	Size distribution: 0.1-3.0μm	1s
Micro-Orifice Uniform Deposit Impactor (MOUDI)	Size-classified filter sampling	Variable (Hours)

2.3 Background

Previous attempts to match predicted CCN concentrations with those directly observed have met with mixed success. The methods by which these studies were conducted vary considerably, and by examining the details of these methodologies one can determine those elements required for a successful experiment.

Only three studies in the literature present results that can be considered successful in terms of aerosol/CCN closure. All were ground-based studies: *Liu et al.* [1996] made measurements in Nova Scotia as part of the North Atlantic Regional Experiment (NARE), *Cantrell et al.* [2001] used measurements made in the Maldives during the Indian Ocean Experiment (INDOEX), and *Roberts et al.* [2002] collected data in the Amazon Basin during the Cooperative LBA Airborne Regional Experiment 1998 (CLAIRE-98). In the first two studies, the aerosol was split into soluble and insoluble fractions based on filter samples and the soluble fraction was assumed to be ammonium sulfate. *Roberts et al.* [2002] further split the soluble fraction into organic and inorganic components. All three studies averaged the CCN and size spectral data over a substantial period of time to match the filter sampling time. *Liu et al.* [1996] used an isothermal haze chamber to obtain CCN concentrations at a supersaturation, S = 0.06%; these data were compared against integrated size distributions from an optical particle counter (Particle Measurement Systems model PCASP-100X). For each of the twelve samples in the closure analysis, data were averaged for a period of 2-5 hours. In ten of the twelve sampling intervals, the predicted concentration agreed with the measurement within the uncertainty limits; of the other two samples, in one case the measurement was overpredicted, and in one case it was underpredicted. *Cantrell et al.* [2001] measured CCN spectra for supersaturations between 0.1 and 1% using the CCN Remover described by *Ji and Shaw* [1998]; in this case, the aerosol size distribution was measured using a Scanning Mobility Particle Sizer (TSI, Inc.). The average measured spectra from three dates were compared to predicted concentrations based on the filter cut sizes. Eight of ten data points matched within experimental uncertainties; in the other two cases, the predicted CCN spectra exceeded the measurements. In the *Roberts et al.* [2002] study, CCN measurements were made at several supersaturations using a static thermal-gradient chamber. These data were averaged over 48-72 hour periods to match the sampling time for the MOUDI cascade impactors that were the source of the compositional data in the analysis. As in the *Cantrell et al.* [2001] study, aerosol size spectra were measured with a differential mobility analyzer. For each of the four sampling periods, the calculated CCN spectrum agreed with the

observation to within measurement uncertainties. Although these studies were limited in scope, the measured and predicted CCN concentrations agreed well enough to indicate that closure had been achieved.

Other ground-based studies of CCN closure have been less successful. A common characteristic is that measured CCN concentrations were less than would be predicted based on available size and composition information. In measurements carried out at Cape Grim, Australia, *Bigg* [1986] used measured size distributions and assumed the aerosol was composed of either sodium chloride or ammonium sulfate; this produced reasonable results at low CCN concentrations, but there were large discrepancies at higher CCN concentrations. Studies by *Covert et al.* [1998] and *Zhou et al.* [2001] (a ship-based study) each compared two methods for predicting CCN concentrations. Both studies used data from tandem differential mobility analyzers to infer an insoluble fraction using hygroscopic growth information, and assumed the soluble fraction was ammonium sulfate. In the *Covert et al.* [1998] study, the correlation between measured and predicted CCN improved when particle solubility was taken into account. *Zhou et al.* [2001], following the same procedure, did not see an improved correlation, and concluded that this was due to a very low insoluble fraction. In both cases, the measured CCN concentration was, on average, 20-30% lower than that predicted; while this error is, perhaps, not excessive, a consistent overprediction is indicative of either a problem with the measurement or an incomplete understanding of the processes affecting activation.

Airborne closure studies are inherently more difficult than those that are ground-based, and the results of the few available airborne closure studies reflect this difficulty. A moving platform greatly increases the variability in the aerosol population sampled, making rapid measurements necessary. Space considerations on the aircraft often limit the instrumentation available; the resulting sacrifices in the dataset add further uncertainty to an already demanding measurement. In short, aerosol/CCN closure has not yet been demonstrated from an airborne platform. An attempt by *Martin et al.* [1994] consisted of only two data points, one maritime and one polluted. The authors assumed a pure ammonium sulfate aerosol and compared the CCN measurement with an integrated spectrum from an optical particle counter. There was reasonable agreement in the maritime case, but not in the polluted case. In the Second Aerosol Characterization Experiment (ACE-2), *Snider and Brenguier* [2000], using data from the Météo-France Merlin aircraft, compared measured CCN with size spectra from a optical particle sizing instrument (PCASP), assuming a pure ammonium sulfate composition. The measured CCN concentration

(at $S = 0.2\%$) was roughly half that expected from the PCASP data; the difference was attributed to an incomplete understanding of the aerosol composition. *Wood et al.* [2000] undertook a similar analysis during ACE-2, using data from the UK Meteorological Office C-130 aircraft, and attempted to improve the agreement by varying the assumed soluble aerosol fraction. At high supersaturations ($S > 0.5\%$), the CCN concentrations were overpredicted by more than 50%; no explanation was offered for this disagreement. Also during ACE-2, *Chuang et al.* [2000a] measured CCN at $S \sim 0.1\%$ from the CIRPAS Pelican and predicted CCN concentrations based on airborne size distributions and aerosol composition measurements from ground-based filter samples. Measurements were roughly an order of magnitude lower than predictions; the authors surmised that instrumentation problems were the source of most of the discrepancy.

In summary, in most of the published closure studies, measured CCN concentrations are significantly lower than expected based on theoretical activation of the measured aerosol size distributions. This disagreement has usually been attributed to an incomplete understanding of the activation processes, even when sampling relatively clean air masses. However, in three cases closure was generally achieved despite the use of a relatively simple compositional model: *Liu et al.* [1996], *Cantrell et al.* [2001], and *Roberts et al.* [2002]. While, in some cases, a lack of closure may be due to measurement errors, this still leaves open the basic question of whether it is possible to achieve an aerosol/CCN closure.

2.4 CCN Instrument Description

Both CCN counters deployed during CRYSTAL-FACE are based on the instrument described by *Chuang et al.* [2000b], using an improved temperature configuration first identified by *Rogers and Squires* [1977] and brought to fruition by G.C. Roberts and A. Nenes (A continuous-flow longitudinal thermal-gradient CCN chamber for airborne measurements, manuscript in preparation, 2003), hereafter labeled Roberts and Nenes (2003). The instrument described by *Chuang et al.* [2000b] was intended to function as a CCN spectrometer, where the supersaturation at which particles activated could be inferred from the droplet diameter at the outlet. However, during the ACE-II campaign, in which that instrument flew aboard the CIRPAS Pelican, stability and resolution issues limited its usefulness, and data were reported only for a single supersaturation [*Chuang et al.*, 2000a]. Later work also discussed in *Chuang et al.* [2000b] indicated that those resolution issues were characteristic of the temperature configuration employed during ACE-II, a result that was later verified theoretically by *Nenes et al.* [2001a].

Recent work by Roberts and Nenes (2003) indicates that the cylindrical CCN design could be significantly improved by incorporating a different control strategy, where the temperature of the column wall is increased axially to asymptotically approach a constant supersaturation. Because water vapor diffuses more rapidly than heat, the constant streamwise temperature gradient leads to a nearly constant supersaturation on the instrument centerline. The simulated supersaturation profile arising from this new temperature configuration is compared to that of the *Chuang et al.* [2000b] configuration in Figure 2.2. The constant temperature increase clearly creates a more stable saturation profile. The new configuration also significantly simplifies the instrument, since ideally it requires active temperature control only at the beginning and end of the growth chamber, compared to the numerous independently controlled segments in the original configuration.

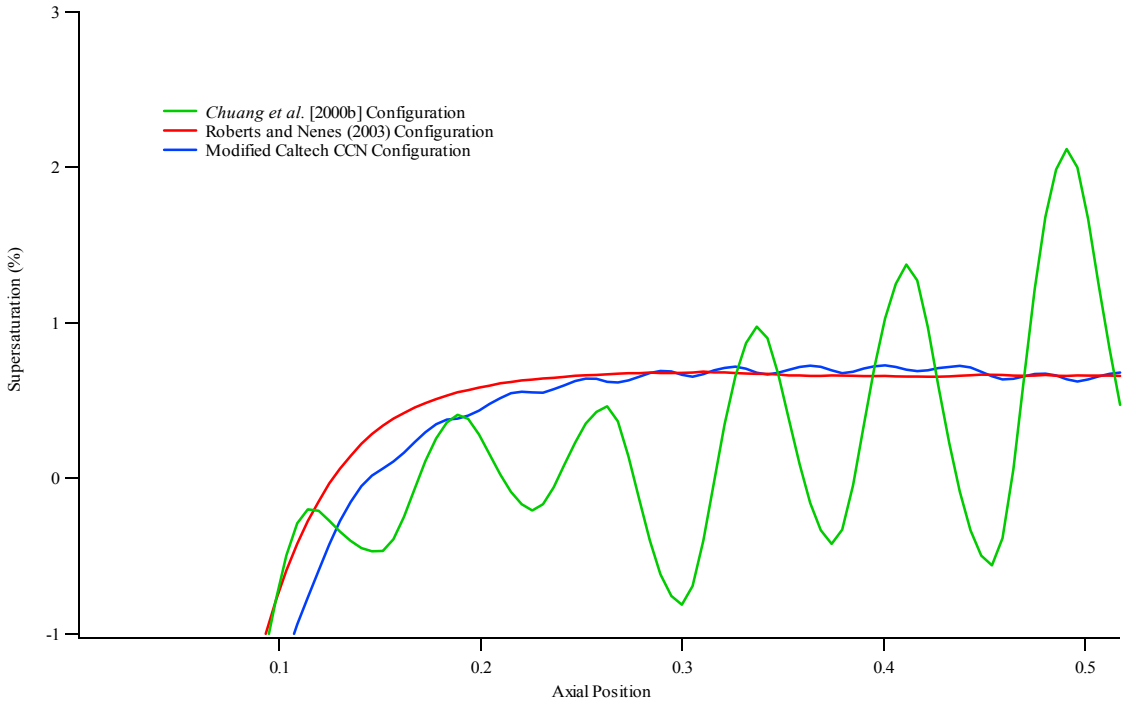

Figure 2.2: Simulated saturation profiles for various configurations for cylindrical CCN instruments. Both the Roberts and Nenes (2003) configuration and the current configuration of the Caltech instrument are substantial improvements over the design described by *Chuang et al.* [2000b].

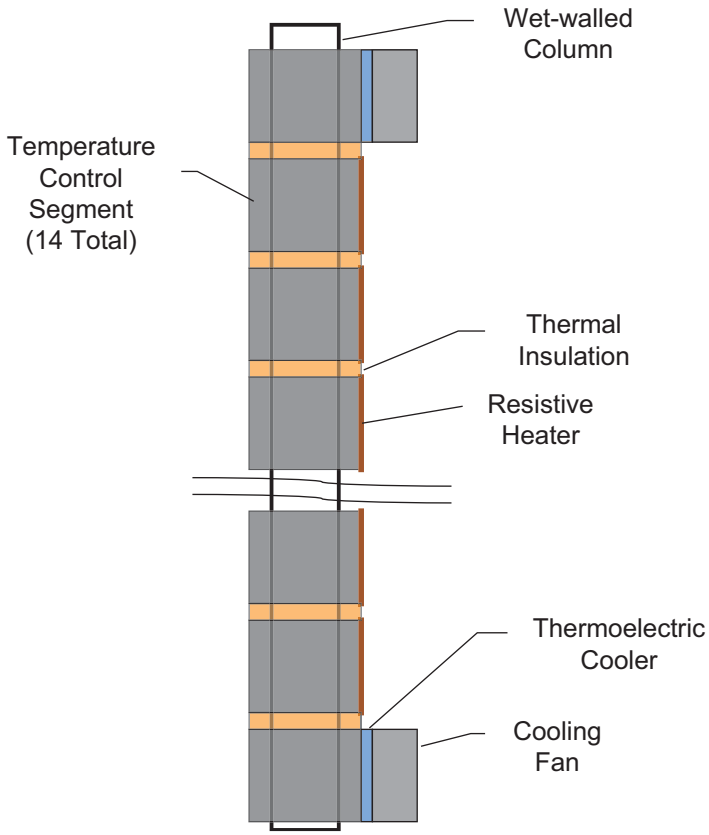

Figure 2.3: Schematic of the Caltech CCN counter as configured during CRYSTAL-FACE.

For the CRYSTAL-FACE campaign, both the instrument described by Roberts and Nenes (2003) (the Scripps CCN counter) and the Caltech CCN counter were onboard the Twin Otter. The Caltech counter, that described in *Chuang et al.* [2000b], was modified to incorporate a variation on the improved temperature profile developed by Roberts and Nenes (2003). Instead of controlling actively only at the top and bottom of the growth chamber, fourteen independent sections are maintained, with a constant temperature increase in each section. The temperatures in the first and last sections are controlled with thermoelectric coolers, and resistive heaters are used to maintain the temperature in the intermediate sections (see Figure 2.3). Using the model described in *Nenes et al.* [2001a], the saturation profile for this configuration was simulated and is presented along with the others in Figure 2.2; the result is close to that of the idealized linear profile. The Caltech instrument was originally designed for stepwise variation in the wall temperature, leading to the slight oscillations in the temperature profile when operated in this mode.

Other technical improvements were made to the Caltech CCN Counter prior to its use in the CRYSTAL-FACE campaign (see *Chuang et al.* [2000b] for details on the original instrument configuration). The sheath flow is controlled on a volumetric rather than on a mass basis, using volumetric flow controllers from Alicat Scientific Instruments. The humidification of the sheath air is now accomplished using Nafion humidifiers from Perma-Pure, Inc. The computer has been upgraded and data acquisition is managed with National Instruments LabView software; a separate multi-channel analyzer card is no longer used since only the number of activated particles must be determined. The thermoelectric coolers are now driven with Wavelength Electronics MPT-5000 temperature controllers, while the resistive heaters are still driven by RHM-4000 units. Controlled resistive heaters have been added to the sheath and sample inlets and to the optical particle counter, to prevent instantaneous supersaturations at the inlet and water condensation at the outlet. Finally, the wetted filter paper on the internal walls of the growth column is periodically re-saturated using a peristaltic pump; while this made the instrument unavailable for data collection approximately 5% of the time, it prevented the more serious flooding and drying problems experienced in the past. These technical improvements all contributed to substantial gains in instrument stability and reliability.

2.5 Instrument Verification

2.5.1 Scripps CCN Counter

The principle of the Scripps CCN instrument has been validated in controlled laboratory experiments using aerosol with known activation properties. A detailed description of the calibration and results is presented by Roberts and Nenes (2003). Monodisperse aerosol of a known composition (*i.e.*, ammonium sulfate) and size was generated by a differential mobility analyzer (DMA; TSI Model 3081). Particle diameters between 0.01 and 0.6 μm were chosen to observe various degrees of activation at a particular supersaturation. The aerosol at a selected size was simultaneously sampled at the outlet of the DMA by a scanning mobility particle sizer (SMPS; TSI Model 3081), a CPC (TSI Model 3010) and the CCN instrument. The SMPS verified the monodisperse output of the first DMA and quantified the amount of multiply charged particles. The scans were averaged, and the median diameter of the distribution was used as the calibration size for the CCN counter. The integrated droplet distribution from the SMPS yielded the total aerosol concentration and was normalized to the average number concentrations recorded by the CPC for the same SMPS scan period. Number and droplet concentrations were recorded every second by the CPC and CCN, respectively, and ranged between zero and 10^4 cm^{-3}.

The CPC has detection efficiency near 100% for particles with diameters larger than 0.018 μm and was used as a reference for comparing the activated fraction of CCN to total aerosol concentration. The median diameter of the selected monodisperse size distribution that activated 50% of the aerosol to CCN was used to calculate the corresponding supersaturation using Köhler theory.

The calibration of the instrument yielded sharp activation curves, presented in Roberts and Nenes (2003), and verified the novel technique of generating a supersaturation profile. At a flow rate of 500 cm^3 min^{-1} and temperature difference between the ends of the column of 5 °C, a sharp rise in the activated droplet concentration occurred at a median diameter of 72 nm. Theory predicts that, for ammonium sulfate aerosol, the corresponding critical supersaturation of 72 nm diameter particles is 0.24%. These calibrations were performed at ambient pressure (ca. 1000 mbar) and need to be corrected for airborne measurements at higher altitudes. The flights during CRYSTAL-FACE occurred mostly in the boundary layer around 900 mbar, which slightly lowers the supersaturation to 0.2%

2.5.2 Caltech CCN Counter

To verify the effective supersaturation of the Caltech CCN instrument in its new configuration, a laboratory calibration was carried out. In this experiment, the instrument was set up in the laboratory in parallel with a CPC, and either ammonium sulfate or sodium chloride particles of known size were fed simultaneously to both instruments. Laboratory pressure and temperature were approximately 980 hPa and 293 K, respectively. The activation properties of these particles were calculated using Köhler Theory as it is presented in *Seinfeld and Pandis* [1998]; constant van't Hoff factors ($\nu = 2$ for sodium chloride and $\nu = 3$ for ammonium sulfate) were used. Polydisperse aerosol distributions of each composition were generated with a nebulizer and passed through a diffusion dryer before being classified with a cylindrical DMA. The resulting monodisperse aerosol was then sampled by both the Caltech CCN counter and a TSI 3010 CPC. The sample concentrations were kept between 800 and 1500 particles cm^{-3}, somewhat above what were commonly observed during the CRYSTAL-FACE campaign.

The results of the verification experiments are given in Figures 2.4 and 2.5. Figure 2.4 shows the CCN ratio (measured CCN concentration/particle concentration as measured by the TSI 3010) as a function of dry particle size. For both ammonium sulfate and sodium chloride, the data

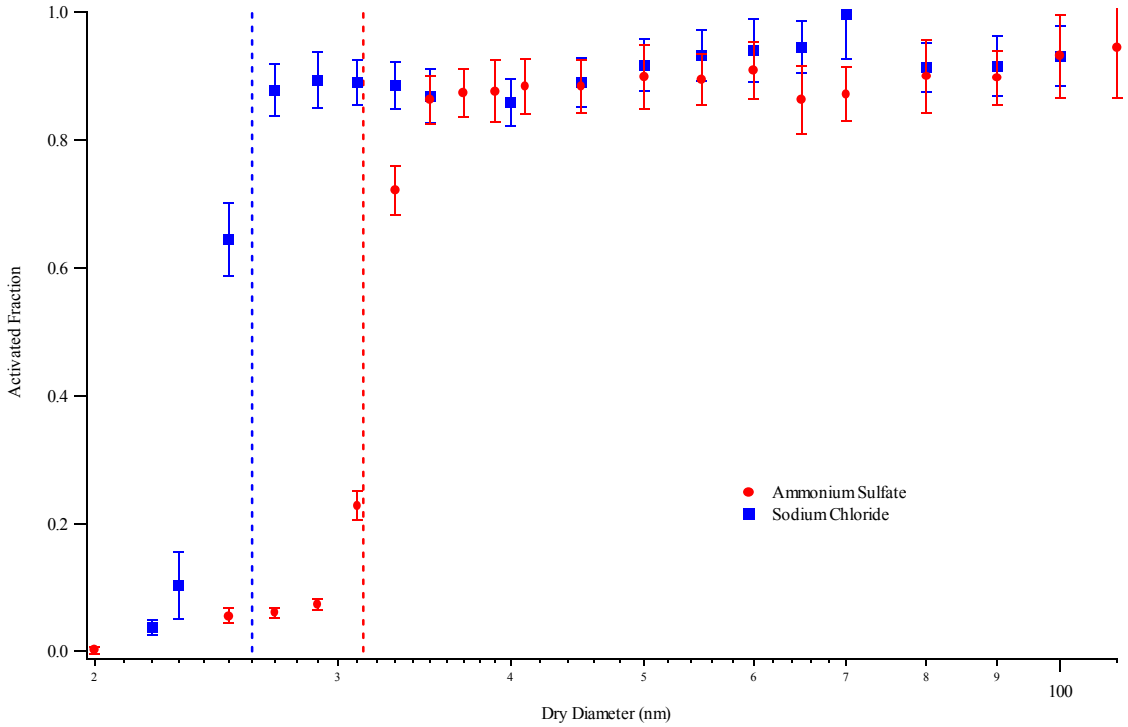

Figure 2.4: Activated fraction versus dry diameter from the laboratory verification experiments for the Caltech CCN instrument. The dashed lines represent the cut size predicted from the instrument model described in *Nenes et al.* [2001].

indicate a sharp activation transition. Vertical lines indicate the smallest dry diameters that activate in the column for each species, as predicted by the instrument model developed by *Nenes et al.* [2001a]. As expected, the size at which this transition takes place is smaller for NaCl than for $(NH_4)_2SO_4$. When the CCN ratio is plotted as a function of critical supersaturation (Figure 2.5), the instrument's response for each species is found to be nearly identical, with the transition occurring at approximately 0.85%. During CRYSTAL-FACE, housekeeping data from the CCN counter for level legs were frequently inserted in the instrument model to determine the effective supersaturation in the instrument during that period; the results indicate that the supersaturation over the course of the campaign was typically within 5% of the value determined by the laboratory experiments.

2.5.3 Field Instrument Intercomparison

Making airborne aerosol measurements is inherently difficult, and it is impossible to completely mimic flight conditions in the laboratory. A well-characterized instrument in the laboratory is necessary but not sufficient for a well-characterized flight instrument. As a means of verifying the *in situ* performance of both CCN counters, the temperature gradient of the

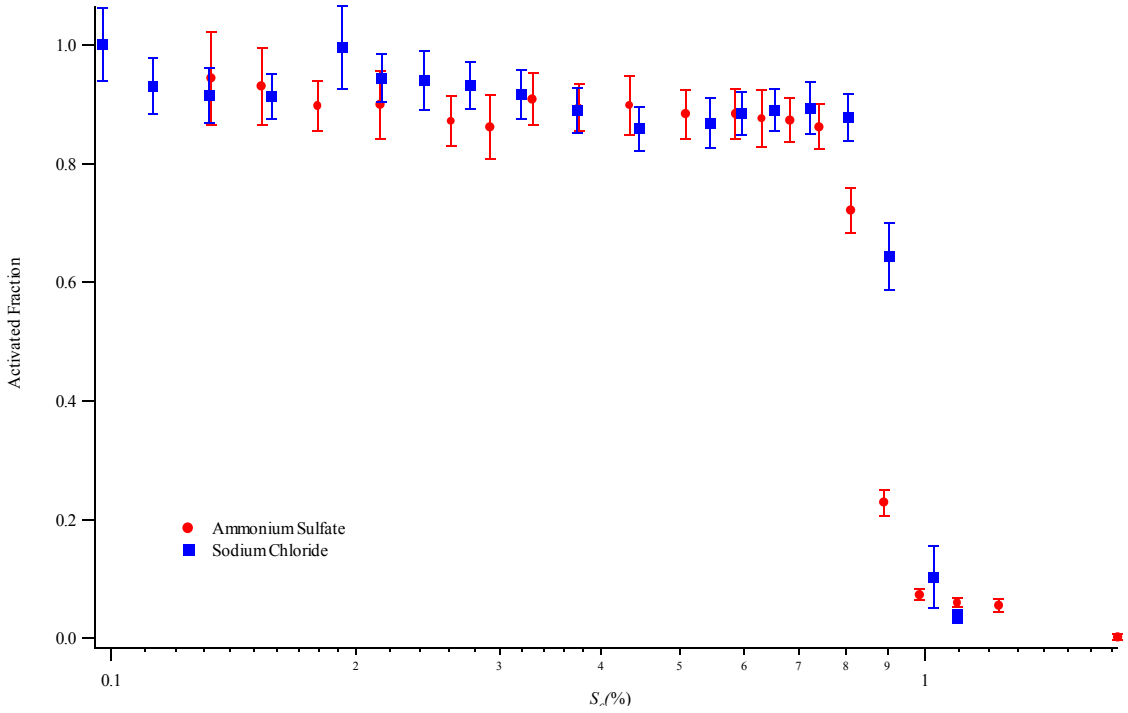

Figure 2.5: The data from Figure 2.4, plotted versus particle critical supersaturation.

Scripps counter was temporarily adjusted so that each had an effective supersaturation of ~0.85%. The comparison took place during CF-11, from 19:14 to 19:32 UTC; this time period included samples in and out of cloud, and at several altitudes between 1000 and 1700 m. The time series for this period is presented in Figure 2.6; for easier comparison, the data from the Scripps counter are given as two-second averages to match the slower sampling rate of the Caltech instrument. Brief gaps in the data from the Scripps instrument occur during altitude changes. For the purposes of the statistical comparison, these time periods are also removed from the Caltech CCN dataset.

The two instruments agree quite closely over the course of the comparison, except for two brief periods, each less than 20 s, where the concentration indicated by the Scripps counter decreased significantly relative to data from both instruments over the rest of the time period. Overall, agreement was excellent: the mean ratio ($N_{Scripps}/N_{Caltech}$) was 0.917, with a standard deviation of 0.115. When the two brief periods of large disagreement are omitted, the mean increases to 0.929, with a standard deviation of 0.086. In either case, the data indicate agreement between the instruments to within the standard deviation, indicating that both instruments work reliably onboard the aircraft and the slightly different configurations produced similar results.

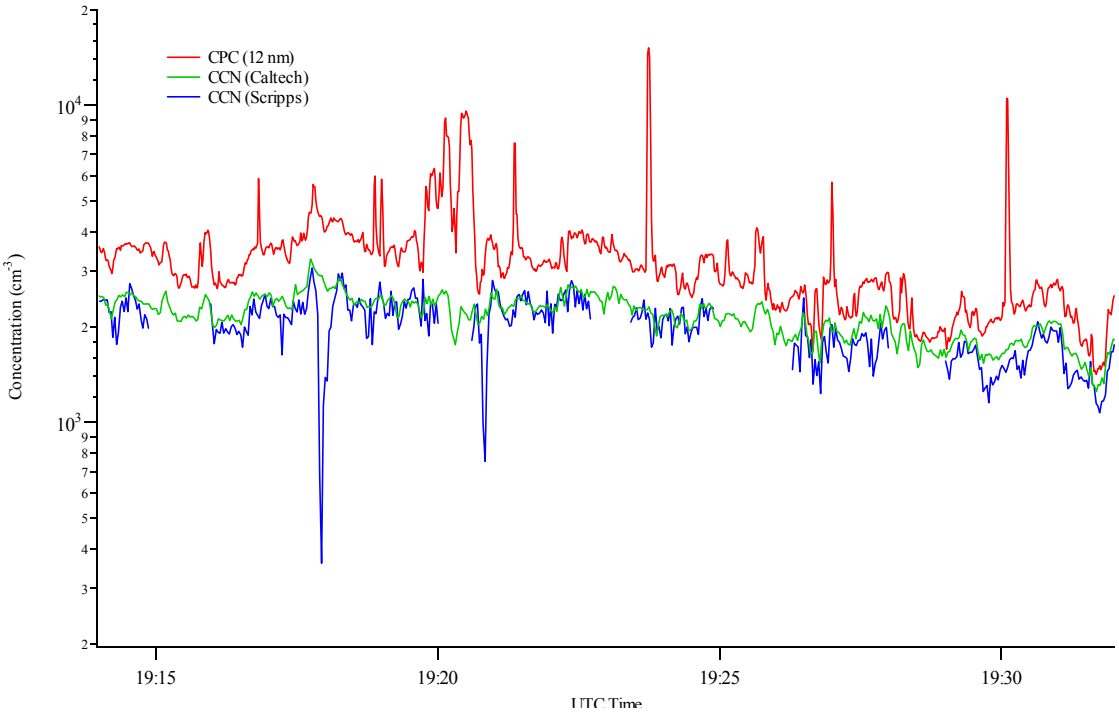

Figure 2.6: Time series from the in situ intercomparison of CCN instruments conducted during flight CF-11. The brief gaps in the data from the Scripps instrument occurred during altitude changes.

2.5.4 Instrument Response

Another test of the validity of the CCN measurements in the field is to examine the instrument response to rapid changes in atmospheric concentrations, which can occur frequently on airborne platforms. During CRYSTAL-FACE, three TSI condensation particle counters were onboard the Twin Otter, and sampled from the same inlet as the CCN counters. Figure 2.7 displays a 30-minute time series from CF-20 for one of these particle counters (operating at a nominal cut size of 12 nm), along with the corresponding data from both CCN counters. The gaps in the time series for $S = 0.2\%$ are the result of the removal of data during altitude changes. The CCN counters record several rapid changes in concentration that correspond closely with concurrent transitions in the total particle concentration measured by the CPC. For example, several sharp transitions occur between 17:32 and 17:35 that are seen clearly in the time series for all three instruments, indicating that the response times of the CCN counters to changes in the sample concentration are similar to that of the CPC. However, there are also several instances where a pulse is seen by the CPC that is not seen by one or both of the CCN counters (*e.g.*, at 17:49, 17:52, and 17:54). This does not necessarily indicate a problem with the CCN instruments: the CPC has a smaller cut size and these pulses in the time series probably

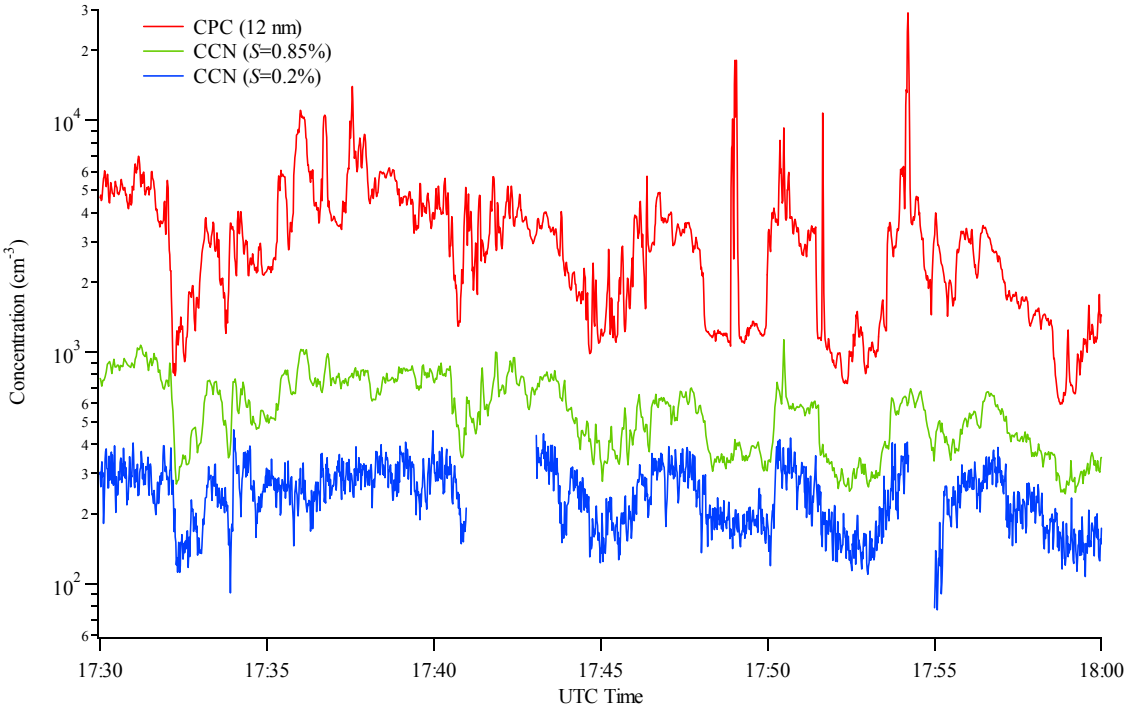

Figure 2.7: Time series data from flight CF-20. The altitude of the aircraft was ~1000 m until 17:42, and ~1500 m thereafter. The gaps in the data at S=0.2% are due to occasional instabilities in the instrument.

correspond to particles too small or too insoluble to activate. The time series data confirm that changes in the observed CCN concentration *in situ* correspond to actual changes in the aerosol population.

2.6 Trends in CCN during CRYSTAL-FACE

Previous studies have shown that CCN concentrations, like all aerosol properties, vary substantially in space and time; therefore, when comparing CCN concentrations with those of previous surface and airborne studies, the conditions of the measurements must be considered. CCN concentrations are typically lowest (N_{CCN} < 250 cm^{-3} for S > 0.5%) under remote marine conditions in either hemisphere [*Hegg et al.*, 1991; *Hudson,* 1993; *Hegg et al.*, 1995; *Covert et al.*, 1998; *Cantrell et al.*, 2000]. In contrast, concentrations can be on the order of several thousand cm^{-3} where a heavy anthropogenic influence exists [*Hudson and Frisbie*, 1991; *Hitzenberger et al.*, 1999; *Cantrell et al.*, 2000].

Earlier published measurements of CCN concentrations in eastern and southern Florida indicate substantial variation depending on the recent history of the air mass. *Hudson and Yum*

[2001] described measurements made along the eastern coast of Florida; these data were classified based on the origin of the air mass, each flight designated either maritime or continental. Over 28000 separate measurements were included in the analysis with an average duration of 3.5 s. At a supersaturation of 1%, the average concentration was 359 cm^{-3} for the maritime flights and 1411 cm^{-3} for the continental flights. Concentrations were slightly lower at S = 0.85% (~320 and 1300 cm^{-3}, respectively) and significantly lower at S = 0.2% (~200 and 500 cm^{-3}, respectively). An earlier study by *Sax and Hudson* [1981] presented ground measurements of CCN in south-central Florida and airborne measurements from east-west transects of the southern Florida peninsula. For the airborne measurements (S = 0.75%), concentrations peaked at 2500 cm^{-3} over the east coast, but dropped to between 250 and 500 cm^{-3} over the center of the peninsula. Ground measurements from the following year supported these data, and demonstrated that the local concentrations in the boundary layer were dependent on wind speed and direction. Such a result is intuitive, given the nature of the Florida peninsula: large population centers along both coasts surround a rural interior. Off the eastern coast is the open Atlantic Ocean, where maritime conditions are the norm, while off the western coast lies the Gulf of Mexico, where there is often more recent continental influence.

The range of CCN concentrations observed during the CRYSTAL-FACE campaign is in general agreement with these earlier studies. During CRYSTAL-FACE, data were collected both over land and the Gulf of Mexico near the southwestern coast of Florida (Figure 2.1). For this description of the general trends in CCN concentrations and the closure analysis that follows, the data from both CCN counters were averaged over 103 seconds to match the time scale of the individual size distributions from the DMA. Only data from level legs were included in the analysis. In this presentation, in-cloud data are included; cloud passes were brief relative to the averaging time, and it will be demonstrated in a later section that removing in-cloud data has a negligible impact on the results. As mentioned previously, the 0.85% S counter required periodic re-saturation, and was out of service ~5% of the time. The 0.2% S counter experienced temperature and pressure stability problems throughout the campaign that required some data filtering; these problems were usually seen at high altitudes and during changes in altitude.

Table 2.3: CCN data summary at S = 0.85%. Each observation is averaged over 103 s. The coefficient of variation is the ratio of the standard deviation of each observation to the observed concentration.

Flight Number	Date	Number of Observations	Measured Concentration (cm^{-3})		Coefficient of Variation	
			Range	Mean	Range	Mean
CF-1	July 3	45	324-1040	660	0.03-0.20	0.07
CF-2	July 3	57	288-801	514	0.03-0.99	0.09
CF-3	July 6	44	155-872	606	0.03-0.19	0.07
CF-4	July 7	29	399-935	554	0.03-0.41	0.22
CF-5	July 7	93	70-391	185	0.04-1.44	0.20
CF-6	July 10	14	427-851	614	0.04-0.23	0.08
CF-10	July 18	18	1138-2332	1413	0.03-0.19	0.07
CF-11	July 18	34	407-1661	1052	0.03-0.31	0.09
CF-12	July 19	20	287-640	456	0.04-0.20	0.08
CF-13	July 19	96	195-515	313	0.04-0.67	0.13
CF-14	July 21	52	225-1105	615	0.03-0.32	0.09
CF-15	July 23	84	218-720	326	0.04-1.28	0.13
CF-16	July 25	60	199-774	305	0.04-0.38	0.10
CF-17	July 26	27	261-402	314	0.03-0.53	0.09
CF-18	July 28	89	286-5999	1283	0.03-0.90	0.22
CF-19	July 29	38	84-436	215	0.04-0.50	0.16
CF-20	July 29	68	151-1193	385	0.05-0.56	0.15
Overall		**868**	**70-5999**	**533**	**0.03-1.44**	**0.13**
Omitting CF-18		**779**	**70-2332**	**447**	**0.03-1.44**	**0.12**

Table 2.3 summarizes the data from the Caltech CCN counter during the CRYSTAL-FACE campaign. For this instrument, operating at S = 0.85%, there are 868 measurements collected during 17 flights. Figure 2.8 shows a histogram of these data. The concentrations ranged from a low of 70 cm^{-3} (during CF-5) up to 5999 cm^{-3} (during CF-18); the average over the entire duration of the campaign was 533 cm^{-3}. However, Figure 2.8 indicates that the mean is skewed by a small number of data points at the upper end of the range; the vast majority of measured concentrations were below 1000 cm^{-3} and the peak in the histogram lies between 250 and 300 cm^{-3}; the median is at 371 cm^{-3}. Almost all of the very high concentration measurements (> 2000 cm^{-3}) are from CF-18, on July 28. The final line on Table 2.3 indicates that if the data from CF-18 are omitted, the mean falls to 447 cm^{-3}, and the upper boundary of the remaining data is 2332 cm^{-3}.

The summary data for the Scripps CCN instrument, operating at S = 0.2%, are presented in Table 2.4. Over 12 flights, there were 353 sampling intervals, with measured concentrations ranging from 33 cm^{-3} (during CF-15) to 1553 cm^{-3} (during CF-10). The mean of these measurements is 306 cm^{-3}, but the histogram in Figure 2.9 shows that, as is the case for the higher

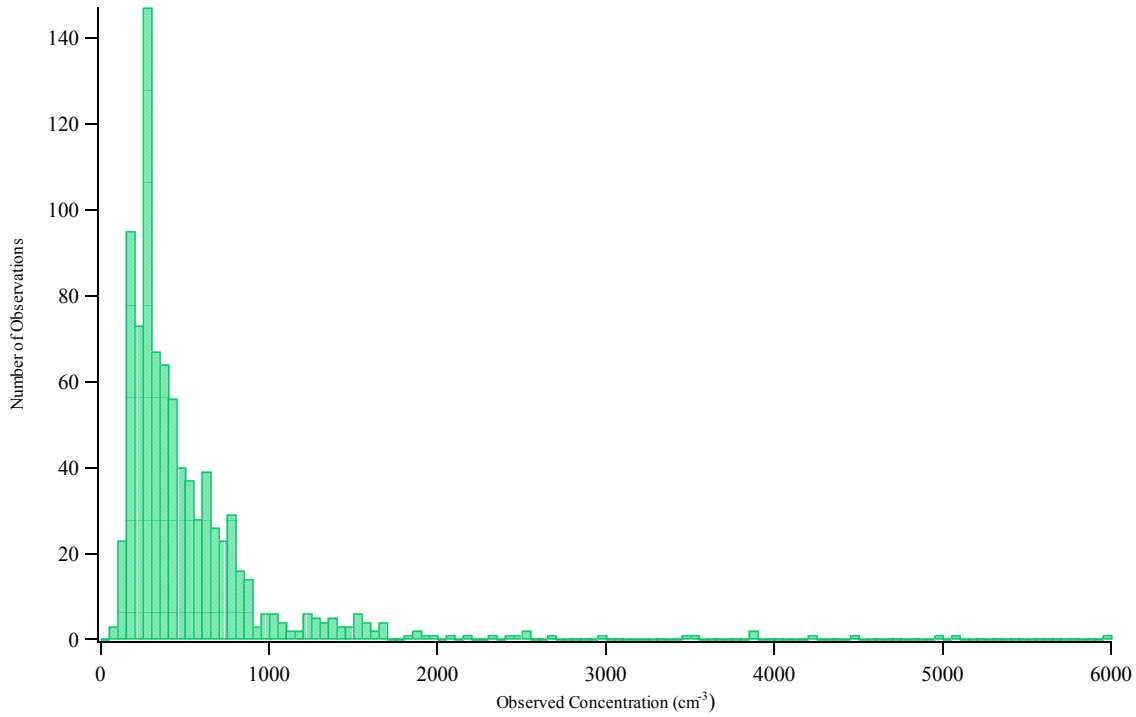

Figure 2.8: Histogram of CCN observations at S = 0.85%.

supersaturation measurements, the mean is skewed by a proportionally small number of high-concentration measurements. The median concentration is 233 cm^{-3}, and the peak in the histogram lies between 50 and 150 cm^{-3}.

Table 2.4: Same as Table 2.3, but at S = 0.2%.

Flight Number	Date	Number of Observations	Measured Concentration (cm^{-3})		Coefficient of Variation	
			Range	Mean	Range	Mean
CF-08	July 13	9	269-702	501	0.12-0.25	0.17
CF-09	July 16	36	129-582	391	0.07-0.27	0.13
CF-10	July 18	18	679-1553	850	0.10-0.49	0.22
CF-11	July 18	26	106-1310	649	0.10-0.76	0.36
CF-12	July 19	18	120-347	225	0.12-0.31	0.18
CF-13	July 19	25	39-80	55	0.25-0.76	0.46
CF-14	July 21	7	281-641	475	0.13-0.33	0.20
CF-15	July 23	55	33-304	141	0.12-0.68	0.28
CF-17	July 26	15	163-263	211	0.10-0.23	0.15
CF-18	July 28	52	219-1275	447	0.10-0.82	0.24
CF-19	July 29	28	50-261	109	0.13-0.43	0.25
CF-20	July 29	64	94-462	175	0.12-0.44	0.21
Overall		**353**	**33-1553**	**306**	**0.07-0.82**	**0.24**

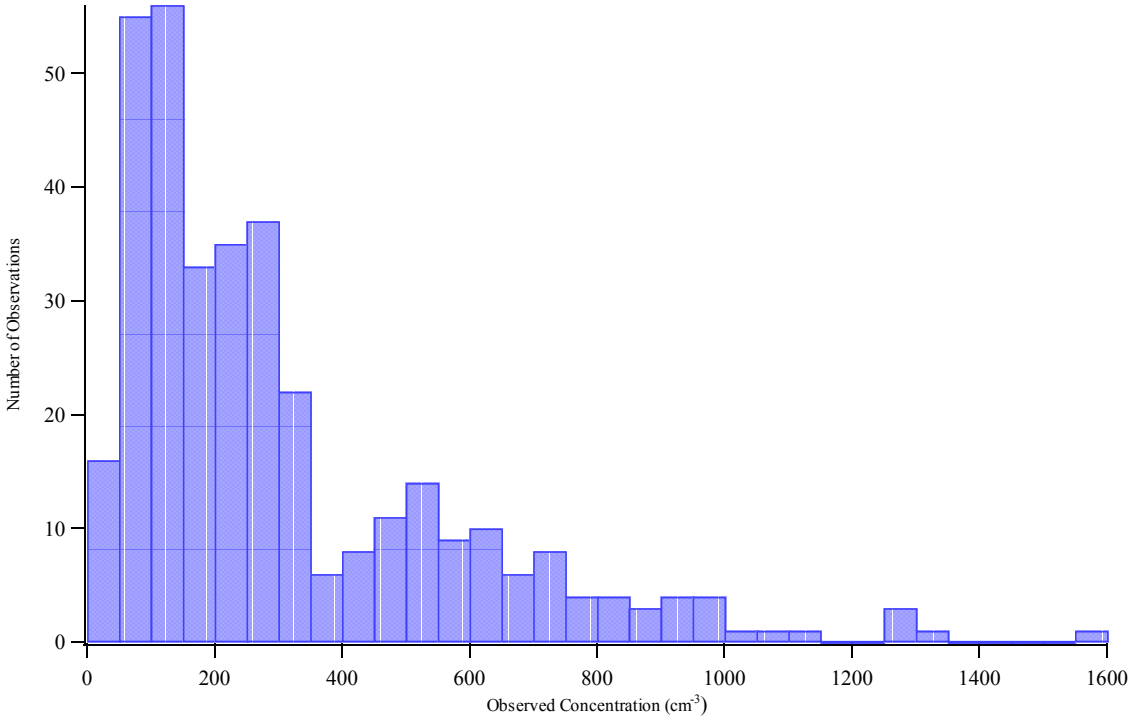

Figure 2.9: Histogram of CCN observations at $S = 0.2\%$.

The histogram data at both supersaturations indicate that the air sampled during the campaign was typically marine and modified marine in character; air masses with more distinct continental and anthropogenic influence were encountered, but infrequently. At both $S = 0.2\%$ and $S = 0.85\%$, the peak in the histogram is below the mean reported by *Hudson and Yum* [2001] for marine aerosol, and the median concentrations from CRYSTAL-FACE are only slightly larger. The data ranges in Tables 2.3 and 2.4 may lead to the conclusion that the continental samples were spread over numerous flights; only during CF-10 was the continental influence obvious throughout the flight.

The flight path of the Twin Otter during a CRYSTAL-FACE mission usually involved multiple altitudes with different patterns on each flight; much of the intraflight variability indicated in Tables 2.3 and 2.4 is a result of these complex flight patterns. Figures 2.10 and 2.11 show the relationship between CCN concentration and altitude. For clarity, the data from CF-18 are omitted from Figure 2.11 and from the present discussion; the very high concentrations at $S = 0.85\%$ during that flight all occurred at altitudes between 700 and 1500 m. The outstanding feature in both figures is the group of high concentration observations at about 1600 m. Although

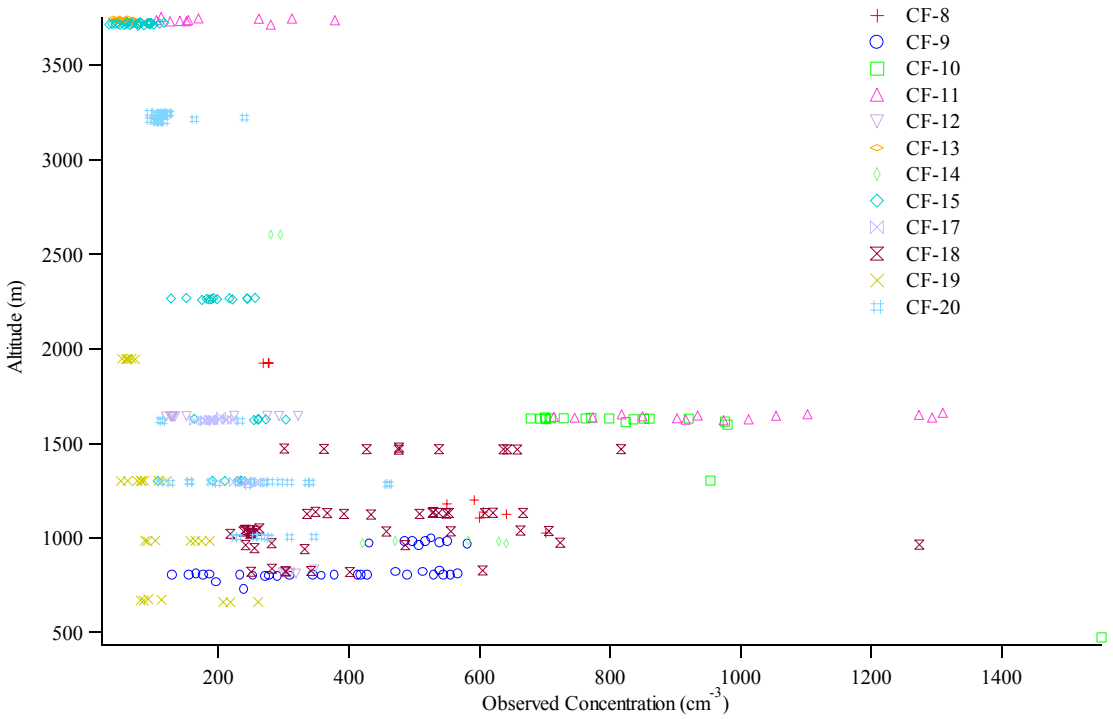

Figure 2.10: Altitude versus observed CCN concentration at $S = 0.2\%$.

concentrations sufficiently high to be considered continental were seen on several flights, only during CF-10 and CF-11, the two flights on July 18, was an air mass of apparent continental origin sampled for an extended time period. The lower concentrations also observed during CF-11 were from another flight leg at a higher altitude; the variation of concentration with altitude is much stronger than during other flights. The difference is explained by examining the back trajectory of the air mass for that day, using the NOAA HYSPLIT model [*HYSPLIT4,* 1997]. For most of the mission, the air mass sampled by the Twin Otter had been aloft and/or over water for several days prior to being sampled. Figure 2.12 indicates a different history for July 18: the air had been over the land for several days, and the air at 1600 m had been at ground level 48 hours before. This air mass history explains the elevated concentrations seen on that day. For the rest of the dataset, there appears to be some altitudinal dependence in CCN concentrations, but the temporal and local spatial variation appears to be more important.

2.7 Comparison of CCN Data with Aerosol Size Distributions

The importance of aerosol/CCN closure, and the difficulty in achieving it, is the primary motivation for this work. The activation properties of the atmospheric aerosol determine in large part the extent of cloud formation and propagation, but our understanding of the processes

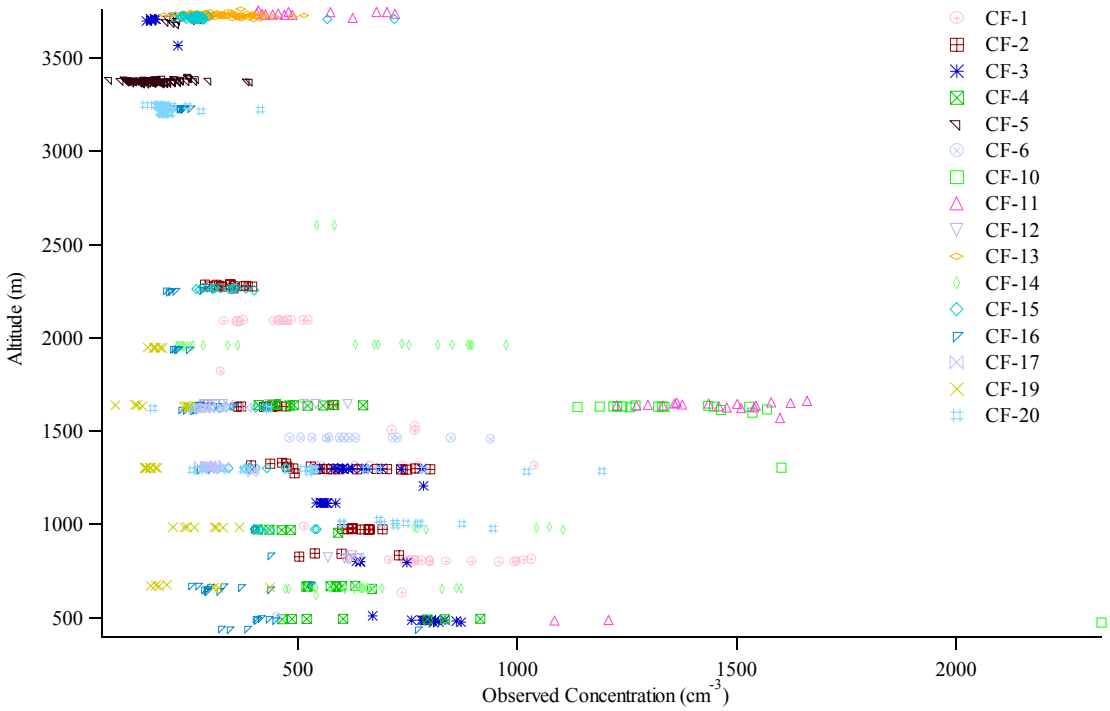

Figure 2.11: Altitude versus observed CCN concentration at S = 0.85%. The observations from CF-18 are omitted for clarity.

involved is incomplete. Comparing measurements of CCN concentrations to predictions based on activation theory serves to validate both the measurement and the theory. During the CRYSTAL-FACE campaign, the DMA measured aerosol number size distributions, with an operating range of 10-900 nm. The scans from this DMA system last 103 seconds, and the instrument sampled from the same inlet as the CPC and CCN instruments; the data from both CCN counters were averaged to match the sampling interval of these size distributions. The operating range of the DMA includes the vast majority of the particles in the atmosphere, thus the CCN population can be effectively assumed to be a subset of the measured size distribution.

For this analysis, the entire aerosol population was assumed to be pure ammonium sulfate. This is clearly a simplification, but it can be considered an obvious first step in estimating CCN concentrations from aerosol size distributions, and the same assumption has been used in similar analyses previously (*e.g.*, *Bigg* [1986], *Martin et al.* [1994], and *Snider and Brenguier* [2000]). Furthermore, the choice is supported in general by unpublished data obtained during CRYSTAL-FACE using the Aerosol Mass Spectrometer (AMS) (R. Bahreini, personal communication, 2003). The assumed composition leads directly to a predicted cut size corresponding to the effective supersaturation in each CCN counter, calculated using Köhler theory where the van't

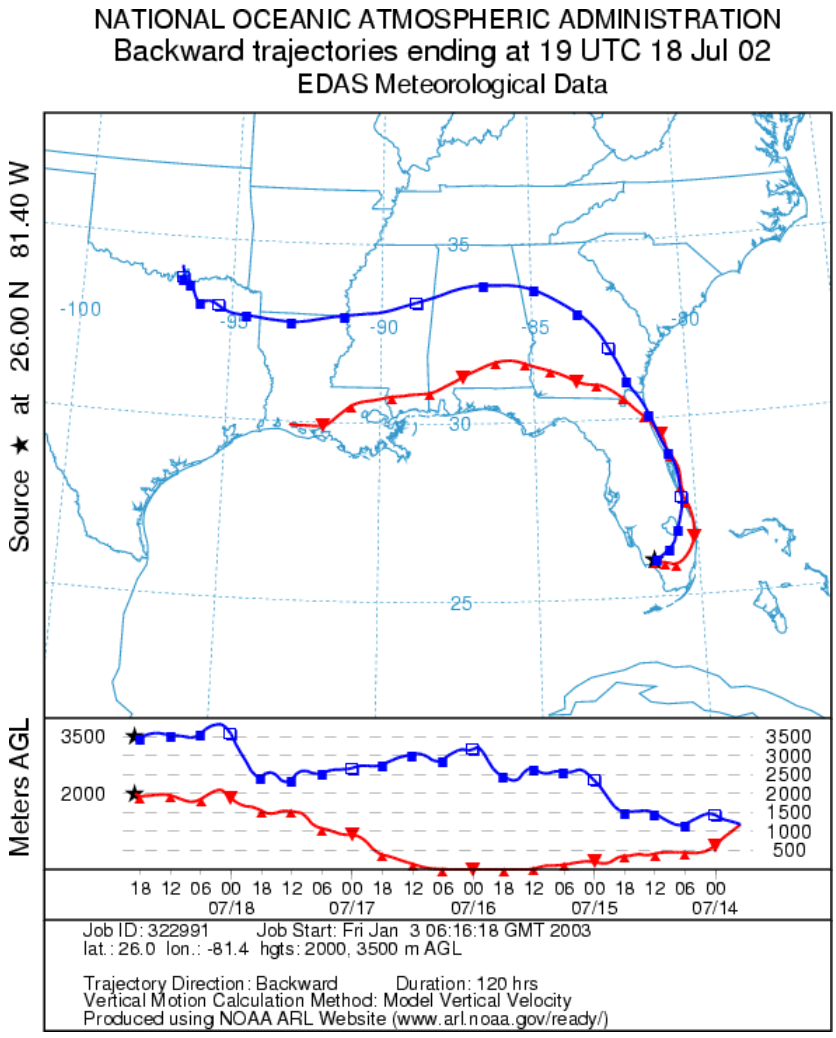

Figure 2.12: Simulated 120 hour back-trajectories for the airmass sampled during flights CF-10 and CF-11. The plot is a product of the NOAA Air Resources Laboratory HYSPLIT model [*HYSPLIT4*, 1997].

Hoff factor for ammonium sulfate is held constant at three (cf. *Seinfeld and Pandis* [1998]). For the counter operating at S = 0.2%, this calculated cut size was 79 nm; for the Caltech instrument, which operated at S = 0.85%, the cut size was 32 nm. The predicted CCN concentration is calculated by integrating upwards from the cut size to the upper boundary of the size distribution.

The long sampling time of the DMA system relative to other aerosol instruments limits its resolution during airborne measurements. During CRYSTAL-FACE, the nominal airspeed of the Twin Otter was 50 m s^{-1}; thus the spatial resolution of the DMA was approximately 5 km. The concentration at a given size is only measured at one point during each scan, and the data analysis implicitly assumes that the aerosol size distribution is uniform over this spatial scale. In reality,

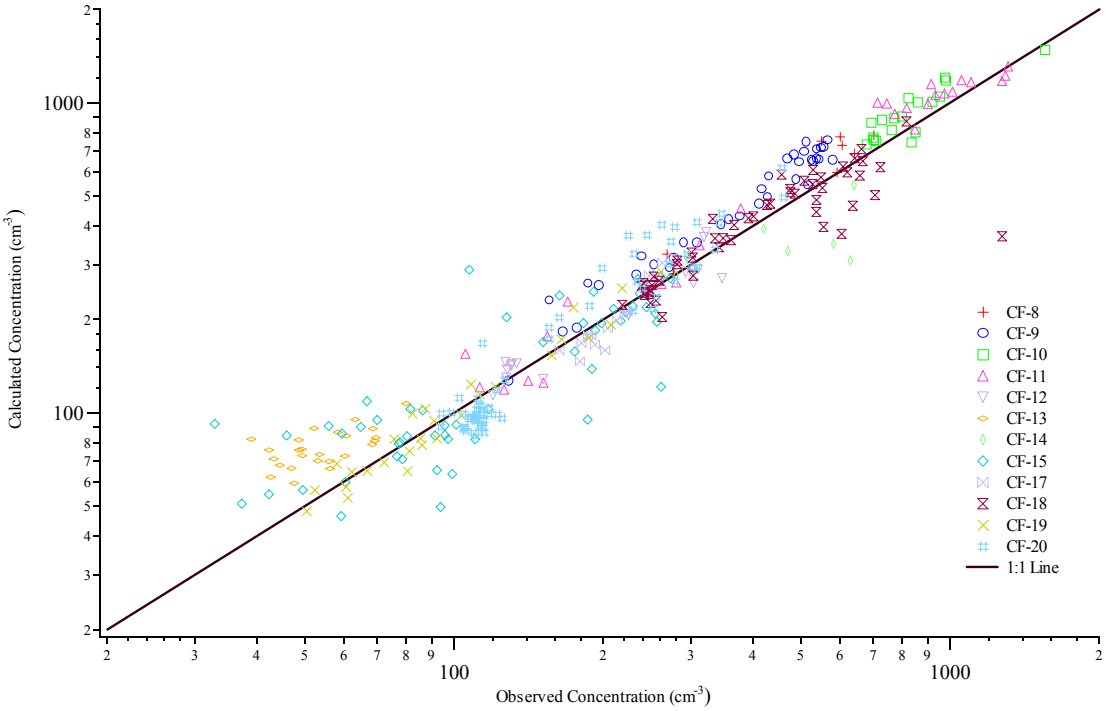

Figure 2.13: Scatterplot of the simplified closure analysis at $S = 0.2\%$.

the aerosol population frequently varies on scales shorter than 5 km. For this reason, it is not necessarily expected that any individual comparison in the simplified closure analysis would indicate good agreement, but the uncertainties would presumably average to zero over the course of many measurements.

The results of this simplified closure analysis are shown in scatterplot form in Figures 2.13 and 2.14. At $S = 0.2\%$, the agreement is excellent throughout the entire dataset. A linear regression of predicted vs. observed concentrations produces a slope of 1.026 and an intercept of 11.1 cm^{-3}, with an R^2 value of 0.912. If the intercept is forced to zero, the slope increases only slightly, to 1.047 ($R^2 = 0.911$). The overall correlation at $S = 0.85\%$ indicates some moderate overprediction: a slope of 1.264, with an intercept of -70.5 cm^{-3} ($R^2 = 0.840$); forcing a zero intercept reduces the slope to 1.201 ($R^2 = 0.835$). However, as was noted earlier, during portions of CF-18, both the CN and CCN (at $S = 0.85\%$) concentrations were much higher than were seen at any other point during the campaign. Omitting this flight from the regression reduces the slope to 1.093, with an intercept of -5.2 cm^{-3} ($R^2 = 0.770$); with a forced zero intercept, the slope is 1.085 ($R^2 = 0.770$).

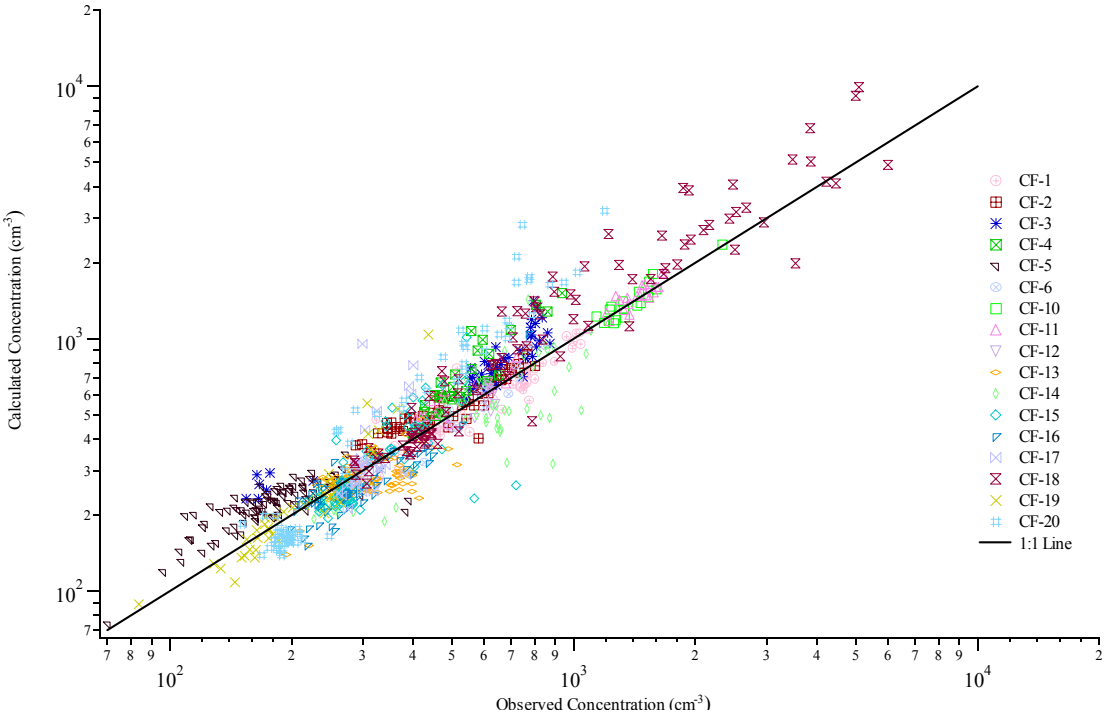

Figure 2.14: Scatterplot of the simplified closure analysis at $S = 0.85\%$.

Based on these linear regressions, the overprediction of CCN at $S = 0.2\%$ is on average only 5%, when assuming the idealized composition. At $S = 0.85\%$, the predicted concentration is 9% greater than the observation, when omitting CF-18. These overestimates are very small, compared to the earlier studies discussed in Section 2.3, and are within estimated measurement uncertainties (note that in the verification study for the Caltech instrument, Figure 2.4, the counting efficiency appears to be near 90%). Obviously, the compositional assumption is not strictly correct. The present analysis is as much a test of the assumption as of anything else, and the results support its use in cases like this one. The sensitivity of the results to the compositional assumption is examined further in the next section. In summary, the overpredictions are small, and the analysis validates the CCN measurements and the theory upon which the predicted concentrations are based.

2.8 Discussion

The CCN population over southwest Florida and the surrounding waters during CRYSTAL-FACE is primarily marine in character, and can be accurately calculated using the aerosol size distribution. However, some assumptions used in the analysis can be scrutinized, particularly the

inclusion of in-cloud data in the analysis and the assumption of a pure ammonium sulfate aerosol. Also, at several points in the analysis, the CCN observations at $S = 0.85\%$ from CF-18 have been omitted. The reasoning behind these decisions and the impact they have on the analysis are discussed below.

2.8.1 In-Cloud Sampling

The decision to include in-cloud observations in the analysis was primarily one of convenience. Cloud passes were usually very brief, and it was assumed that the impact of including these data would be negligible. To confirm this, the CCN data at $S = 0.85\%$ were filtered to remove data collected in-cloud, and the results were compared to the unfiltered data. The filter removed observations where the average liquid water content (over the 103 s sampling period), as measured by a Forward Scattering Spectrometer Probe (FSSP, from PMS, Inc.), was greater than 500 μg cm^{-3}. This effectively removed all data points wherein a portion of the sample time was in-cloud, 17% of the dataset. The average CCN concentration of the filtered dataset is 518 cm^{-3}, a decrease of 3%. The effect on the closure analysis was even smaller: after removing the in-cloud samples, the slope of the curve fit (predicted vs. observed concentration) increases to 1.240 ($R^2 = 0.826$, intercept forced to zero), a 1% difference. This confirms that the inclusion of in-cloud samples has a negligible impact on the overall analysis.

2.8.2 Aerosol Composition

For the simplified closure analysis in Section 2.7, the aerosol was assumed to be composed entirely of ammonium sulfate. The results indicate that this was a viable procedure in this case, even though the assumption could not have been strictly true. Each of the successful closure analyses discussed in Section 2.3 relied on more detailed compositional assumptions, as did nearly all of the studies where closure was not achieved. Incomplete understanding of the role of composition in establishing the aerosol/CCN relationship was cited in many cases as a primary reason why the closure analysis was unsuccessful.

One reason the idealized ammonium sulfate compositional assumption works so well here may lie in the mixing state of the aerosol. The viability of the assumption provides strong evidence of an internally mixed aerosol. Substantial external mixing of the population would mean that some fraction of the aerosol would have little or no ammonium sulfate. Whatever their actual composition, these particles (at equivalent diameters) would almost certainly activate at higher critical supersaturations; sodium chloride is the only common atmospheric species that

activates more readily than ammonium sulfate, and *Twomey* [1971] determined that most atmospheric CCN are not NaCl. Explaining the results in Section 2.7 using an externally mixed aerosol requires that the concentration of smaller NaCl particles that activate at 0.85% (or 0.2%) supersaturation be consistently offset by an equivalent number of larger, less readily activated particles; this result is highly unlikely..

However, if the aerosol is internally mixed, it is expected that the population, as a whole, would be relatively insensitive to the presence of insoluble species. *Roberts et al.* [2002] demonstrated using a prescribed size distribution that replacing half of the soluble mass (in that case, ammonium bisulfate) with insoluble organic material throughout the entire aerosol population reduced the activated fraction by only about 10% (at S = 0.85%). The effect is somewhat more pronounced at lower supersaturations; the same replacement of soluble mass with insoluble mass leads to a drop in activated fraction on the order of 35% at S = 0.2%. This result is not surprising; although the replacement of soluble mass with insoluble mass can have a large effect on activation properties for particles whose critical supersaturations are near the effective supersaturation of the instrument, the integral nature of the measurement means that the overall impact will be substantially less important. In practical terms, substituting insoluble mass for soluble mass would cause the activation cut size to shift by some undetermined number of channels. This relative insensitivity to the presence of insoluble compounds lends credence to the idealized ammonium sulfate composition used in this analysis.

The selection of ammonium sulfate as opposed to other species also impacts the analysis. The choice reflects the predominance of ammonium and sulfate in the atmospheric aerosol particles smaller than 1 μm, as a result of cloud processing [*Seinfeld and Pandis,* 1998]. However, the composition of the resultant particle is influenced by the relative abundance of ammonia and sulfur dioxide at the time of processing. Ammonium sulfate production dominates at high ammonia concentrations; at lower ammonia concentrations, ammonium bisulfate is the more common product. To determine the sensitivity of the closure analysis to the particular species chosen as the solute, the statistics were re-calculated using a different composition, ammonium bisulfate. In practical terms, this means increasing the cut size from 79 nm to 87 nm for the comparison at S = 0.2%, and from 32 nm to 35 nm for the analysis at S = 0.85%. At S = 0.2%, the adjustment resulted in a decrease in the slope of the fitted line from 1.047 to 0.939; the R^2 is nearly unchanged (0.911 and 0.909, respectively). At S = 0.85%, the re-analysis results in the slope of the fitted line dropping from 1.234 (R^2 = 0.822) to 1.201 (R^2 = 0.835). If the data

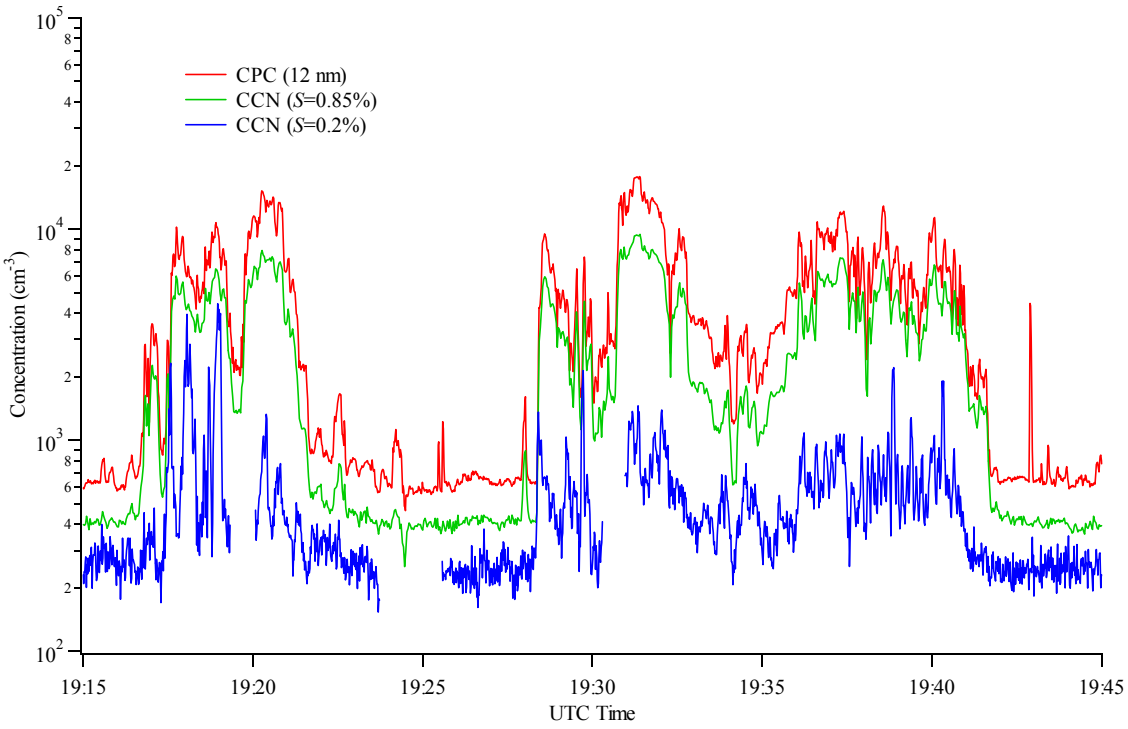

Figure 2.15: Time series for a portion of flight CF-18. Note how the aerosol concentrations measured by the CPC change rapidly by more than an order of magnitude. The high concentrations were atypical of the conditions normally encountered during CRYSTAL-FACE.

from flight CF-18 are omitted, the slope drops to 1.085 (R^2 = 0.770). Thus, if the aerosol is assumed to be ammonium bisulfate rather than ammonium sulfate, the size distribution underpredicts the CCN concentration somewhat at S = 0.2% and overpredicts somewhat at 0.85%. This confirms that the success of the analysis is not entirely dependent on the precise soluble species used to define the aerosol composition.

2.8.3 Flight CF-18

During the July 28 flight, CF-18, several instruments on the CIRPAS Twin Otter measured particle concentrations far greater than at any other time during the CRYSTAL-FACE campaign. The source or sources of these particles is not immediately clear, but the result was that aerosol (and CCN) concentrations rapidly changed by more than an order of magnitude, as can be seen in Figure 2.15. The CCN concentration at S = 0.85% tracks closely with the total aerosol concentration, while CCN at S = 0.2% appear to correlate less well; this is an indication that the particles were too small to be activated at the lower supersaturation. The size distribution data corroborate this (Figure 2.16); the vast majority of particles are smaller than 80 nm, the nominal

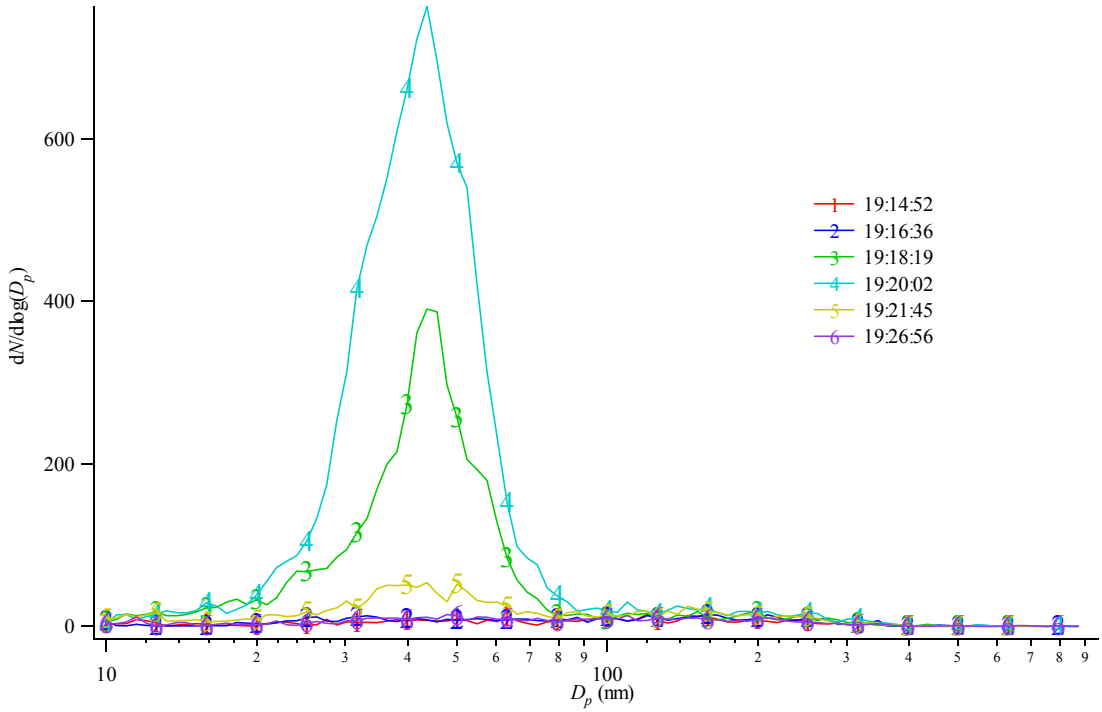

Figure 2.16: Consecutive size distributions from the DMA for the first half of the time series in Figure 2.15. The large peak that dominates the spectrum at 19:20:02 disappears almost completely in the next scan. Nearly all of the particles in the scans showing elevated concentrations are below the size at which ammonium sulfate particles would activate at S = 0.2% (i.e., 80 nm).

cut size at which ammonium sulfate particles activate when S = 0.2%. This explains why the concentrations at the lower supersaturation are not atypically high. Figure 2.16 also provides some explanation as to why the closure analysis from CF-18 involved large underpredictions as well as overpredictions. The consecutive size distributions show how rapid the transitions were between elevated and normal particle concentrations. As was discussed in the previous section, the scan time for the DMA was sufficiently long that it could miss these particles: if the transition occurs while the DMA is scanning at the upper end of the size range, the huge numbers of small particles would not be observed. This is true at all times, but usually the atmospheric particle concentrations are spatially stable enough that the scan rate is not an issue; that does not appear to be the case here. The extremely high concentrations and large spatial variation for the small particles on this flight are very interesting and worthy of further study. However, the atypical concentrations on this day justify omitting them from the closure analysis, and from the description of the CCN trends for the region.

2.9 Discussion

Information gathered from the CIRPAS Twin Otter during the July 2002 CRYSTAL-FACE campaign provides a clear picture of the character of the atmospheric aerosol along the coast of southwest Florida. Included in the Twin Otter payload were two cloud condensation nucleus counters that employed a recently developed technique for maintaining a stable constant supersaturation in order to make continuous real-time measurements of CCN. These instruments, operating at supersaturations of 0.2% and 0.85%, were well characterized in the laboratory and in the field, and their performance was consistent with those of other aerosol counters onboard the aircraft.

The CCN concentrations measured over the course of the campaign by the two instruments were in general agreement with those from earlier studies in the region. At S = 0.2%, the mean concentration over the course of the campaign was 306 cm^{-3}, while the median was 233 cm^{-3}. At S = 0.85%, the mean and median were 533 and 371 cm^{-3}. These data indicate that the majority of observations are best described as marine in character. Of the 19 flights for which data are available, only two air masses were sampled that had a distinct continental influence.

The extensive dataset from the CRYSTAL-FACE campaign was used as the basis for a simplified closure analysis to determine whether the CCN concentration could be accurately predicted by assigning an assumed composition to a measured aerosol size distribution. The analysis proved successful: at S = 0.2% the calculated concentration was on average 3% greater than the prediction, with an R^2 value of 0.91. At S = 0.85%, the overall ratio of calculated to measured concentrations was 1.09 (R^2 = 0.77), when the atypical data from CF-18 are excluded. The analysis indicates that, for conditions like those encountered during the CRYSTAL-FACE campaign, it may be possible to accurately calculate the concentrations of CCN over a range of supersaturations from the aerosol size distribution by assuming a pure ammonium sulfate composition.

More study is required in order to determine whether it is a generally applicable practice to predict CCN concentrations from the aerosol size distribution using an idealized composition. There are certainly conditions, like the elevated concentrations encountered during CF-18, where assuming a pure composition is not sufficient for characterizing the CCN population. The measurements made during the CRYSTAL-FACE campaign establish new instrumentation for accurate in situ CCN measurements for use in future campaigns.

2.10 Acknowledgements

The authors acknowledge Athanasios Nenes for assistance with simulating the performance of the CCN instruments. This work was supported by National Aeronautics and Space Administration grant NAG5-11549 and the Office of Naval Research.

3 Boundary Layer Aerosol Gradients and Convective Cloud Microphysics: A Case Study

3.1 Introduction

The impact on clouds of enhanced aerosol levels as a result of anthropogenic influences has been the focus of numerous studies. *Twomey* [1974] suggested that when the concentration of CCN is enhanced, more sites are available for condensation, leading to a cloud with more droplets, but a smaller average droplet size. Such a cloud would be more reflective than a cloud with fewer, larger droplets. *Albrecht* [1989] suggested that shifting the cloud droplet size distribution towards smaller diameters would also inhibit the growth processes that lead to precipitation, thereby increasing cloud lifetime. These phenomena, together known as the indirect aerosol effects, could be significant to the global radiative balance, but understanding of the complex processes involved is far from complete.

The reasoning leading to each of the indirect aerosol effects requires that when more particles compete for a fixed liquid water content (LWC), the resulting cloud droplet population is more numerous and skewed toward smaller sizes. Such a connection between the aerosol population and the cloud droplet population has been observed in stratocumulus clouds where particle concentrations have been enhanced locally. For example, *Ferek et al.* [1998] and *Durkee et al.* [2000] found that, in regions impacted by ship exhaust, cloud droplets were significantly smaller and more numerous than in the surrounding air. These studies indicate that the bright cloud lines known as "ship tracks" in marine stratus layers result from the Twomey effect; the connection is also evidenced by simulation results [*Ackerman et al.*, 1995]. Satellite data have indicated that phenomena similar to ship tracks occur in clouds downwind of biomass burning [*Kaufman and*

Nakajima, 1993; *Kaufman and Fraser*, 1997] and industrial sources [*Rosenfeld*, 2000; *Keil et al.*, 2002]. The influence of enhanced aerosol loadings on clouds is most evident in stratocumulus layers, because the clouds are more spatially extensive and homogeneous than other cloud types.

Presumably the same connection between enhanced aerosol loadings and increased cloud droplet concentrations found in stratocumulus layers also exist in more isolated convective clouds. Several recent studies indicate that this is likely, but the evidence is not conclusive. *Heymsfield and McFarquhar* [2001] analyzed in situ microphysical data in and around trade wind cumulus clouds during the Indian Ocean Experiment (INDOEX). The analysis compared data from the relatively pristine tropical Southern Hemisphere (SH) to measurements in the more heavily polluted Northern Hemisphere (NH); droplet concentrations were greater in the more polluted regions by a factor of three, and the effective droplet diameters were 35% smaller. *Hudson and Yum* [2001] found a similar correlation using in situ data collected in eastern Florida during the Southern Cumulus Microphysics Study (SCMS). Small cumulus clouds in airmasses of continental origin had higher concentrations of smaller cloud droplets than clouds that formed in more pristine marine air.

To date, there have been no in situ measurements examining how boundary layer aerosol concentrations affect cloud droplet and ice crystal concentrations in large mixed-phase convective clouds. In simulations of such systems *Phillips et al.* [2002] predict that both droplets and ice crystals will be smaller and more numerous when the aerosol concentration in the boundary layer is increased above the typical continental background. This result is consistent with conclusions drawn from analyses of satellite data. *Sherwood* [2002] found a negative correlation between the aerosol index as measured by the Total Ozone Mapping Spectroradiometer (TOMS) and the effective ice crystal diameter derived from data from the Advanced Very High Resolution Radiometer (AVHRR). *Rosenfeld* [1999] presented data from the Tropical Rainfall Measuring Mission (TRMM) satellite showing the effect of smoke from biomass burning on convective cloud systems. In the latter study, the effective droplet radius near cloud top in areas unaffected by smoke was roughly twice that derived from the polluted regions.

The recent CRYSTAL-FACE campaign provided an opportunity to explore the relationship between the boundary layer aerosol and the microphysical properties of mixed-phase convective cloud systems. The campaign was based in the Florida Keys in July 2002; six research aircraft and extensive ground-based radar facilities were employed to better understand the physical

processes involved in the development of cirrus anvils, which are thought to affect the global radiative balance [*Ramanathan et al.*, 1989]. The CRYSTAL-FACE website provides more details about the campaign (http://cloud1.arc.nasa.gov/crystalface/index.html). Data from two of the research aircraft participating in CRYSTAL-FACE are used in this study. The CIRPAS Twin Otter had the dual role of characterizing the boundary layer aerosol feeding the convective systems and making radiation measurements below the cirrus anvils. The University of North Dakota Citation II made microphysical measurements near the top of the convective systems and in the lower parts of the cirrus anvils. Measurements from these aircraft are compared in the following analysis to determine whether the correlation observed in stratocumulus and small convective clouds between boundary layer CCN concentrations and cloud particles also exists for more strongly convective mixed-phase systems.

This study examines a convective system sampled by both the Twin Otter and Citation aircraft on July 28, 2002. The Twin Otter flew in the boundary layer near the base of the cloud, and the observations from that period reveal several periods of atypically high aerosol concentrations. These enhanced concentrations are likely the result of encountering a plume originating at a power plant near Miami. At approximately the same time, the Citation aircraft made multiple passes through the same convective system near its top. These coordinated observations provide an opportunity for the first time to examine the effect of a highly inhomogeneous feed aerosol on a strongly convective system. The data from the Citation show a spatial gradient in the ice particle concentration that may be a result of the inhomogeneities in the boundary layer, but the evidence is inconclusive. The case study is ongoing; additional insight may be gained from ground-based radar observations and from simulations of the convective system.

3.2 Instrumentation

3.2.1 Twin Otter

During CRYSTAL-FACE, the Twin Otter payload included a wide range of aerosol and trace gas instrumentation; included in this study are observations from several of them (see Table 2.2 for the complete list). Total particle concentration was measured at 1 Hz using a condensation nucleus counter (TSI model 3010, with a 50% cut size of 12 nm). Two cloud condensation nucleus (CCN) counters operated at supersaturations (S) of 0.2% (1 Hz) and 0.85% (0.5 Hz); these instruments are described by *Roberts and Nenes* [2003] and *VanReken et al.* [2003]. A

differential mobility analyzer (DMA) system (described by *Wang et al.* [2003]) measured dry and ambient aerosol size distributions for particle diameters from 0.010 to 0.90 μm, with a sample time of 103 s. An aerosol mass spectrometer (AMS) provided size-resolved aerosol composition for particles larger than 0.1 μm [*Jayne et al.,* 2000; *Jimenez et al.*, 2003].

In addition to the aerosol payload, the Twin Otter was equipped with extensive navigational and meteorological instrumentation. Position was measured at 10 Hz using a NovAtel Differential GPS unit (NovAtel, Inc.). A Rosemount 5-hole flow angle sensor (Model 858) provided static and dynamic pressure, and pressure differentials; pressure altitude, true air speed (TAS), angle of attack, and mean wind velocity (three-dimensional) were calculated from these data. Total temperature was measured using a Rosemount Model E102AL probe, and a EdgeTech Model 137-C3 hygrometer provided the dew point temperature. Additional information on these instruments is available on the CIRPAS website (http://web.nps.navy.mil/~cirpas/).

3.2.2 Citation

The instrumentation onboard the Citation during CRYSTAL-FACE was designed to make detailed observations of cloud microphysics above the freezing level. For the current study, observations of cloud particle size and concentration are of particular interest. A Forward Scattering Spectrometer Probe (FSSP-100, manufactured by Particle Measurement Systems, Inc.) measured size distributions of droplet-sized particles. The FSSP has a nominal particle diameter range of 2-47 μm, based on a size calibration with liquid water droplets; the cloud particles sampled and presented here were almost certainly frozen. The reliability of the FSSP in measuring ice particles was discussed by *Gayet et al.* [1996], who concluded that the data are quantitatively reliable when the ice particles are primarily small and spherical. The FSSP can grossly overpredict the actual particle concentration when large ice particles are present [*Field et al.*, 2003]. In this study, data from the Cloud Particle Imager (CPI, manufactured by SPEC, Inc.) mounted on the wing of the Citation are used to qualitatively assess the shape, or habit, of the crystals in the cloud particle population.

Condensed water content is of significant interest for the analysis presented in later sections. A Rosemount icing probe (Model 871FA) gave no indication of liquid water on any of the cloud passes included in this study. This is not surprising given the air temperature (approximately -35

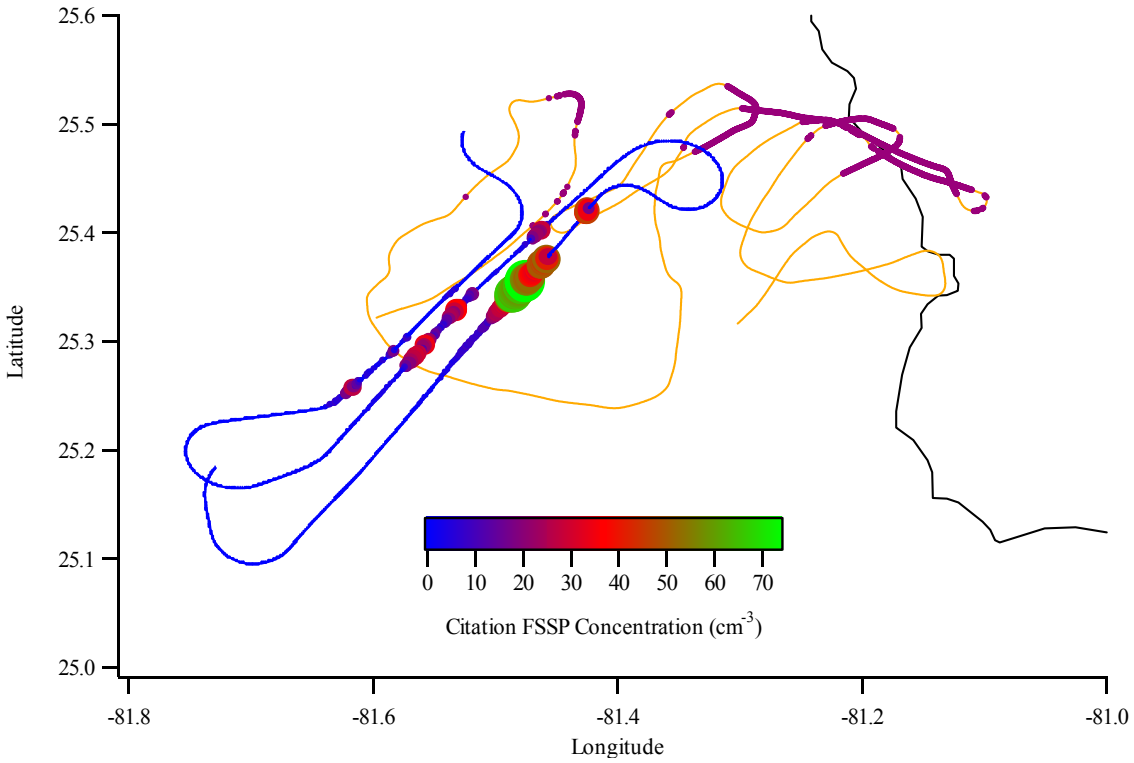

Figure 3.1: Flight tracks for the Twin Otter and Citation aircraft for a portion of their July 28 flights. The Twin Otter's track is orange, with dark red markings denoting locations where the aerosol concentration exceeded 3000 cm^{-3}. The Citation's track is blue, with larger and differently shaded markers indicating the cloud particle concentration as measured by the FSSP-100.

°C), and it is therefore assumed that the condensed water is entirely frozen. A Couterflow Virtual Impactor (CVI) separated particles larger than a controlled cut size (here, D_p > ~8 μm) from the rest of the sample volume; the particles were then evaporated and fed into a Lyman-α hygrometer, which measures water vapor concentration. The technique was described in detail by *Twohy et al.* [1997], who demonstrated that the condensed water content measured by this technique compares favorably with values derived from other instruments. The condensed water content measured by the CVI system is used in this analysis, with a value derived from the FSSP size distribution (assuming frozen spherical particles) included for comparison.

In addition to its microphysical instrumentation, the Citation was equipped with a suite of navigational and meteorological sensors to record position, altitude, pressure, temperature, frost point, and the three-dimensional wind field. This portion of the payload is described in detail on the aircraft's website (http://www.aero.und.edu/ats/citation.htm).

3.3 Boundary Layer Conditions

3.3.1 Observations

On July 28, both the Twin Otter and Citation aircraft sampled in the vicinity of a convective system just off the western coast of South Florida; the flight tracks of both aircraft are shown in Figure 3.1. The Twin Otter flew outside the cloud within the boundary layer for approximately 90 minutes (UTC 19:00-20:30) at an altitude of approximately 1000 m. During this period, atypically high aerosol number concentrations were observed in the same vicinity on several passes; the locations of these observations are indicated in the figure. As shown in Figure 3.2, the total particle concentration in these, as measured by the CPC, reached peaks exceeding 10000 cm^{-3}, more than an order of magnitude greater than the background concentration, which was less than 1000 cm^{-3}. There were four such periods of elevated concentrations during the 90 minutes of observation in the vicinity of the convective system; in each case the aerosol loading rapidly increased over a short distance (~0.5 km) and remained above background levels over 10-50 km. The time series data from the two CCN counters onboard the Twin Otter are also presented in Figure 3.2. Gaps in the data correspond to periods during which the instrument was being re-

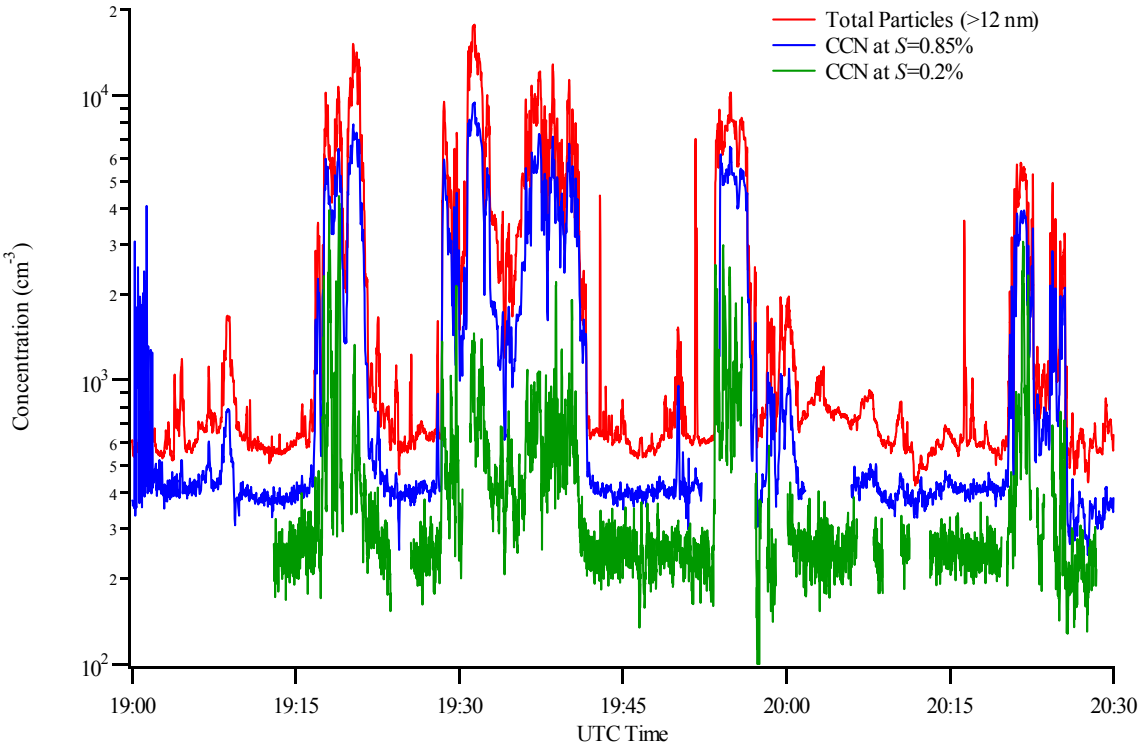

Figure 3.2: Time series for total particle concentration and CCN concentration at $S = 0.2\%$ and $S = 0.85\%$.

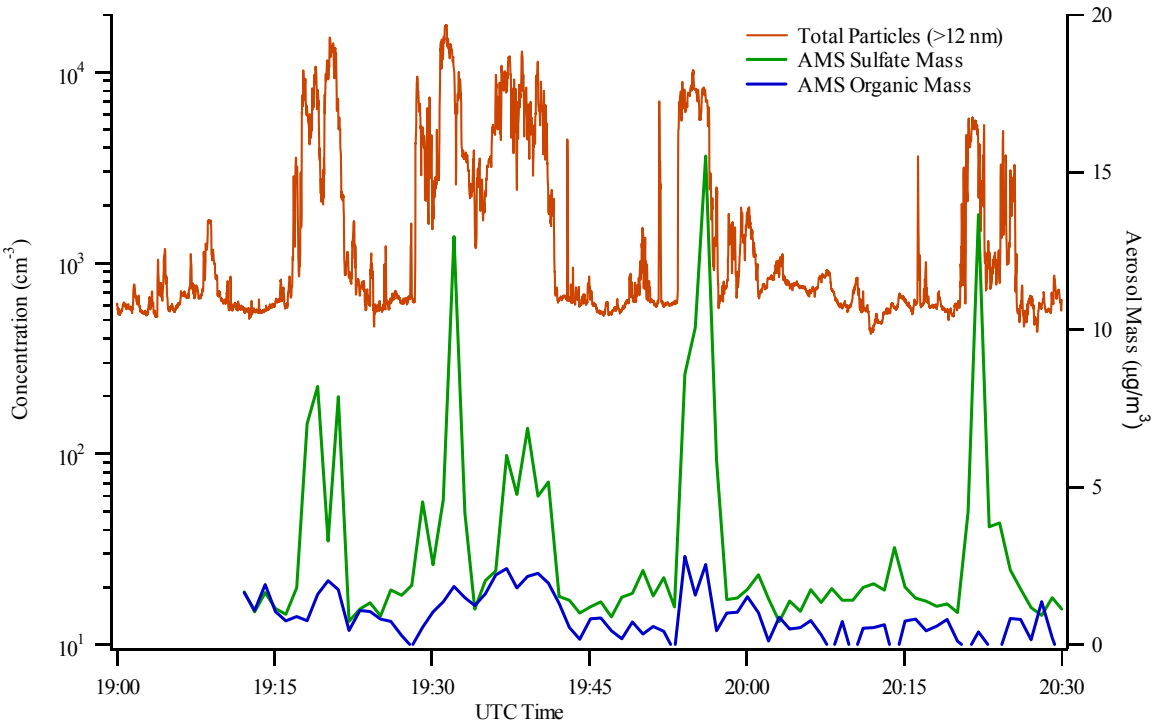

Figure 3.3: One-minute averages of aerosol sulfate and organic mass as measured by the AMS. The total particle concentration is again included for comparison.

saturated (for the S = 0.85% counter) or when the instrument was not operating within normal parameters (for the S = 0.2% counter). More than half of the particles measured in the regions of enhanced loading were active at S = 0.85%, while a much smaller fraction were active at S = 0.2%. This suggests that the particles were either too small or had insufficient soluble mass to activate at the lower supersaturation. Data from the Aerodyne Aerosol Mass Spectrometer (AMS) (Figure 3.3) indicate that even though the organic mass was enhanced in the regions of high particle concentrations, the aerosol was primarily sulfate. According to Köhler theory [*Seinfeld and Pandis*, 1998], the minimum dry diameters at which ammonium sulfate particles would activate for supersaturations of 0.2% and 0.85% are 79 nm and 32 nm, respectively. The dry aerosol size distributions from the DMA, shown in Figure 3.4, indicate that the majority of the particles in the regions of high aerosol number concentrations had diameters between 32 and 79 nm, which is consistent with activation at S = 0.85%, but not at S = 0.2%.

As indicated in Figure 3.1, each occurrence of elevated aerosol loading occurred while the Twin Otter was sampling along the northern side of the convective system, while air sampled at other locations around the base of the cloud remained at background aerosol levels. Thus the air converging into the convective cell was spatially inhomogeneous; in the boundary layer, the

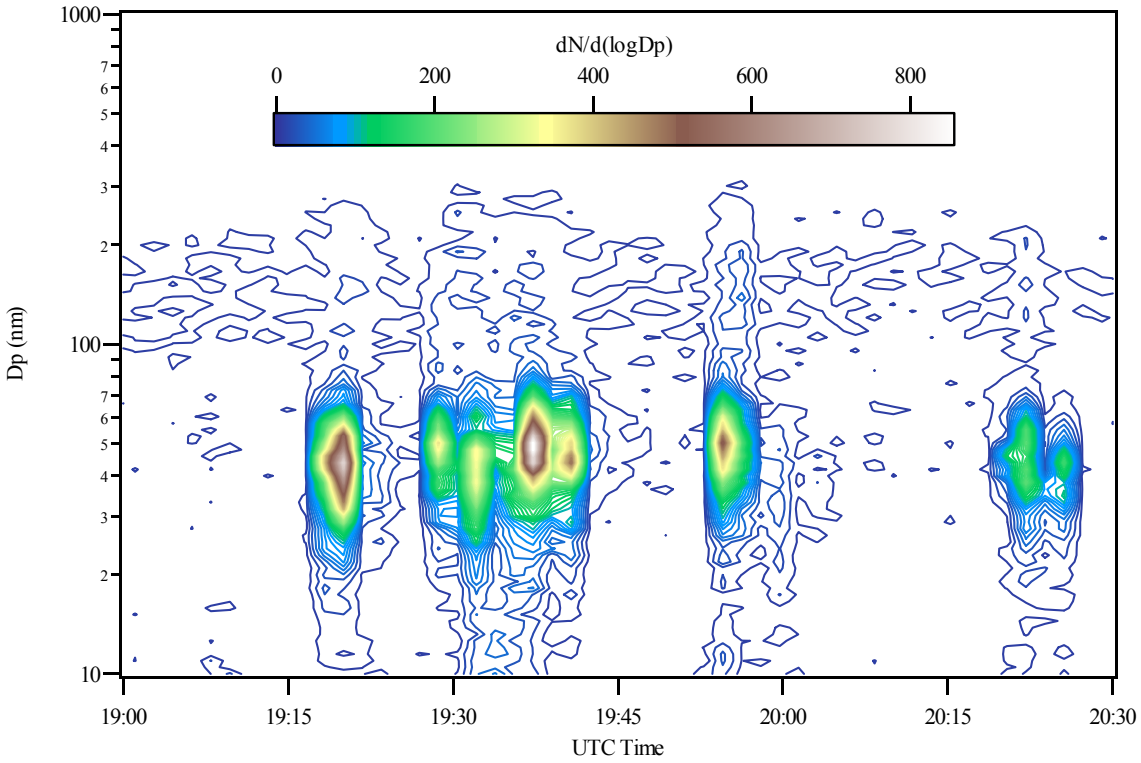

Figure 3.4: Time series contour plot of dry aerosol size spectra as measured by the DMA.

system was drawing in many more particles at its northern edge than elsewhere. The CCN counters on the Twin Otter confirm that these particles readily activated at supersaturations similar to those expected in strongly convective regions. The presence of highly enhanced CCN concentrations in one portion of the air mass at cloud base would presumably cause spatial inhomogeneities in the cloud droplet concentration inside the cloud at low levels. Unfortunately, the convective strength of the cloud made it impossible for the Twin Otter to pass through it to measure in situ microphysics.

3.3.2 Origin of Enhanced Aerosol Concentrations

There are several possible sources of the enhanced boundary layer particle concentrations near the convective system. An elevated layer of Saharan dust was predicted for the region on that day, and evidence of such a layer was seen by the Citation at higher altitudes (28 July 2002 Mission Report, http://cloud1.arc.nasa.gov/crystalface/mission_report/MissionRpt_020728.pdf). It was thought initially that this layer may have been the source of the particles observed by the Twin Otter. However, the concentrations were much higher than could be expected after long-range transport, and the large sulfate mass is incompatible with such a source [*Prospero,* 1999].

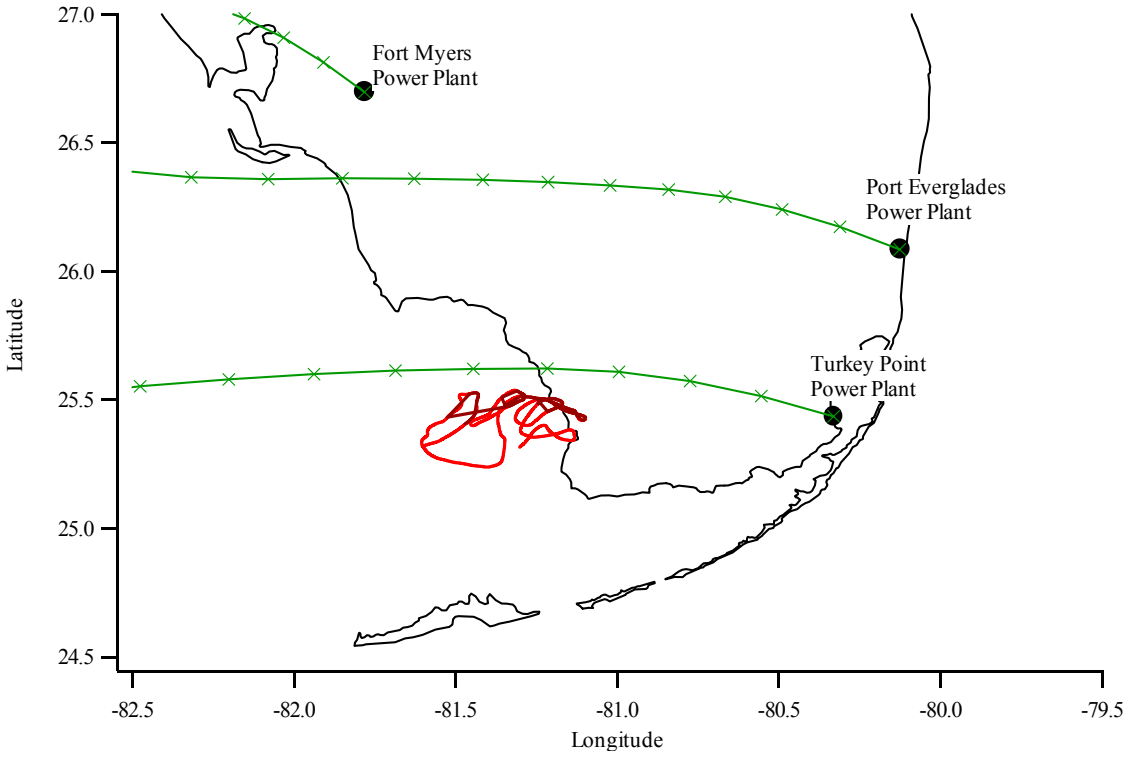

Figure 3.5: Simulated plume trajectories for three South Florida oil-burning power plants. The flight track of the Twin Otter is marked as in Figure 3.1. Note that the trajectory indicates the centerline of the plume; after five hours significant horizontal and vertical broadening would be expected.

Homogeneous bi-molecular nucleation of sulfuric acid and water was also considered as a potential particle source; however, earlier studies have indicated that such events occur generally in very clean air, where the available aerosol surface area is less than about 10 $\mu m^2 cm^{-3}$ [*Clarke et al., 1998*; *Clarke et al.,* 1999]. At no point did the aerosol surface area approach this low level, which is circumstantial evidence that the particle concentrations seen are not the result of recent new particle formation.

Since it is unlikely that the instances of elevated aerosol concentrations observed on July 28 were the result of either Saharan dust or recent nucleation, the only other reasonable source is from the ground. Figure 3.5 gives a broader view of the flight track of the Twin Otter, again highlighting the points where the aerosol concentration exceeded 3000 cm^{-3}. The measurements were made over Everglades National Park along the southwest coast of Florida, where there are no major anthropogenic sources. However, there are three major oil-burning power plants in the larger area (Fort Myers, Turkey Point, and Port Everglades), as well as the city of Miami itself. The sulfate levels were much higher than is typical for pollution from an urban center (cf. *Brock*

et al., [2003]), but were consistent with what might be emitted from the combustion of large amounts of unrefined fossil fuels. Data available online indicate that the three power plants emit large amounts of sulfate and other species; Table 3.1 provides 1999 emissions data for the three plants from the Aerometric Information Retrieval System (AIRS) database (available at http://www.epa.gov/air/data/) [*Environmental Protection Agency,* 1994]. Numerous studies have demonstrated that power plants of this size can produce aerosol plumes like those seen during the July 28 flight [*Brock et al.,* 2002; *Brock et al.,* 2003].

Table 3.1: Emissions from South Florida power plants from EPA AIRS database.

Plant Name	**Fort Myers**	**Turkey Point**	**Port Everglades**
Address	10650 SR 80 Fort Myers, FL 33905	9760 SW 344 St. Florida City, FL 33035	8100 Eisenhower Blvd. Fort Lauderdale, FL 33316
Latitude	26.6969°	25.4356°	26.0853°
Longitude	-81.7819°	-80.3308°	-80.1261°
VOCs (Mt/yr [a])	121.6	128.6	197
NO_x (Mt/yr)	12235.8	7196.4	10887
CO (Mt/yr)	448.3	821.6	951
SO_2 (Mt/yr)	29939.0	11559.7	19591
PM_{10} (Mt/yr)	100.4	59.1	123
$PM_{2.5}$ (Mt/yr)	90.4	54.4	114
NH_3 (Mt/yr)	70.9	68.2	107

[a] Mt = metric tons

Using the NOAA HYSPLIT model [*HYSPLIT4,* 1997], plume trajectories were calculated for the three power plants on July 28, approximately five hours prior to the time the elevated concentrations were observed (Figure 3.5). The simulated plume from the Turkey Point plant passed close to the Twin Otter's flight track about five hours after emission. The highly elevated sulfate mass concentrations measured during that period would be expected in a power plant plume, and is corroborated by the available emissions data. The dry particle sizes measured by the DMA are similar to those seen in the vicinity of Nashville, Tennessee by *Brock et al.* [2002] and near Houston, Texas by *Brock et al.* [2003]. Taken together, the available evidence points to the Turkey Point power plant as the probable source of these elevated concentrations.

Similar trajectory simulations for the other Twin Otter flights during CRYSTAL-FACE were also performed using HYSPLIT. During four additional flights (July 23, 26, and two flights on July 29) the results indicate that the Twin Otter may have encountered an air mass that had recently (within six hours) been influenced by emissions in the Miami area. During the latter three of these flights, particle concentrations exceeding 10000 cm^{-3} were observed near the point where the simulated trajectory crossed the flight track. This lends further support to the

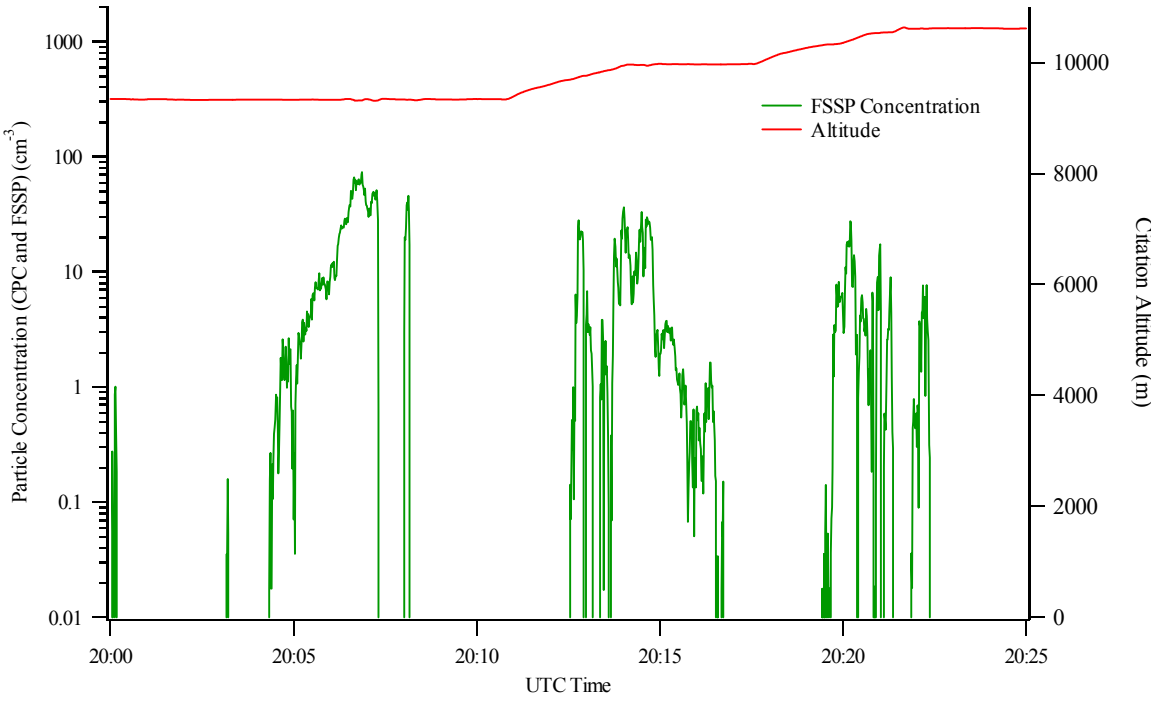

Figure 3.6: Altitude and cloud particle concentration as measured by the FSSP-100. The Citation was flying from southwest to northeast for the first and third passes through the cloud, and in the opposite direction during the second pass.

hypothesis that the power plants near Miami were, on occasion, a major source of elevated particle concentrations during CRYSTAL-FACE.

3.4 Upper-level Microphysics

3.4.1 Observations

During the same period that the Twin Otter was sampling the boundary layer in the vicinity of the convective system under consideration here (i.e., between UTC 20:00 and UTC 20:25), the Citation made three passes through the upper levels of the cloud. The first pass was a level leg at an altitude of 9300 m, while the aircraft was climbing during the latter two encounters: from 9600 to 10000 m during the second pass and from 10200 to 10600 m on the final pass. The aircraft's flight path during this period is presented in Figure 3.1; to denote the boundary of the cloud near its top, the markers for the Citation track are colored and sized to indicate the ice particle concentration as measured by the FSSP-100.

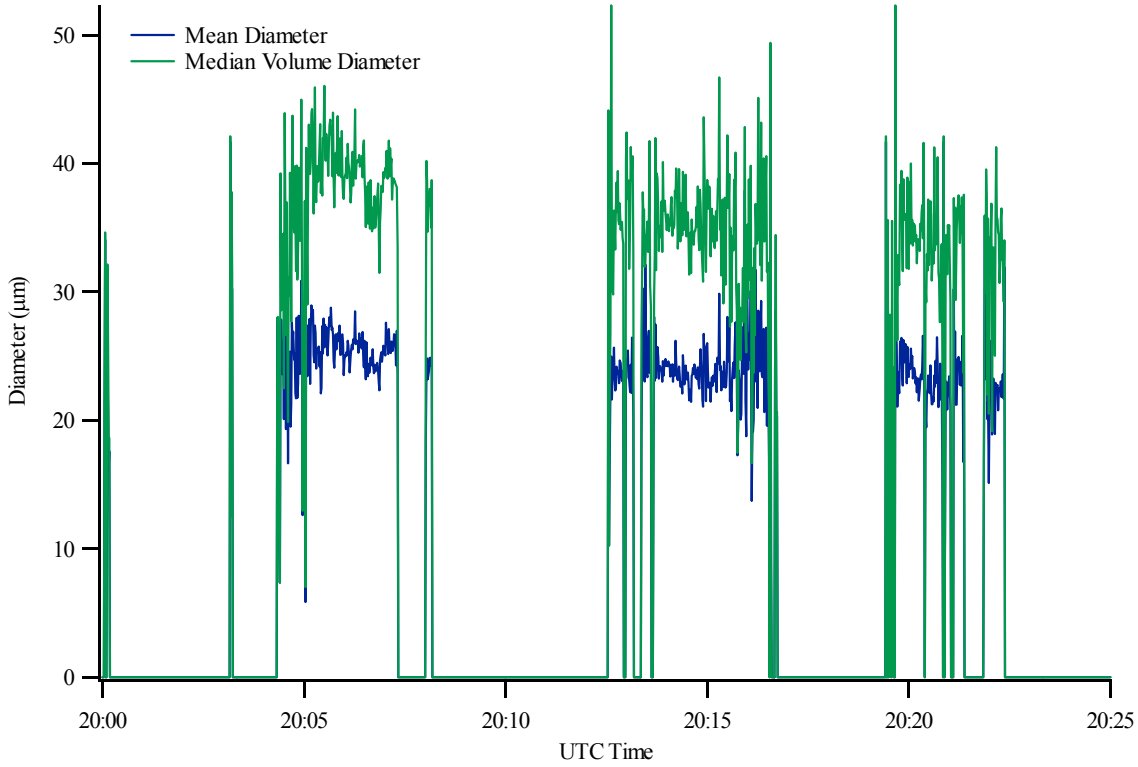

Figure 3.7: Mean and median volume cloud particle diameters derived from the FSSP-100 on the Citation.

In the upper levels of the cloud, there was a spatial distribution of cloud particle concentration; the trend was most obvious at the lowest altitude sampled by the Citation, where the highest concentrations were observed (i.e., the first pass through the cloud). As might be expected from the location of the enhanced aerosol concentrations in the boundary layer, Figure 3.1 indicates that the highest concentrations of cloud particles were seen on the northern side of the system. This trend can be seen more clearly in Figure 3.6; during the first and third passes (UTC 20:04-20:08 and UTC 20:19-20:22, respectively) the Citation flew from southwest to northeast, and in the opposite direction on the second pass (UTC 20:13-20:17). The spatial variation is most clearly seen in the first pass, and is also distinguishable in the second pass. In both cases, the particle concentration measured by the FSSP-100 is an order of magnitude greater on the northern end of the cloud than on the southern end. Such a trend was not observed during the third pass; however, that pass was at the highest altitude and the cloud appeared to be broken at that level.

The presence of the strong gradient in the upper levels of the cloud is quite interesting given the high spatial variability of aerosol concentrations found in the boundary layer. A qualitative

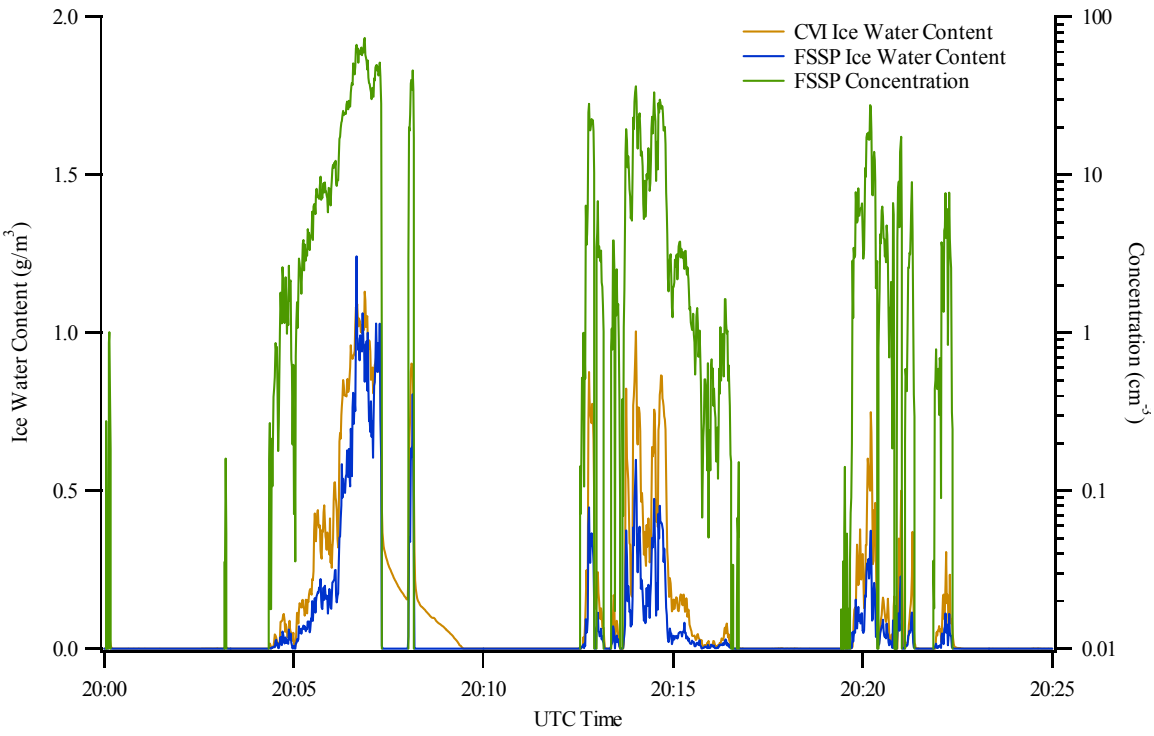

Figure 3.8: Ice water content as measured by the FSSP-100 and the CVI on the Citation. The total concentration as measured by the FSSP is included to denote the cloud boundary.

analysis of the habit of the crystals indicates that they are primarily frozen water droplets, presumably uplifted from lower levels (A. Heymsfield, personal communication). However, it is not immediately clear whether the variation at the top of the cloud is due to the inhomogeneity of the aerosol at cloud base or to other factors; for example, there is some evidence that the gradient in the ice particle concentration across the cloud is instead the result of entrainment. Figure 3.7 displays both the mean diameter and median volume diameter (i.e., the diameter which splits the total aerosol volume in half) derived from the FSSP-100 data for the three passes through the cloud. There is no strong spatial trend in the observations. If the observed gradient in concentration were due exclusively to a gradient in CCN concentrations at the base of the cloud, then the condensed water content would be expected to be constant. From that expected result it follows that the ice particles should be smaller where they are more numerous; this does not occur for the system examined here. Indeed, the condensed water content is not constant across the cloud; independent observations from the FSSP-100 and the CVI confirm that the peak condensed water content for each pass through the cloud collocated with the peak in ice particle concentration (Figure 3.8).

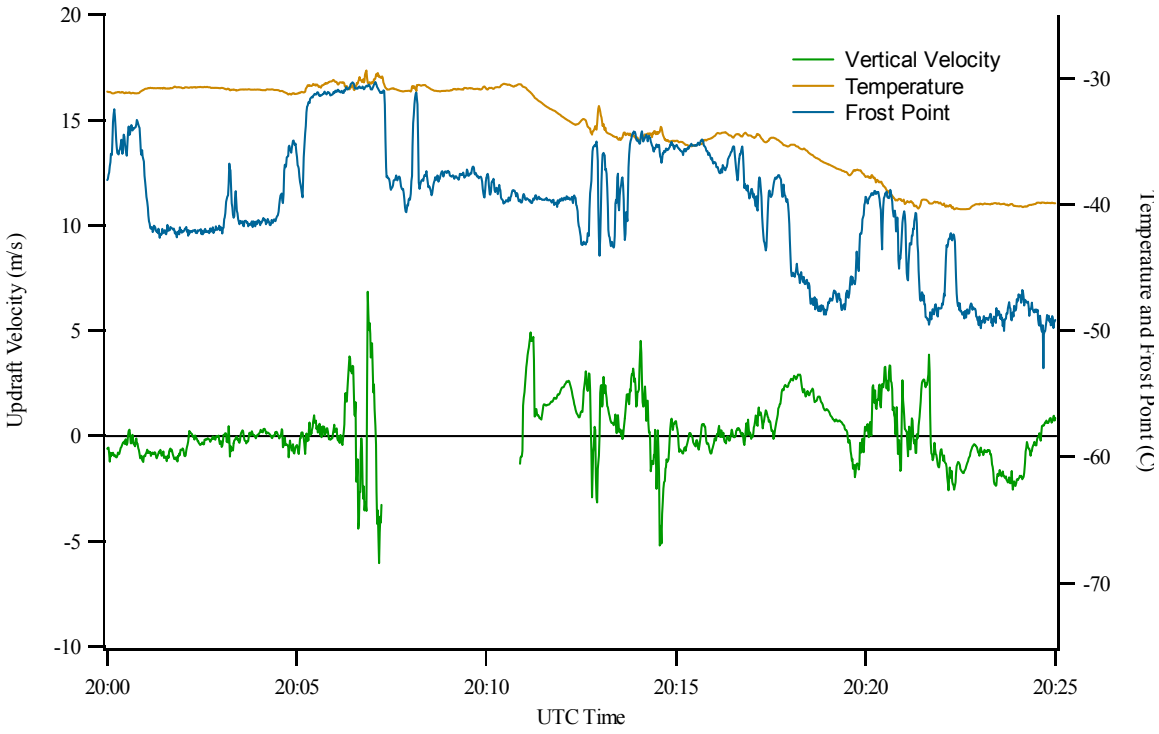

Figure 3.9: Vertical velocity, temperature, and frost point observations for the three passes through the convective system by the Citation.

One explanation for the relative homogeneity in ice particle size across the top of the cloud is that as the updraft weakens, it is diluted with air from outside the cloud. Such dilution would reduce the concentration of cloud particles, but may not immediately lead to particle evaporation. The peak updraft velocity does appear to be collocated with the peak in ice particle concentration (Figure 3.9), as would be expected if the particle concentration gradient were a result of dilution. However, there are reliability concerns with the wind data; a portion of the time series (from UTC 20:07 to 20:11) has been filtered from the data set, and *Stith et al.* [2002] noted that in a previous campaign frozen water in pressure sampling lines resulted in large errors in the measured wind. Furthermore, the frost point temperature observations (also in Figure 3.9) do not indicate significant dilution across the top of the cloud. If significant mixing was occurring, a spatial gradient in the difference between the temperature and the frost point temperature would be expected that roughly corresponded to the gradient in ice particle concentration, particularly since the particle size data does not show that evaporation is occurring. Instead, the temperature is very close to the frost point across most of the cloud, meaning that the cloud is near its saturation point with respect to ice.

The observations of the upper-level cloud microphysics from the Citation aircraft are difficult to interpret in the absence of in situ measurements of the cloud at lower levels. While a gradient in ice particle concentration is observed, there is not a strong gradient in particle size; the existence of a Twomey effect in mixed phase convective clouds is not supported by these data. However, it is not possible to determine why the effect is not observed without additional information. While no additional in situ data are available for this case, it may be possible to reconstruct the cloud to a greater degree using ground-based radar and computer simulations. These possibilities are discussed in the next section.

3.5 Future Work

There are several possible causse why the data from the cloud under consideration here were not consistent with the Twomey effect. Certainly one possibility is that the observed concentration gradient at the top of the cloud is not directly connected to the spatial variability in the boundary layer. In this scenario, any initial variability in the droplet population at cloud base would be mixed together as the air was lifted, and the cloud properties at the top of the updraft would be relatively uniform. Another possibility is that the spatial gradient at altitude is connected to the boundary layer variability, and that the lack of size variability at the top of the cloud is an indication that the Twomey effect is not sufficient for describing the relationship between CCN and cloud particles in mixed-phase convective systems. It is also possible that the variability observed in the aerosol properties around the base of the cloud is not representative of the air entering the cloud, in which case no variability would be expected at the top of the cloud.

In any case, the in situ observations from the Twin Otter and Citation are not enough to draw any conclusions. As part of the CRYSTAL-FACE campaign, a ground-based radar system was stationed near the location of the cloud. Data from this system can be used to reconstruct the cloud, and thereby determine the strength of convection and gain some insight as to the microphysical structure at lower altitudes. There are also simulations underway using the Regional Atmospheric Modeling System (RAMS); this model has be used extensively to simulate the development of convective systems, and will provide a basis for comparing the observed cloud properties and perhaps determining whether the variability in the boundary layer aerosol population could be expected to impact cloud properties in the manner observed by the Citation at the top of the cloud.

For this system, the available observations may not be sufficient to determine conclusively whether aerosol plumes in the boundary layer have a significant impact on the development of mixed-phase convective clouds. However, the possibility that they do makes this an important question worthy of further study. Aerosol plumes are common features over much of the United States [*Brock et al.*, 2002; *Brock et al.*, 2003], and could potentially impact regional climate in areas where convective cloud systems are common. Since it is not difficult to predict the location of these plumes, it should be possible to predict where convective systems may be collocated with aerosol plumes. In future field campaigns where airborne platforms are equipped to sample inside convective clouds, selecting clouds that are likely to be influenced by power plant or other industrial plumes would allow for a better understanding of the interrelationship between aerosols and clouds.

4 Design for a New Cloud Condensation Nuclei (CCN) Spectrometer

Note: This chapter has been submitted to *Aerosol Science and Technology*.

4.1 Abstract

The design of a new cloud condensation nucleus (CCN) spectrometer based on a modifications to the original design of *Fukuta and Saxena* [1979a] is presented. The key modifications include introducing a trapezoidal geometry and orienting the chamber vertically. A series of simulations demonstrate the broadening of the effective range of the instrument to include supersaturations lower than those reported for the original instrument, without reducing the maximum resolvable supersaturation. A design criterion is developed to eliminate configurations that would result in secondary flows in the growth chamber resulting from buoyancy effects. Using instrument configurations that satisfy this criterion, the effects of variations in the chamber geometry, the imposed temperature gradient, and the total volumetric flow are evaluated. A new configuration is identified that could produce real-time CCN spectra with an effective range including at least supersaturations between 0.07% and 1.2%,. Further improvements for the inlet and droplet detection regions of a new instrument are also discussed.

4.2 Introduction

In order to improve our understanding of the role of aerosols in cloud development and propagation, it is necessary to measure the cloud-forming ability of the aerosol population under a wide variety of conditions. Those particles that have the potential to form cloud droplets at water vapor supersaturations in the range of those typically encountered in clouds are denoted cloud condensation nuclei, or CCN. CCN are characterized by their critical supersaturation (S_c), the

supersaturation at which the particles can activate and form cloud droplets. Supersaturation, *S*, is defined as the amount by which the ratio of the water vapor pressure to the saturated vapor pressure exceeds unity. The critical supersaturation of a particle depends on its size and composition, and the cloud-forming potential of the aerosol population can be characterized by expressing the CCN concentration as a function of supersaturation.

In practice, CCN concentrations are typically measured by exposing an aerosol sample to a known saturation profile for a period sufficient for growth to droplet size, at which point the grown droplets can be readily detected using standard light scattering techniques. The supersaturation required to activate droplets is most commonly induced in an instrument by maintaining two parallel wet surfaces at different temperatures. The linear temperature and water vapor concentration profiles between the two surfaces lead to a supersaturation in water vapor between them, since the saturation water vapor pressure is a sub-linear function of temperature. Larger temperature differences lead to larger supersaturations, and the maximum supersaturation is approximately midway between the two surfaces. Several distinct designs employ this same basic concept [*Twomey*, 1963; *Sinnarwalla and Alofs*, 1973; *Fukuta and Saxena*, 1979a]; others employ a cylindrical geometry and take advantage of the different diffusion rates of heat and water vapor [*Chuang et al.*, 2000b; *Roberts and Nenes*, 2003]. Regardless of design, all aforementioned instruments are characterized by an important limitation: they can only measuring one supersaturation at a time. To produce CCN spectra with a time resolution sufficient for airborne measurements, an instrument should employ continuous flow, and should be able to make measurements at multiple supersaturations simultaneously. While single supersaturation CCN counters are frequently used for field measurements [*Chuang et al.*, 2000a; *Snider and Brenguier*, 2000; *VanReken et al.*, 2003] and can provide valuable information regarding the activation properties of the aerosol population, they do not unambiguously characterize the CCN spectrum on a timescale appropriate for airborne measurements.

There are instruments capable of measuring the activation properties of an aerosol sample simultaneously over a broad range of supersaturations. One such instrument that has been widely used for airborne measurements is the CCN spectrometer developed by *Hudson* [1989]. This instrument exposes the aerosol sample to a supersaturation that increases in the direction of flow. CCN with different critical supersaturations activate at different points along their streamline, and thus have different growth times. The CCN spectrum is inferred from the size distribution of the droplets at the outlet of the instrument. The relationship between particle critical supersaturation

and outlet diameter is derived from calibrations using particles of known size and composition; implicit in the calculation of the CCN spectrum is the assumption that particles with the same critical supersaturation will always grow at the same rate. This assumption does not always hold for particle compositions different from that of the calibration aerosol; studies have shown that organic compounds can affect both the equilibrium droplet diameter [*Shulman et al.*, 1996; *Facchini et al.*, 1999] and the rate at which the droplets grow to their equilibrium size [*Feingold and Chuang*, 2002; *Chuang*, 2003]. When there is a significant organic component to the atmospheric aerosol, reliable CCN data would be quite valuable, since the importance of organic species in cloud processes is largely uncertain. In such a situation, an inferred CCN spectrum based on calibration with a salt aerosol may lead to an inaccurate result.

Fukuta and Saxena [1979a, 1979b] developed an instrument that is able to measure the activation properties of an aerosol population without relying on the final size of the resultant droplet. Instead of exposing the entire sample to an identical saturation profile, this instrument, denoted hereafter as the Fukuta-Saxena CCN Spectrometer (FSCS), imposes a transverse saturation gradient in the growth chamber, so that different streamlines are exposed to different supersaturation profiles. The principle is described in detail by *Fukuta and Saxena* [1979b]. Additional insight was provided by later simulations of the instrument [*Nenes et al.*, 2001a]. In the FSCS, both the top and bottom plates of the growth chamber have an imposed temperature gradient perpendicular to the direction of flow, so that the temperature difference between the plates (and, therefore, the supersaturation) is greater at one side of the rectangular chamber than at the other. The gradient is maintained by controlling the temperature of both the top and bottom plates at one end of the growth chamber (Figure 4.1a); the side wall at the temperature controlled end is made of a material with low thermal conductivity, while the opposite side wall and both plates are constructed of a highly conductive material. Heat therefore flows from the high temperature edge through the conductive material to the low temperature edge. The activated droplets exiting the growth chamber on different streamlines are counted separately, so that the supersaturation at which a droplet activated is determined by its position on the transverse axis and not by its outlet size.

The utility of the FSCS is somewhat limited by a relatively small dynamic range. *Fukuta and Saxena* [1979a] gave the range as $0.15 < S < 1.2\%$; data presented in later studies [*DeFelice and Saxena*, 1994; *Saxena*, 1996] all fall within those limits. *DeFelice and Saxena* [1994] stated that higher or lower supersaturations could be attained by adjusting the temperatures of the saturated

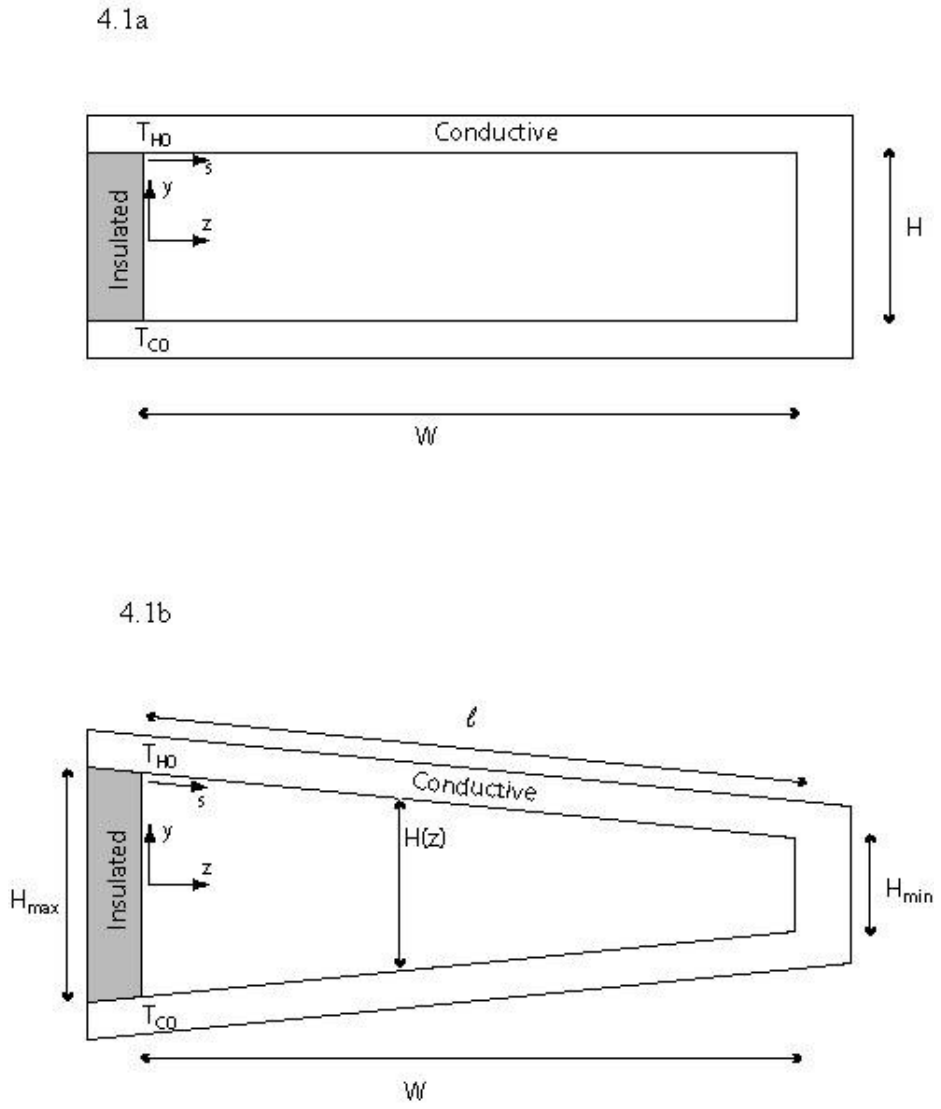

Figure 4.1: Schematics of cross sections for (a) the rectangular geometry of the original FSCS and the Baseline design; and (b) the proposed trapezoidal geometry. In both cases, heat travels from T_{H0} to T_{C0} through the conductive material along the coordinate *s*.

plates; a reduction in the lower bound would be a significant improvement, since clouds with maximum supersaturations less 0.1% are thought to be common and climatically important [*Pruppacher and Klett*, 1996]. This sensitivity arises mostly under continental and polluted conditions, where large number of CCN lead to clouds with low supersaturation [*Nenes et al.*, 2001b]. Under these conditions, only those CCN with low critical supersaturations will activate; thus resolving the CCN spectrum for values under 0.1% becomes essential. *Roberts et al.* [2003]

found that when biomass burning is occurring in the Amazon Basis, cloud properties were strongly influenced by the portion of the CCN spectrum below S = 0.1%. Unfortunately, detecting those CCN active at such low supersaturations is very difficult due to the long growth times required to reach detectable droplet sizes.

Nenes et al. [2001a] developed a model to simulate the FSCS and determine the theoretical limitations to its dynamic range. They concluded that the instrument could not resolve the CCN spectrum when S < ~0.1%, due to insufficient growth times. Increasing the growth time (either by lengthening the growth region or reducing the flow rate) did not improve performance, since growing droplets will tend to gravitationally settle out of the region of maximum supersaturation, further reducing the growth rate and causing particle losses. A vertical orientation for the growth chamber, where the flow is downward (in the direction of gravity), was simulated as an alternative and found to be generally more effective, since the problem of gravitational settling is eliminated. However, operating the FSCS vertically introduces a new complication, that of buoyancy-induced secondary flows. If the imposed temperature difference between the two plates is too large, the variations in air density cause flow reversals along some streamlines. In the end, *Nenes et al.* [2001a] concluded that orienting the growth chamber vertically would match, but not significantly improve upon, the empirically demonstrated performance of the instrument.

Although the simulations conducted by *Nenes et al.* [2001a] indicate that the accessible supersaturation range of the original FSCS design could not be improved by orienting the growth chamber vertically, their results suggest potential mechanisms by which the minimum resolvable supersaturation might be reduced. For particles of low critical supersaturation, the rate of droplet growth is effectively proportional to the supersaturation [*Seinfeld and Pandis*, 1998], so much more time is required to separate activated droplets from other particles at low supersaturations. In a vertical orientation, the minimum resolvable supersaturation could be decreased by increasing the residence time for those streamlines, either by reducing the flow velocity or by lengthening the column. Gravitational settling would no longer pose a significant problem because the settling would be in the direction of flow and would therefore not change the supersaturation to which the CCN are exposed. In any event, the settling velocity would be much smaller than the flow velocity. However, the flow velocities along the high supersaturation streamlines must be large enough that buoyancy-induced flow reversals do not significantly impact the flow of the aerosol sample through the growth chamber. The dynamic range of the

FSCS could be significantly increased if the flow velocity for the low supersaturation streamlines could be reduced without reducing the velocity significantly on the high supersaturation streamlines.

The current work details a means of doing this through the design of a new CCN spectrometer. By redesigning the geometry of the FSCS growth chamber, a transverse gradient in the flow velocities of streamlines can be achieved, so that streamlines exposed to low supersaturations have significantly longer residence times than more highly supersaturated streamlines. A trapezoidal geometry is chosen here (Figure 4.1b), but other more complex geometries can have similar effects, potentially with even more dynamic range. The design of the growth chamber depends largely on three parameters: the shape of the chamber, the imposed temperature gradient, and the volumetric flow rate through the instrument. The simulations in this work use a model similar to that used by *Nenes et al.* [2001a] to examine how varying these parameters affects supersaturation profiles and particle growth in the instrument. The modifications to the model necessary to simulate the alternate geometries will be discussed, and the potential impact of buoyancy forces will be evaluated. Each design parameter will then be varied independently to determine its relative importance. By optimizing these parameters, a growth chamber can be designed to resolve droplets at supersaturations significantly lower than is possible using the FSCS, with little variation in performance based on the composition of the sample aerosol. The instrument design is augmented by outlining a novel droplet detector that would allow the particles on all streamlines to be detected simultaneously, increasing the time resolution of the spectra produced. If these design modifications are implemented in the future, along with technological improvements to reduce the size and weight, the new CCN spectrometer would be able to produce activation data over the entire range of interest rapidly enough for airborne measurements without being sensitive to the variations in droplet growth rate introduced by variations in chemical composition.

4.3 Instrument Model

To evaluate the performance of several existing CCN instrument designs (including the FSCS), *Nenes et al.* [2001a] developed a model that determines the theoretical temperature, water vapor, and supersaturation distributions as a function of position. These distributions were then used to calculate particle growth and. activation In the case of the FSCS, the authors chose to treat the growth chamber as a series of two-dimensional flow fields where each streamline is

treated as flow between two infinite plates; any perturbations to the velocity field arising from the proximity of the side walls is neglected. This approach is based on scaling arguments [*Nenes et al.*, 2001a] and is consistent with experimental data reported by *Fukuta and Saxena* [1979a]; the simulations are valid if the distance from the chamber side walls for the chosen streamlines for the simulations is not significantly less than the distance between the hot and cold plates. This work uses the numerical model developed by *Nenes et al.* [2001a] to examine the effects of replacing the rectangular shape of the FSCS with a trapezoidal geometry (Figure 4.1b). The specifics of the model formulation are discussed at length in the earlier work, and will not be repeated here.

Some minor modifications to the model developed by *Nenes et al.* [2001a] are required to accommodate a trapezoidal geometry. In the original formulation used to simulate the FSCS, the temperature of the hot and cold plates varied based on the chosen value of the z coordinate (Figure 4.1a), but the distance between the plates and the initial velocity profile did not. For a trapezoidal geometry (Figure 4.1b), both the distance between plates and the velocity profile at the inlet become a function of the z position, and the dependence on z of the temperatures of the hot and cold plates changes. The ensuing analysis is presented to show how the velocity field is affected by the choice of geometry.

The distance between the plates is a linear function of z:

$$H(z) = H_{\max} - \frac{(H_{\max} - H_{\min})}{W} z \,. \qquad [4.1]$$

For this study, the inlet velocity profile is assumed always to be parabolic, and the flow direction is downward, in the direction of the gravitational force. The velocity (u) profile at a given z position depends on the distance between the plates and the pressure drop (ΔP) across the length (L) of the column, as well as the air viscosity (μ):

$$u(y,z) = \frac{\Delta P\left(H(z)\right)^2}{8L\mu}\left[1 - \left(\frac{2y}{H(z)}\right)^2\right]. \qquad [4.2]$$

The volumetric flow (Q) is actually a more convenient design parameter than the pressure drop across the growth chamber. The relationship between the velocity and the volumetric flow rate is

$$Q = \int_0^W u_{avg}(z) H(z) dz \,. \qquad [4.3]$$

As for the case of flow between parallel plates, the average velocity (u_{avg}) for a given z position is equal to two-thirds of maximum velocity (u_{max}) for that position. Therefore,

$$Q = \int_0^W \frac{\Delta P (H(z))^3}{12 L \mu} dz \,. \qquad [4.4]$$

Evaluating the integral and rearranging terms yields

$$\frac{\Delta P}{8 L \mu} = \frac{6Q}{W (H^*)^3} \,, \qquad [4.5]$$

where

$$(H^*)^3 = \mathrm{H}_{\max}^3 + H_{\max}^2 H_{\min} + H_{\max} H_{\min}^2 + H_{\min}^3 \,. \qquad [4.6]$$

The inlet velocity distribution is then

$$u(y,z) = \frac{6Q}{W (H^*)^3} (H(z))^2 \left[1 - \left(\frac{2y}{H(z)} \right)^2 \right]. \qquad [4.7]$$

Note that, for a fixed ΔP, the velocity is greater where $H(z)$ is greater. Since the goal in modifying the geometry is to allow longer residence times for streamlines exposed to lower supersaturations, the greatest temperature difference between the plates should occur where the distance between plates is largest. The temperatures of the hot and cold plates (T_H and T_C respectively) are determined here by defining a coordinate s that runs along the conductive wall from the hot tip to the cold tip:

$$T_H(z) = T_{H0} - \left(\frac{dT}{ds} \right) \left(\frac{\ell}{W} \right) (W - z) \;;\; T_C(z) = T_{C0} + \left(\frac{dT}{ds} \right) \left(\frac{\ell}{W} \right) (W - z) \,, \qquad [4.8]$$

where

$$\frac{dT}{ds} = \frac{T_{H0} - T_{C0}}{2\ell + H_{\min}} \qquad [4.9]$$

and

$$\ell = \sqrt{W^2 + \left(\frac{H_{\max} - H_{\min}}{2} \right)^2} \,. \qquad [4.10]$$

All of these initial conditions are calculated at the start of a simulation; once the simulation begins, the calculations are performed just as described by *Nenes et al.* [2001a].

4.4 Effect of Buoyancy Forces

When a chamber with a temperature difference between two plates is oriented vertically, so that the flow moves downward in the direction of the gravitational force, there exists a buoyancy force that acts to perturb the expected laminar parabolic flow profile. The perturbation is strongest where the temperature difference between opposite plates is greatest (i.e., for low values of z), and can be large enough for the flow to reverse direction near the warm plate. Such a reversal in fact occurs when the chamber design of the original FSCS is oriented vertically (Figure 4.2). The velocity profiles shown are at a point midway down the length of the growth chamber, after the equilibrium velocity field is established. The occurrence of flow reversal within the growth chamber might not appear significant when examining simulation results, but as a practical matter would complicate instrument design; recirculation of activated droplets would be likely, and flow oscillations or significant flow across the width of the chamber might also occur.

It is important to establish the conditions under which a proposed growth chamber design is

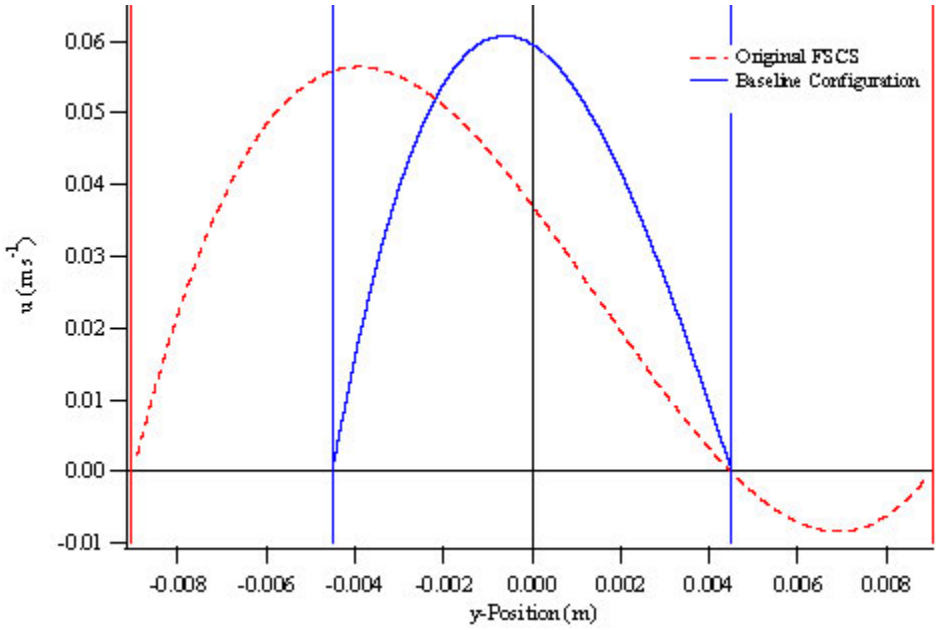

Figure 4.2: Equilibrium velocity profiles near the high supersaturation end of the growth chamber for the original FSCS configuration and this study's Baseline configuration. The FSCS profile is taken at z =0.015 m, and the Baseline profile is from z =0.010 m. The centerline of each chamber is located at y = 0.000 m, and dotted lines represent the hot and cold plates. Negative velocities in the original FSCS profile indicate flow reversal occurs for the conditions simulated.

not susceptible to flow reversals. A design criterion can be derived to determine whether for a set of design parameters the possibility exists for a negative value of u at any location in the chamber. Following *Bird et al.*[1960], and employing the Boussinesq approximation, the velocity field at a given value of z between infinite vertical plates of temperature difference ΔT is

$$u(\eta, z) = \frac{g\rho\Delta T}{48T\mu}(H(z))^2\left[\eta^3 - A\eta^2 - \eta + A\right], \qquad [4.11]$$

where $\eta = (2y/H(z))$ and A is an undetermined constant. For the purpose of deriving a design criterion, the density, ρ, and the viscosity, μ, can be treated as constant. The terms on the right side of the equation outside the brackets can be grouped and denoted Γ. To determine the value of A, we integrate the velocity over all values of η:

$$u_{avg}(z) = \int_{-1}^{1} u(\eta, z)d\eta, \qquad [4.12]$$

Which results in

$$A = \frac{3u_{avg}(z)}{4\Gamma}. \qquad [4.13]$$

Substituting this result into equation [4.11] and rearranging terms:

$$u(\eta, z) = \left[\frac{3}{4}u_{avg}(z) - \Gamma\eta\right]\left(1 - \eta^2\right). \qquad [4.14]$$

Since the range of possible values for η is between -1 and 1 (inclusive), for the velocity to be less than zero (indicating flow reversal), the first bracketed term on the right side of the equation must be less than zero. Therefore, flow reversal will not occur if

$$\frac{4\Gamma}{3u_{avg}(z)} < 1. \qquad [4.15]$$

Equation [4.15] assumes that $\eta = 1$; this gives the largest possible value to the numerator, making the design criterion as conservative as possible. Substituting for Γ and $u_{avg}(z)$ (which is two-thirds of $u_{max}(z)$ from equation [4.7]) yields the buoyancy criterion, B, in a form more convenient for design purposes:

$$B = \frac{1}{144}\frac{g\rho}{\mu}\frac{(\Delta T)}{T}\frac{WH^*}{Q} < 1. \qquad [4.16]$$

Equation [4.16] is the desired design criterion that should be satisfied to ensure that flow reversal would not occur in a proposed instrument configuration. Calculating B for the original FSCS configuration confirms that flow reversal would be expected (Table 4.1). Likewise, if a set

of instrument parameters is selected so that the design criterion is satisfied (the "Baseline Configuration" in Table 4.1), then flow reversal does not occur (Figure 4.2). There exist some configurations where $B > 1$ that still would not result in a flow reversal, but this study will only consider configurations where the criterion is satisfied.

Table 4.1: Operating Conditions and Parameters for the Original FSCS Design [*Fukuta and Saxena*, 1979a] and the Baseline Design.

Parameter	Original FSCS	Baseline
Length of chamber from inlet to exit, m	0.838	0.838
Width (W) of chamber, m	0.191	0.070
Height (H) of chamber, m	0.018	0.018
Distance at which walls become saturated, m	0.168	0.168
Inlet Pressure, Pa	1.013×10^5	1.013×10^5
Inlet Relative Humidity, %	100	100
Inlet Temperature, K	283	283
Hot Tip Temperature, K	288	288
Cold Tip Temperature, K	283	283
Volumetric Flow Rate, $m^3\ s^{-1}$	8.5×10^{-5}	3.5×10^{-5}
Design Criterion, B	4.48	0.70

4.5 Instrument Design Simulations

The primary motivation for exploring alternative designs for a transverse gradient CCN spectrometer is the need for accurate measurements at supersaturations below 0.1%. Several instrument parameters affect the resolvable supersaturation range; this study will explore the sensitivity of the lower end of the range to changes in the geometry of the growth chamber, the imposed temperature gradient, and the flow rate through the chamber. To provide a reasonable

baseline against which to compare the effects of parameter variations, the performance of the original FSCS design and a smaller chamber with the same geometry are also simulated using the reformulated instrument model.

4.5.1 Baseline Simulations

Nenes et al. [2001a] included instrument simulations of the FSCS in their study of the theoretical properties of various CCN instrument designs, but the volumetric flow rate considered results in higher velocities than reported by *Fukuta and Saxena* [1979a]. To verify the predictive ability of the new model, the original FSCS is again simulated in this study, even though the configuration does not satisfy the design criterion and leads to a reversed flow near the warm plate (Figure 4.2). Also simulated is a theoretical instrument with the same (rectangular) geometry as the FSCS, but with approximately a 60% reduction in width, a 50% decrease in the plate separation, and a 70% reduction in the volumetric flow rate. Reducing the width of the chamber would make the instrument significantly lighter (an important factor in the design of airborne instrumentation), with little change in instrument performance; the values for H and Q were chosen such that the baseline configuration would be similar in performance to the original FSCS while satisfying the buoyancy criterion. The instrument parameters and operating conditions for these simulations are detailed in Table 4.1.

The new baseline configuration results in a reduction in the maximum resolvable supersaturation, but the minimum resolvable supersaturation is not significantly different in the two cases. Supersaturation profiles for the original FSCS design (Figure 4.3a) and for this study's baseline design (Figure 4.4a) show how the equilibrium supersaturation profile depends on the cross-gradient position within the growth chamber. In both figures, each curve represents the centerline supersaturation for a different value of z. Each curve increases to its equilibrium supersaturation from a minimum (not shown in the figures) near the point where the imposed wetted surfaces at the warm and cold plates begin. As expected, the largest supersaturations occur at the lowest values of z, where the difference in temperature between the hot and cold plates is largest; the maximum supersaturation is approximately 1% for the original FSCS configuration, and ~0.8% for the baseline. The saturation profiles also indicate what fraction of the total length of the growth chamber is available for particle growth. In each of these cases, the profiles for low values of z approach their equilibrium values sooner than those profiles at the lower-supersaturation end of the chamber. This results limits the time available for droplet growth for those streamlines where S is lower.

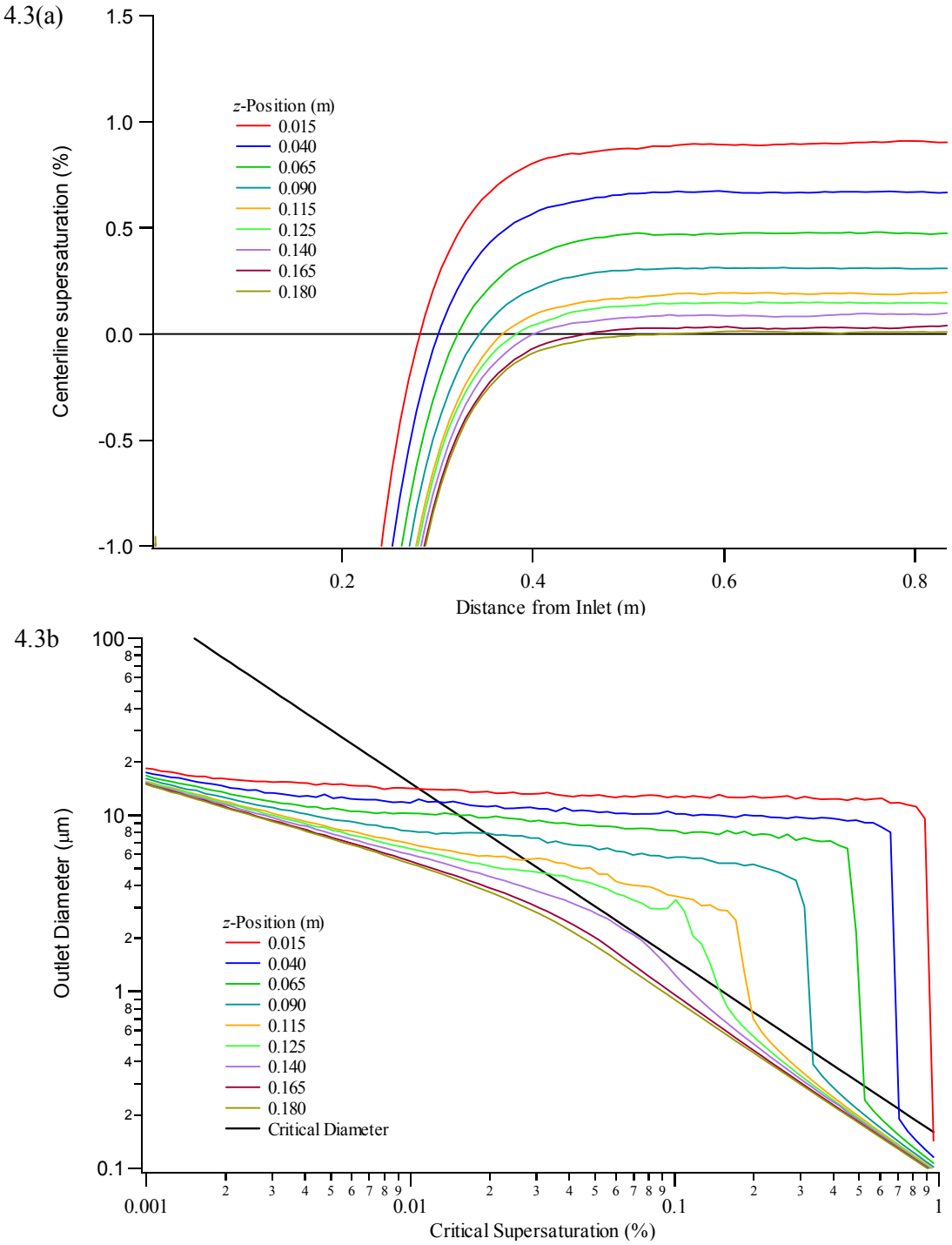

Figure 4.3: Simulation results for the original FSCS design (Figure 4.1a). (a) Centerline supersaturation profiles for several values of z; and (b) particle growth curves for those streamlines. These results are for an ammonium sulfate aerosol with an assumed accommodation coefficient of 1.0.

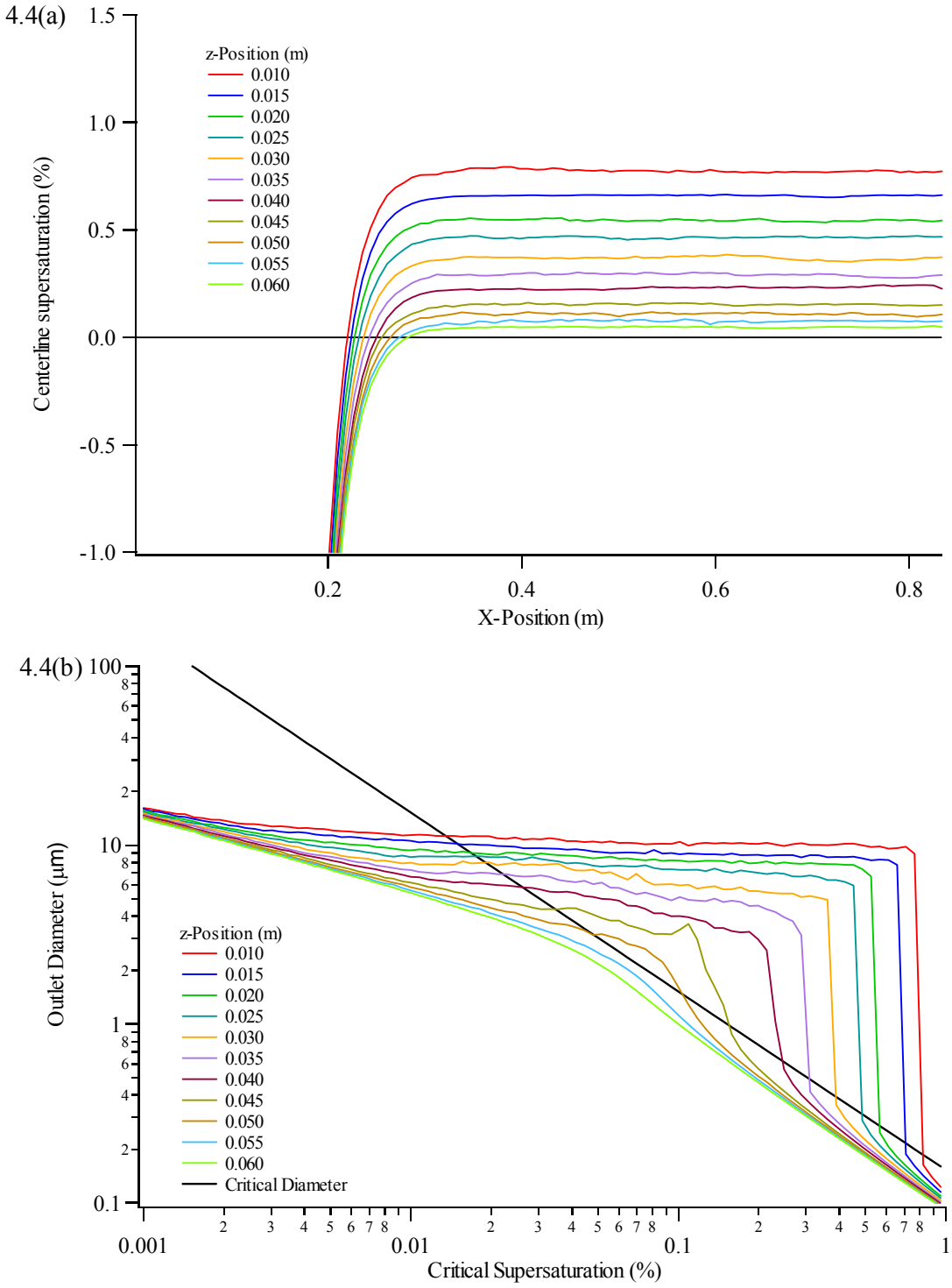

Figure 4.4: As in Figure 4.3, but for the Baseline instrument design.

The effect of the limited growth times at low supersaturations can be seen in the particle growth curves (Figures 4.3b and 4.4b for the original FSCS and baseline designs, respectively).

The curves display the outlet droplet diameter as a function of the critical supersaturation of the dry particles entering the instrument. As before, each curve represents the performance on the centerline for the given value of z. The critical supersaturation of a particle is a function of its size and composition (as described by Köhler theory [*Seinfeld and Pandis*, 1998]); these simulations assume a pure ammonium sulfate composition, and that the water accommodation coefficient (α) is 1.0. The solid black line in each figure represents the critical diameter, which is the size of the droplet when it has reached its critical supersaturation. If the outlet diameter at a given supersaturation is greater than the critical diameter at that point, then those particles have activated. The "sharpness" of the elbow in the individual growth curves is an indication of effectiveness of the instrument in separating the activated droplets from the rest of the sample.

For the original FSCS design (Figure 4.3b) and this study's baseline configuration (Figure 4.4b), those streamlines with equilibrium supersaturations greater than about 0.2% indicate a sharp size differentiation between the particles that activate and those that do not. As the value of z increases and the equilibrium supersaturation decreases, the difference in outlet diameter between activated and unactivated particles diminishes. When the z-value is such that the particles are exposed to a supersaturation of about 0.1% or less (i.e., $z > 0.125$ m for the original design and $z > 0.045$ m for the baseline case), the elbow in the growth curve is not sufficiently distinct to reliably separate the activated particles from unactivated ones; this sets a lower limit on the instrument's resolution. Thus the simulation results indicate for original FSCS configuration, the resolvable supersaturation range is from ~0.1 - 1%; this is in general agreement with the performance of the actual instrument [*Fukuta and Saxena*, 1979a]. In the baseline configuration, the upper end of the resolvable range is somewhat reduced, to ~0.8%.

4.5.2 Variations in Growth Chamber Geometry

As noted earlier, the lower limit to the resolvable supersaturation range is a result of there being insufficient time for the particles on streamlines with low supersaturations to grow to droplet size; the residence time for growth along these streamlines could be increased by implementing a trapezoidal geometry. A series of simulations, where the difference in plate spacing on opposite ends of the growth chamber ($\Delta H = H_{max} - H_{min}$) is gradually increased, show how an alternative geometry can improve the resolvable range. For these simulations, H_{min} is reduced by the same amount that H_{max} is increased from the baseline height (e.g., when ΔH is 0.008 m, H_{max} is set to 0.013 m and H_{min} to 0.005 m); this ensures that the cross-sectional area of the growth chamber remains unchanged.

The centerline velocity variations for these simulations are presented in Figure 4.5. Taken at a point after the flow field is well established, the data clearly show the effect of the trapezoidal geometry on the velocity profiles. The rectangular geometry (where ΔH is zero) produces no velocity gradient across the width of the chamber; the centerline velocity for this geometry is near 0.060 m s^{-1} for all values of z where wall effects can be ignored. As ΔH is increased, and the geometry becomes "more" trapezoidal, the gradient in the centerline velocity across the width of the chamber becomes greater. When the height difference is 0.010 m, the largest considered in this study, the velocity at the low supersaturation end of the column is more than five times smaller than at the opposite end (0.017 m s^{-1} versus 0.089 m s^{-1}). This gives the particles exposed to lower supersaturations the longer residence time required for droplet growth. Compared to the baseline configuration, there is a fourfold increase in the time available for droplet growth when ΔH = 0.010 m for the streamlines exposed to lowest supersaturations.

The effects of modifying the chamber geometry can be seen in the growth curves in Figure

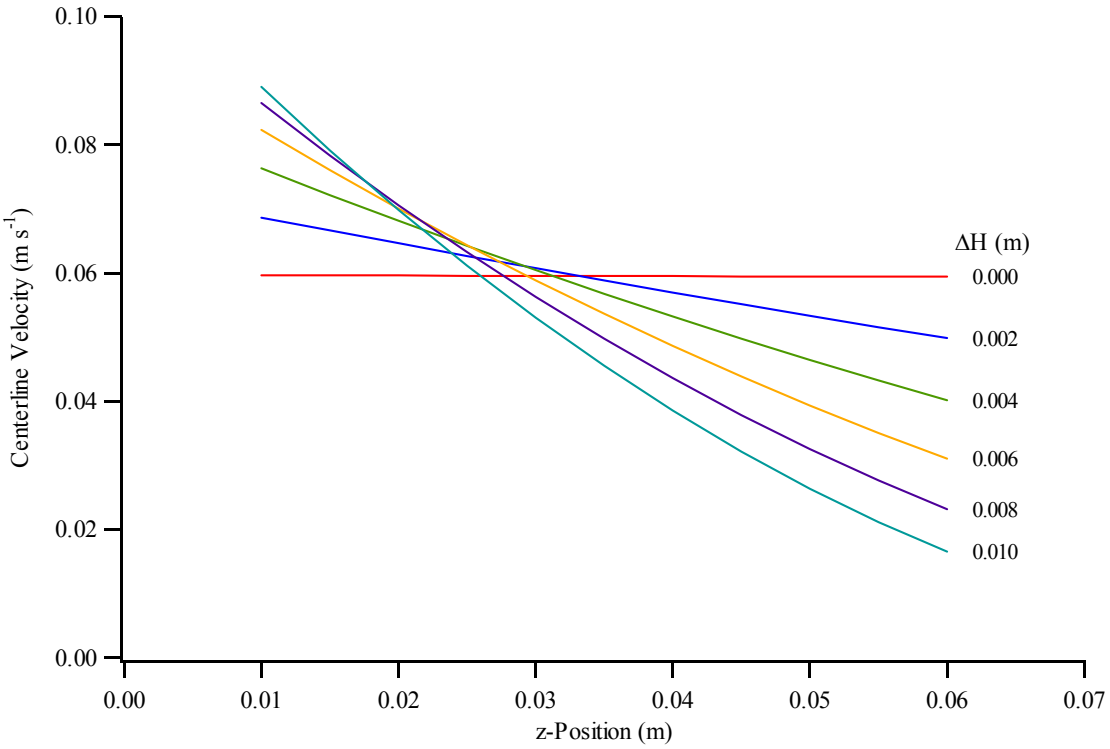

Figure 4.5: The variation in the centerline velocity for several trapezoidal geometries. ΔH = 0.000 m for the Baseline configuration. The velocity values are taken at a point where the equilibrium flow field is established.

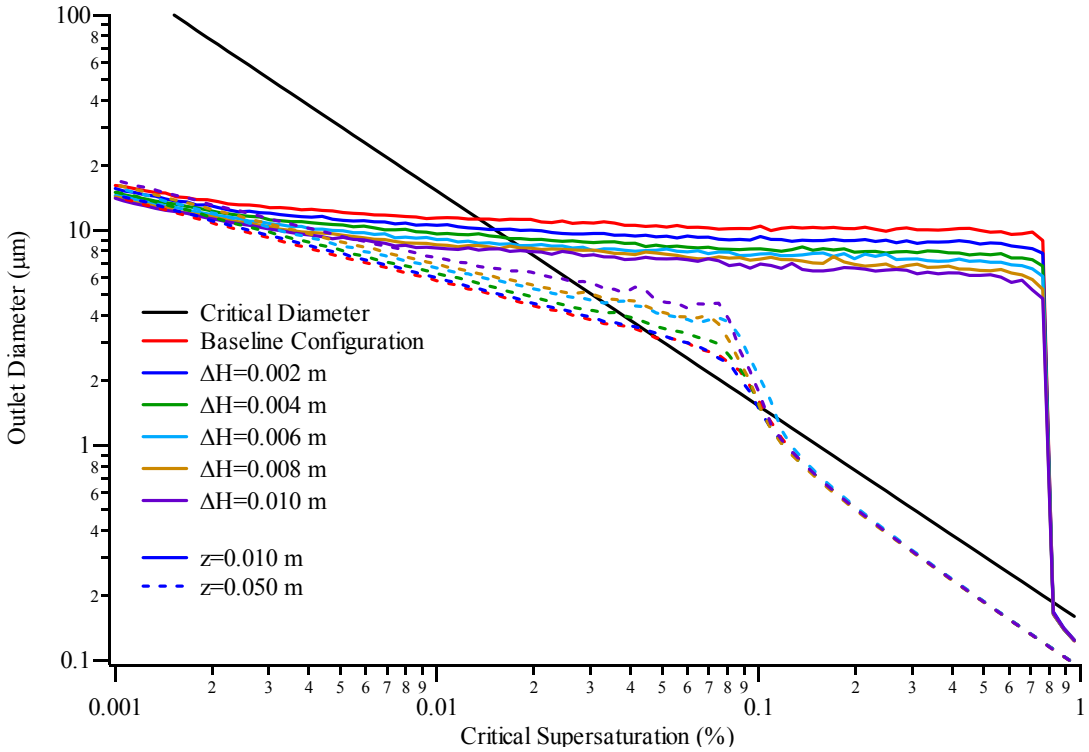

Figure 4.6: Particle growth curves for several values of ΔH. Only the upper and lower boundaries of the resolvable supersaturation range are presented.

4.6. The data from two transverse locations are shown: one at the high supersaturation end of the chamber (z = 0.010 m), and one from the low supersaturation end (z = 0.050 m). On the low supersaturation end, increasing the value of ΔH to 0.010 m (the maximum value considered here) results in an approximate doubling of the outlet droplet diameter. At z = 0.050 m, this doubling increases the size difference between activated and unactivated particles, thereby reducing the minimum resolvable supersaturation to approximately 0.08%. This improvement at the low end of the supersaturation range is achieved without any corresponding reduction in the maximum resolvable supersaturation. At the high supersaturation end of the chamber, the activated droplets are smaller at the outlet; this is not an issue, since the droplets are still larger than those exposed to lower supersaturations.

Another potential limitation should be noted, even though it does not occur for any of the cases examined here. When the saturation profiles arising from the trapezoidal geometry (Figure 4.7) are compared with the baseline case (Figure 4.3a), the effect of the increased residence times at the low supersaturation end of the chamber is obvious: at high values of z, streamlines reach their equilibrium state much more quickly when ΔH = 0.010 m than in the baseline case.

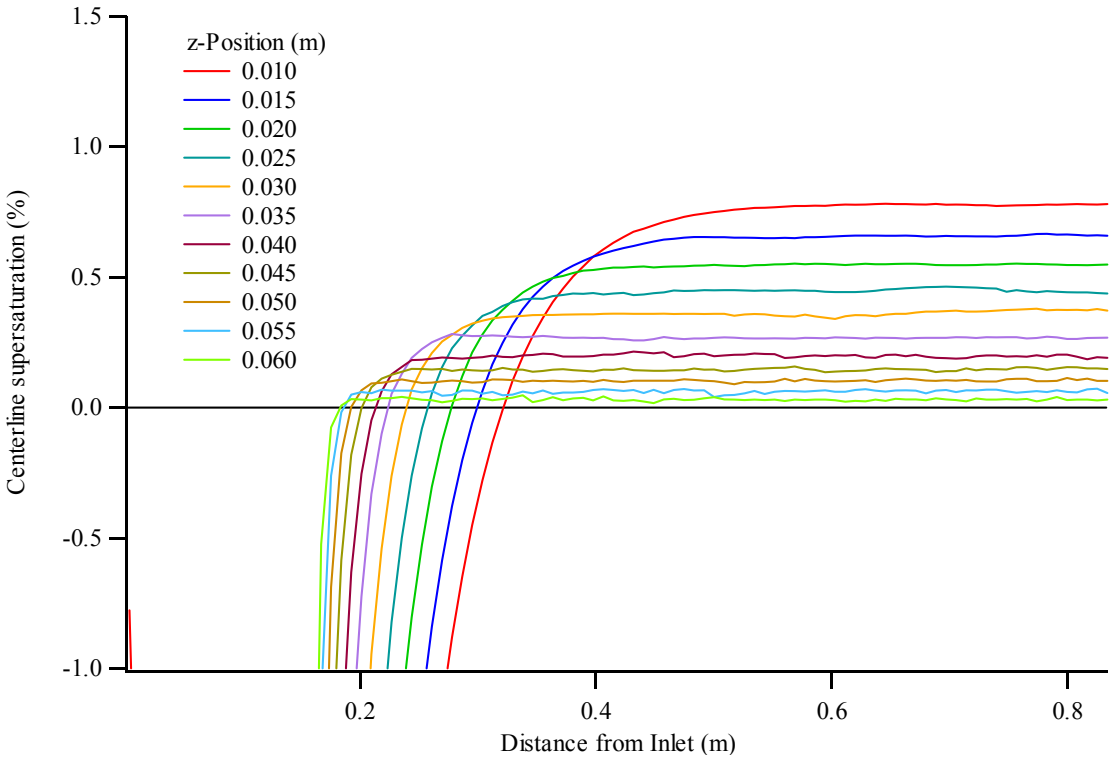

Figure 4.7: Centerline supersaturation profiles for the case where ΔH = 0.010 m. Note the distances required to reach the equilibrium supersaturation on different streamlines, compared with Figure 4.4b.

However, the opposite effect is seen where the equilibrium supersaturation is not reached until the streamlines have proceeded more than halfway down the length of the chamber, due to the higher flow velocities. In an extreme case, the streamlines at the high supersaturation end of the chamber might never reach their equilibrium supersaturations; this would result in a reduction in the maximum resolvable supersaturation in the chamber, an undesirable outcome.

4.5.3 Variations in Temperature Gradient

As has been noted by *Fukuta and Saxena* [1979a] and *DeFelice and Saxena* [1994], the range of supersaturations in the growth chamber can be moved by changing the temperature difference (ΔT) between the hot and cold edges (T_{H0} and T_{C0} in Figure 4.1). The response of a chamber with the proposed trapezoidal geometry to changes in ΔT is explored here by increasing or decreasing T_{H0} without changing T_{C0} (*i.e.*, when ΔT = 3.5 K, T_{H0} = 286.5 K and T_{C0} = 283 K). A value of 0.006 m was chosen for ΔH for these simulations. This maximizes the range over which the temperature can be varied while still ensuring that B is less than unity and retaining the resolution enhancements achieved with the trapezoidal geometry. The effects of the temperature variations

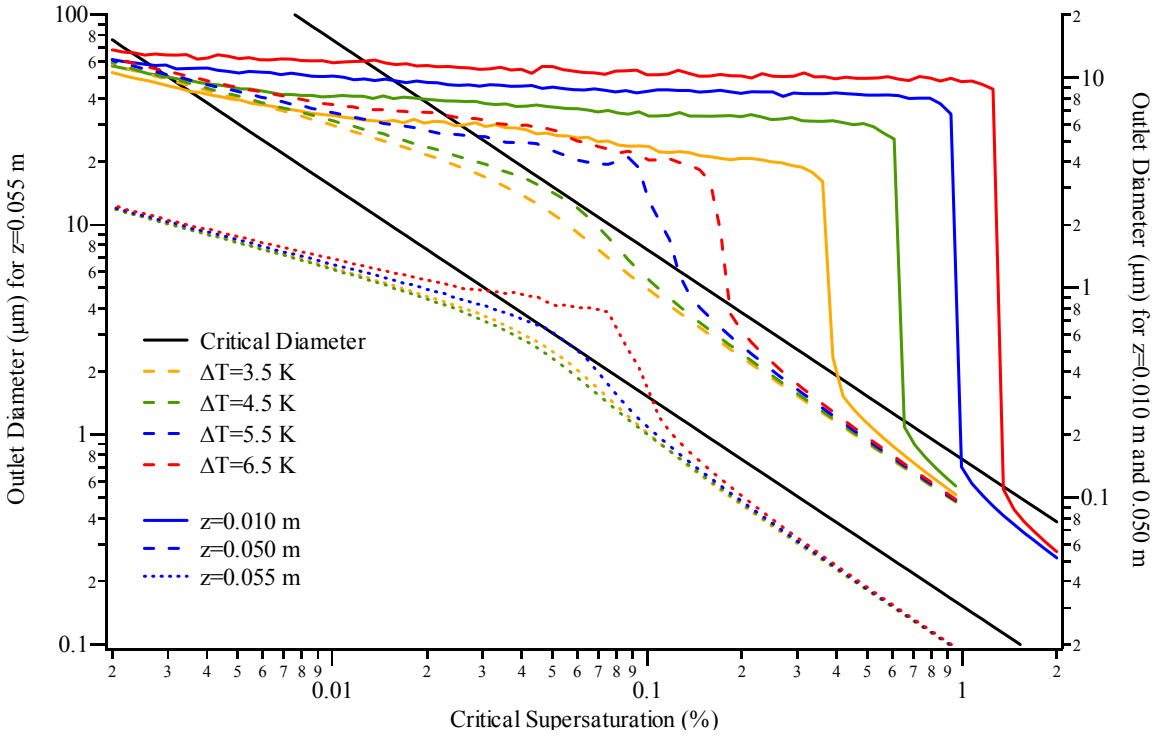

Figure 4.8: Particle growth curves for several values of ΔT. To prevent overlap, the growth curves for z = 0.010 m and z = 0.050 m are offset. The values for these curves are found on the right axis.

on particle growth are as expected (Figure 4.8); as ΔT is increased, the upper boundary of the supersaturation range increases. The effective supersaturations of streamlines at the opposite end of the chamber (i.e., where the distance between plates is smaller) also increase, but this undesirable effect is mitigated because the increase in ΔT also allows activation to occur on streamlines where it had not for lower values of ΔT. For example, when ΔT is increased from 5.0 K (the value for the simulations where the geometry was varied) to 6.5 K, the effective supersaturation increases from ~0.8% to ~1.3% at z = 0.010 m, and from ~0.08% to ~0.2% at z = 0.050 m. However, the increased temperature gradient now allows particles to activate on the z = 0.055 m streamline, where there was no activation before; the effective supersaturation at that position is ~0.07%. Thus by increasing ΔT it is possible to improve both the upper and lower boundaries of the resolvable supersaturation range.

4.5.4 Volumetric Flow Rate Variation

The total volumetric flow rate (Q) through the trapezoidal chamber is also varied to demonstrate its effect on particle growth. From the baseline value of 2.50 x 10^{-5} m^3 s^{-1}, Q is increased by 10% and decreased by 15%, in increments of 5%. To ensure that the buoyancy

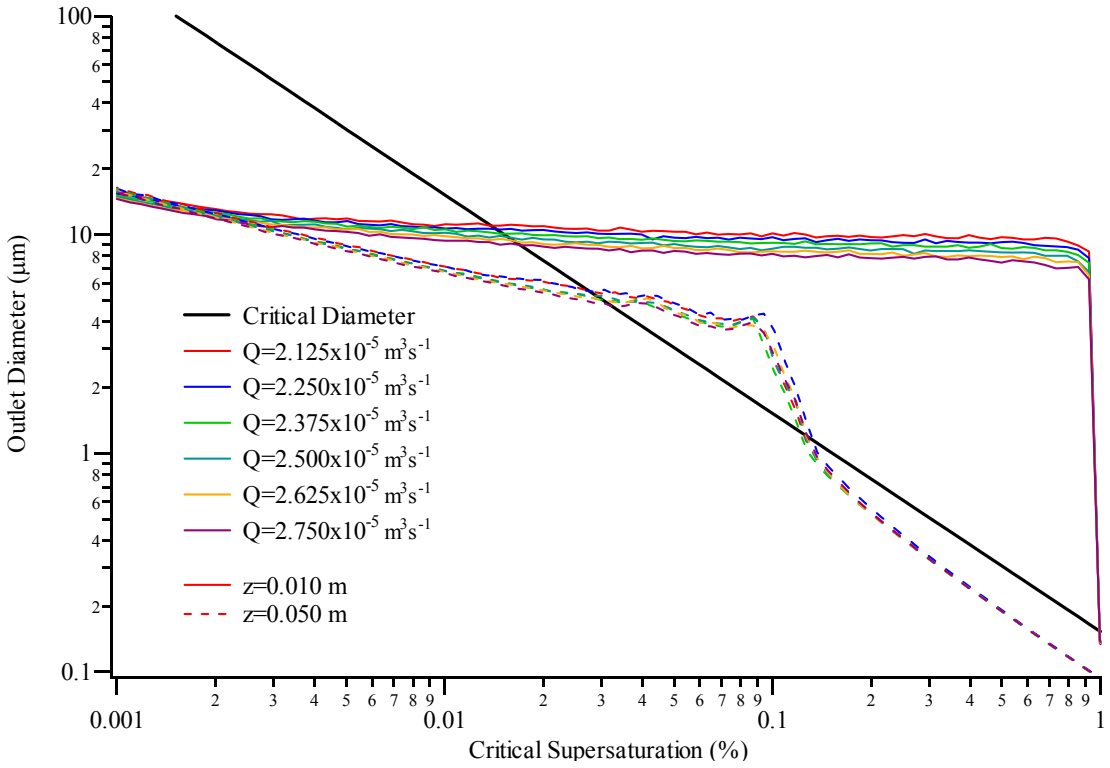

Figure 4.9: Particle growth curves for several values of Q. The upper and lower boundaries to the resolvable supersaturation range are presented.

criterion is satisfied for these simulations, a value of 5.5 K is chosen for ΔT. The results (Figure 4.9) show that lower flow rates lead to somewhat larger outlet diameters, with a negligible effect on the supersaturation range. The highest simulated flow rate, 2.75 x 10^{-5} m^3 s^{-1}, is 30% larger than the lowest value. At z = 0.010 m, this variation results in an increase in the outlet droplet diameter of approximately 30%; at the low supersaturation end of the chamber (i.e., where z = 0.050 m), the improvement is even less, about 15%. Additional reductions to the flow rate could further increase the outlet diameters, but such a configuration would not satisfy the buoyancy criterion. Since the droplets are large enough in all cases examined here to be detected by light scattering, there is little advantage in reducing the volumetric flow rate to increase the outlet diameter. One additional consideration here is that of counting statistics; low flow rates would result in fewer droplets passing through the detection region of the instrument in a given time. The need to obtain a significant sample in such a case could require that the sampling rate be reduced, resulting in a loss of temporal resolution. Since the issue depends heavily on the design of the detection region, this issue is beyond the scope of the current study.

4.6 Response to Aerosol Non-Idealities

The simulations presented in the previous section demonstrate the relative effects of changes in the chamber geometry, the temperature gradient, and the total volumetric flow. The results indicate that larger values of ΔH and ΔT can improve the resolvable supersaturation range of the instrument, but that varying Q has a minimal effect. Although there is no single optimum configuration, it is possible to choose a configuration that results in both a large resolvable supersaturation range and a sharp size differential between activated and unactivated particles while still satisfying the buoyancy criterion to avoid flow reversal.

The simulation results for one such configuration are presented in Figure 4.10. For this design, ΔH is set to 0.010 m and ΔT is 6.0 K. To keep the buoyancy criterion below 1.0, the volumetric flow rate is 2.75 x 10^{-5} m^3 s^{-1}. All other parameters are as in the baseline configuration, and the results are still based on an idealized aerosol (i.e., pure ammonium sulfate aerosol with α set equal to 1.0). The saturation curves in Figure 4.10a indicate that the maximum equilibrium supersaturation is approximately 1.2%, roughly the same as that of the original FSCS. The growth curves confirm this maximum supersaturation, and show that particles with critical supersaturations as low as 0.07% would be easily resolved by the instrument. In fact, the sharp size difference between activated and unactivated droplets at z = 0.055 m in Figure 4.10b implies that particle activation would likely occur on streamlines between z = 0.055 m and z = 0.060 m. This would probably extend the resolvable supersaturation range below S = 0.07%.

The aerosol growth calculations to this point have been based on an idealized aerosol (pure ammonium sulfate, α = 1.0). As was noted in the introduction, a primary advantage of the FSCS (as well as the alternative configuration proposed here) over other designs is its relative insensitivity to variations in droplet size resulting from non-homogeneous aerosol populations. To verify the performance of the proposed configuration, an alternative aerosol growth model was employed that allows more realistic aerosol populations to be simulated. The sensitivity of the proposed instrument configuration to variations in chemical composition was tested by comparing the growth calculations for a pure salt aerosol to a population that is 50% insoluble (internally mixed, by mass) and to one that is 90% insoluble. The results are presented in Figure 4.11a; note that this growth model results in smaller droplets at the outlet for specified inlet composition due to a change in the method for calculating the wet diameter at the inlet. For the two streamlines presented in Figure 4.11a, the results indicate that varying the composition has a

4.10(a)

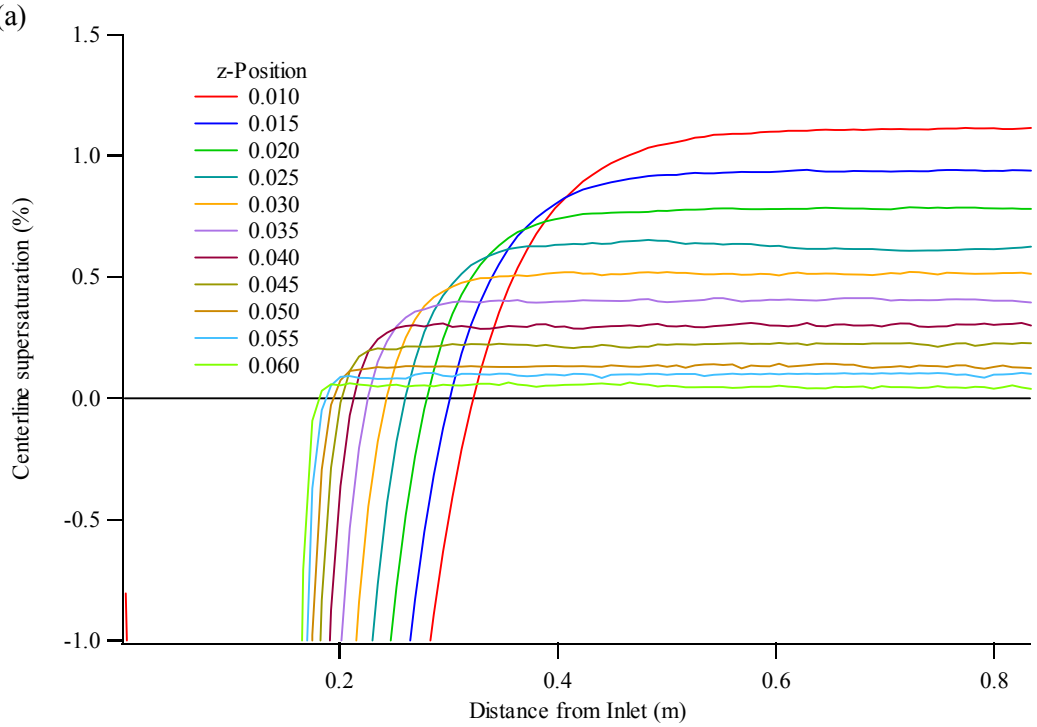

4.10(b)

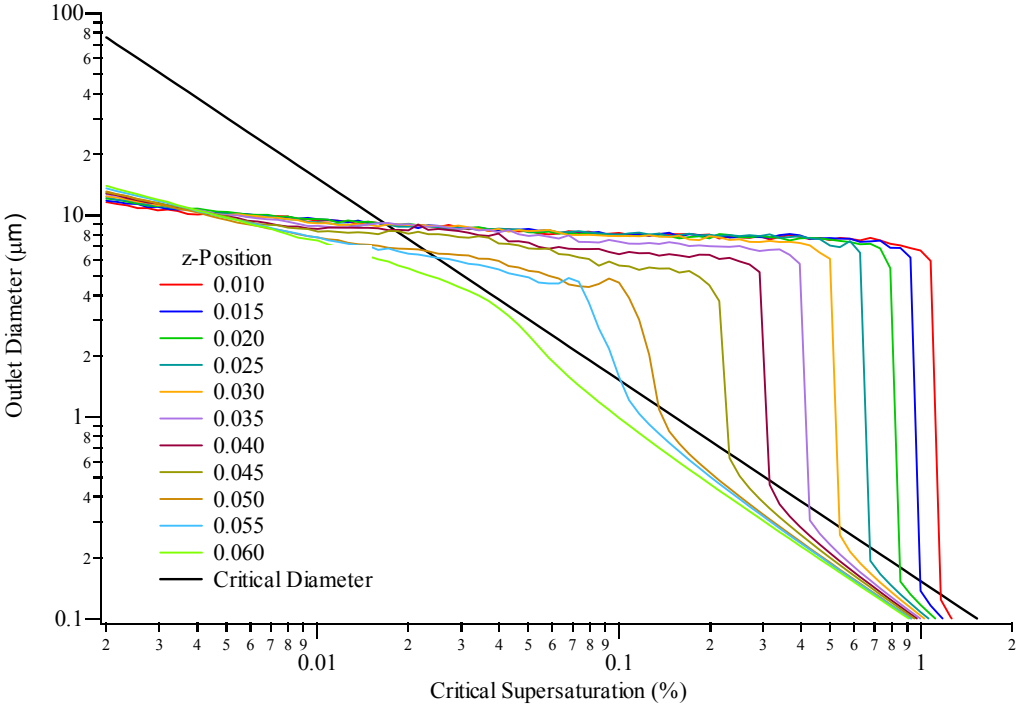

Figure 4.10: As in Figure 4.3, for an optimized instrument configuration.

minimal effect of the effective supersaturation of the streamline. The effect on the outlet diameter is also relatively small at the high supersaturation end of the chamber (i.e., when z =

0.010 m), but at low supersaturations there is a significant reduction in outlet size when the aerosol is primarily composed of insoluble material. However, this does not directly affect the resolution of the instrument; since the "sharpness" of the elbow is not diminished, activated droplets can still be readily distinguished from unactivated particles. It is possible that the apparent reduction in growth rate for slightly soluble particles could cause the minimum resolvable supersaturation to shift slightly toward a larger value.

The effect of the value of the water mass accommodation coefficient on the growth calculation can be seen by comparing Figure 411b with Figure 4.10b. Studies have indicated that for a growing water droplet, α may have values as low as 0.04 [*Chodes et al.*, 1974; *Shaw and Lamb*, 1999]; the growth curves in Figure 4.11b were calculated using this value. The growth curve for $\alpha = 1.0$ at the highest supersaturation streamline (z = 0.010 m) is included for comparison. When the lower value of the accommodation coefficient is used in the calculation, there is a significant (~50%) reduction in the outlet diameter of the activated droplets. While there are still sharp gradients in the growth curves on those streamlines with high effective supersaturations, it is no longer possible to distinguish between the activated droplets and the unactivated particles on streamlines where the effective supersaturation is less than ~0.2%. If the value of α was even less than 0.04, the performance of the proposed instrument (as well as designs currently in use) would break down completely. If the mass accommodation coefficient is significantly greater than 0.04, as has been suggested recently by *Li et al.* [2001], then the performance of the proposed configuration would be closer to the idealized case discussed above.

The results presented here demonstrate that it is possible to design a CCN spectrometer with a broader range than the FSCS. The performance of such an instrument would have a minimal dependence on compositional variability in the sample aerosol, unless the mass accommodation coefficient was affected by those changes; the latter could result in undercounting at supersaturations at the low end of the instrument's resolvable range, but not over the entire range. In that sense, all CCN instruments are susceptible to changes in α. Obviously, alternative configurations to the one described here could have similar characteristics, or different characteristics better suited for a given design goal. Other practical details of the instrument design would also interplay with the parameters considered here, and would influence choices for the chamber design. Some potential improvements for the inlet and detector regions of an instrument design based on the FSCS are discussed in the next section.

4.11(a)

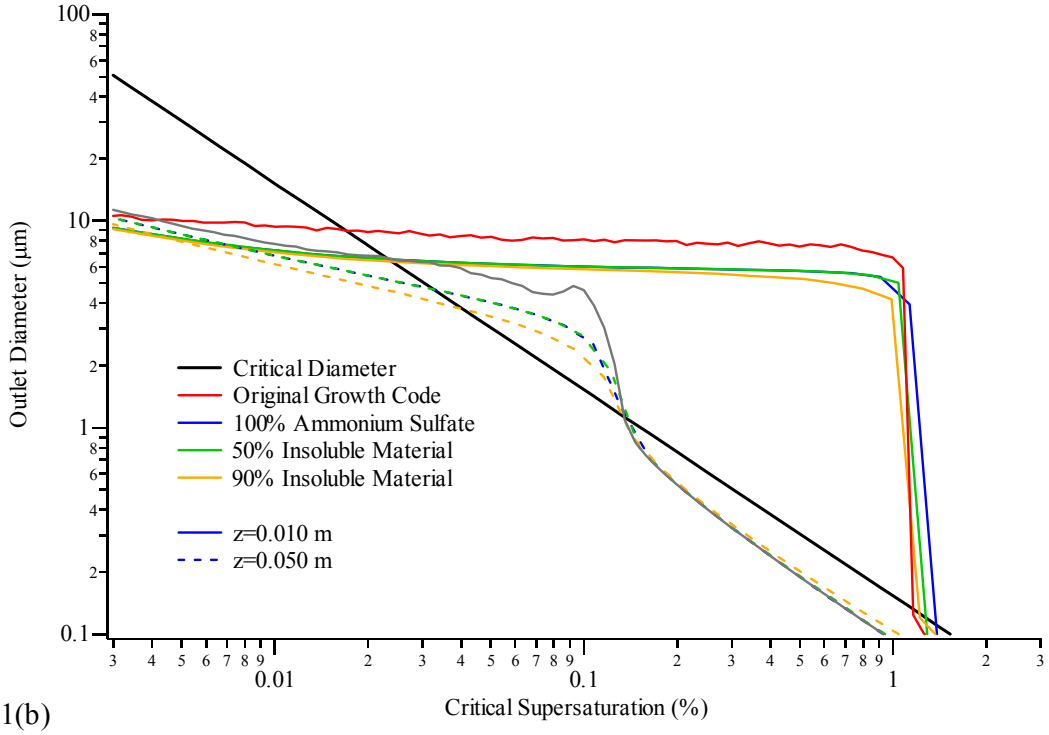

4.11(b)

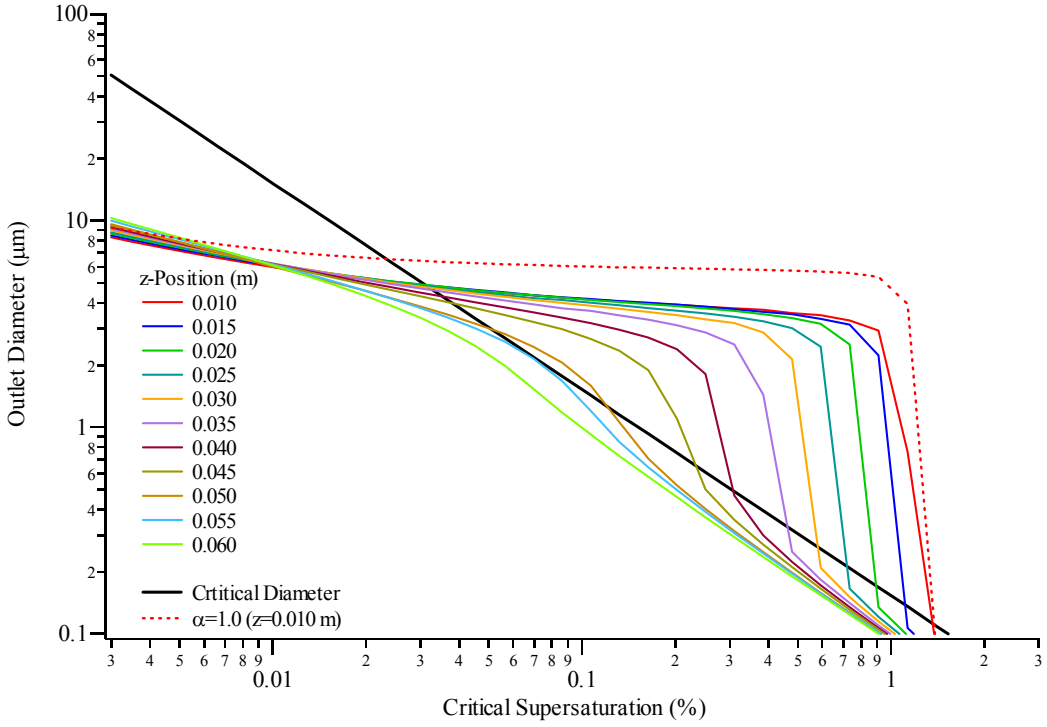

Figure 4.11: Particle growth curves indicating the dependence of the instrument performance on (a) particle composition and (b) the mass accommodation coefficient. The additional curve in (a) is to indicate the difference in the results of the two aerosol growth models (see text).

4.7 Additional Instrument Design Improvements

In the quarter century since the development of the FSCS, there have been vast technological advances that could be implemented to improve the instrument. The size of many components could be reduced; the time resolution of the measurement and the level of automation could both be increased. Most of these potential improvements are not tied to the design of the growth chamber and are therefore outside the scope of this work. However, more fundamental modifications to the inlet region and to the droplet detector would ensure that the gains achieved by modifying the geometry of the growth chamber are fully realized.

4.7.1 Inlet Region

In the FSCS, a single flow enters the growth chamber through a wedge-shaped manifold that widens smoothly from a narrow slit [*Fukuta and Saxena*, 1979a]. This design successfully produces a uniform parabolic flow across the chamber, but it also introduces into the chamber a significant number of particles outside of the region of maximum supersaturation. These particles compete for the limited water vapor in the chamber, and could potentially reduce the maximum supersaturation reached along the centerline. Their presence also further complicates the role of gravitational settling in a horizontally-oriented instrument. As some growing droplets fall out of the detected streamlines, other droplets may fall into that region.

These problems can be avoided by surrounding the sample region with a particle-free sheath flow. Two well-balanced streams, filtered to remove all particles, could be introduced along the hot and cold wall in such a way that the flow is evenly distributed across the width of the chamber; these flow streams would fill nearly the entire height of the chamber. The sheath flows should be kept separate until the streamlines have stabilized, after which the aerosol sample flow can be introduced through a narrow slit along the centerline of the chamber. The sample flow should be small relative to the sheath flows, so that all particles are exposed to essentially the same supersaturation. Any required flow shaping (e.g., shifting from a rectangular geometry to a trapezoidal one) can be accomplished by gradually narrowing or widening one end of the chamber after the two sheath flows and the sample flow have merged into a single laminar, parabolic flow. The shaped, merged flow would then enter the growth chamber and activation could occur along the centerline as described earlier.

4.7.2 Droplet Detector

For an instrument design similar to that of the FSCS to be effective, the activated droplets must be sampled on their growth streamlines; the position of the streamline within the growth chamber is the parameter that determines the supersaturation at which activation occurred. This streamline sampling can be accomplished in several ways. The original FSCS design employed a moving sampling probe at the end of the growth chamber, which pulled a portion of the flow through the chamber into an attached optical particle counter. This apparatus was successful in sampling individual streamlines, but required ~15 seconds to obtain a full CCN spectrum [*Fukuta and Saxena*, 1979a]. This low time resolution is often insufficient for airborne measurements, where particle concentrations can change by an order of magnitude in a period of several seconds (e.g., Chapter 3). The cycle speed of the sampling probe could be accelerated somewhat, but the presence of moving parts within the flow streams distorts the flow, and this effect would be enhanced if the probe were translated across the chamber more rapidly.

Ideally the droplet detector on an instrument based on the FSCS design would be able to obtain a CCN spectrum more rapidly (on the order of one spectrum per second), and would observe the droplets without distorting the flow through the instrument. These goals are most easily achieved by designing a detector as part of the instrument, rather than attaching the growth chamber to an external particle counter. There are two ways to accomplish this; one is to design a scanning device that would illuminate only a small portion of the flow at any given time, so that a droplet in that fraction could be observed by a single photodetector. As for the original FSCS design, the location of an observed droplet within the chamber would be determined by the time at which the observation was made. The scanning mechanism could easily be made fast enough to achieve sufficient time resolution, but would probably require either moving parts or very sensitive electronics.

Another option is available due to advances in photodetector technology. A small linear array photodetector could be incorporated into a design so that each detector in the array collects light from only a small portion of the sample flow after the flow has exited the growth chamber (Figure 4.12). Such an arrangement would only require a single light source, and all streamlines could be monitored concurrently. The time resolution would be limited only by the counting statistics required for the observed concentrations to be significant, an issue that could be addressed to some degree by modifying the sample flow rate. The design does require that light scattered from a given streamline be observed only by a single channel in the array, but this can

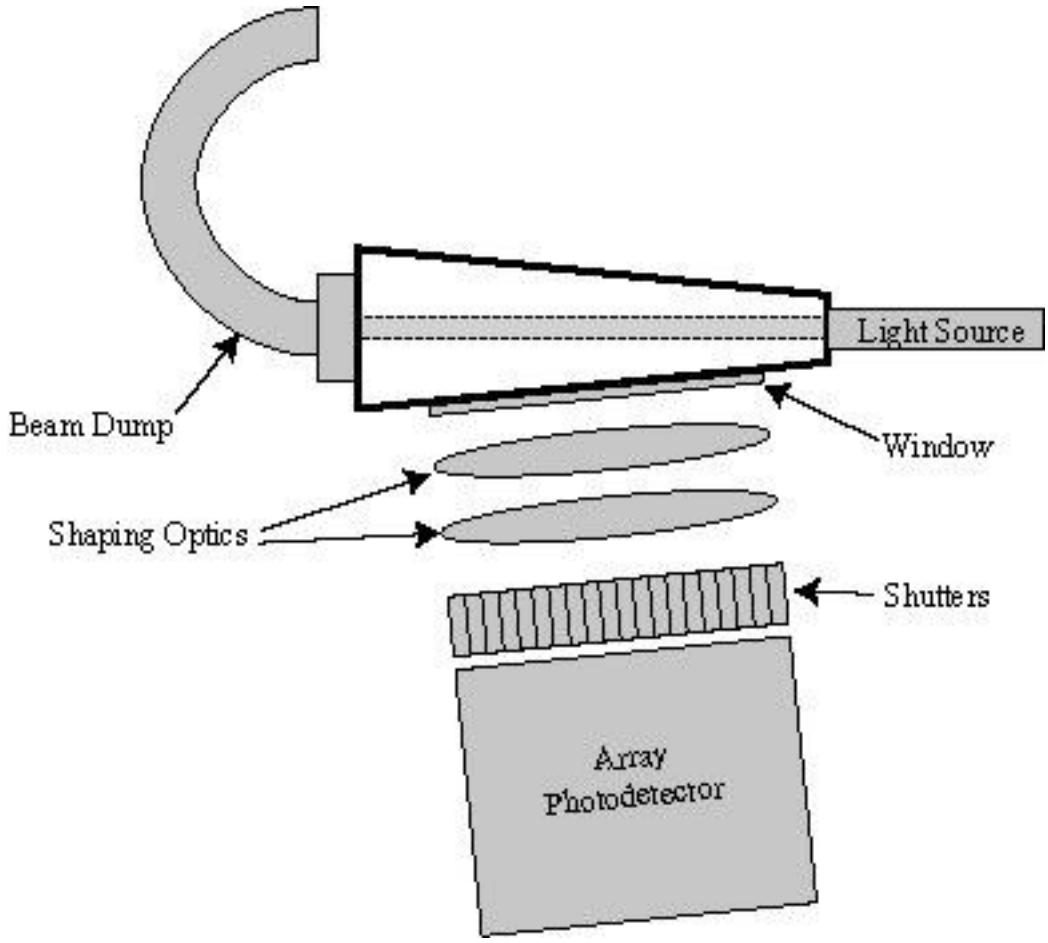

Figure 4.12: Schematic of improvements to the detector region of the proposed instrument.

be accomplished through the use of shutters and shaping optics. The amount of data requiring processing is also significantly greater if an array detector is employed since each channel of the array acts as an individual particle counter, but the analysis of the data would likely be more straightforward, since the supersaturation of the observation would not have to be calculated based on the timing of the measurement.

It is also important to note that if the geometry of the growth chamber were modified to allow longer growth times for those streamlines exposed to lower supersaturations, there would be a corresponding effect on the view volume in the detector region. For an equal sampling period, less flow would pass through the illuminated region on the low velocity, low supersaturation end of the chamber. Since fewer particles activate and grow to droplet size at lower supersaturations, there would also be fewer droplets in a given volume on that same end of the chamber. These effects when compounded might require that the sampling period be extended in cases when the

CCN concentrations are low. However, the advantages of obtaining CCN concentrations at lower supersaturations outweigh any small reduction in time resolution arising from variations in residence times in the growth chamber.

4.8 Summary and Conclusions

This work explores the viability of alternative growth chamber geometries to that used in the original Fukuta-Saxena CCN Spectrometer. By introducing a trapezoidal cross section, the flow within the growth chamber is redistributed to allow longer growth times for those particles exposed to lower supersaturations while minimizing the potential impact of buoyancy forces. A design criterion is derived that determines whether a given design configuration is susceptible to flow reversal under equilibrium conditions. Using only configurations that satisfy this buoyancy criterion, a series of simulations are presented that demonstrate the relative effects of varying the chamber shape, the temperature gradient, and the total flow rate through the instrument.

Simulation results indicate that the incorporation of a trapezoidal geometry significantly increases the growth time available for particles on streamlines at the low supersaturation end of the growth chamber. This allows activated particles on these streamlines to reach a size where they can be easily differentiated from unactivated particles, thereby reducing the minimum resolvable supersaturation of the instrument, without sacrificing resolution at the upper end of the range. Increasing the temperature gradient in a given configuration generally results in an upward shift of the entire resolvable supersaturation range. However, the results here indicate that in some cases increasing ΔT will also result in activation on streamlines where it would not otherwise occur; thus, it is possible to increase the upper limit of the resolvable range without sacrificing resolution at lower supersaturations. Compared with the effects of varying the shape of the chamber and the temperature gradient, modest variations in the total volumetric flow are found to have a relatively small impact on instrument performance.

By using the buoyancy criterion developed in this work and applying the results of the growth chamber simulations, it is possible to design a CCN spectrometer with a broader dynamic supersaturation range that would be better suited for real-time atmospheric CCN measurements than currently available instruments. One such configuration is presented here, which would result in a dynamic range of $0.07\% < S < 1.2\%$. This compares with the FSCS, which has the same maximum resolvable supersaturation, but has not been shown to able to resolve

supersaturations below ~0.1%. This study also proposes improvements to the inlet and droplet detection regions that could be incorporated into a new instrument design.

4.9 Acknowledgements

This work was supported by the Office of Naval Research and the EPA STAR Graduate Fellowship Program.

5 Summary

The goal of this thesis is to advance our understanding of the relationship between aerosols and clouds. While much can be gained by studying particle activation and growth in the laboratory and through theoretical studies, these approaches cannot yet capture the complexity of the real atmosphere. Field observations, while difficult, are a necessary component of the atmospheric sciences; the atmosphere is the original source of all the questions, and ultimate confirmation of all the answers. This thesis demonstrates how field measurements obtained in the natural laboratory can be used to validate our theoretical understanding of atmospheric phenomena and to raise new questions that require further study.

Chapter 2 presents observations of cloud condensation nuclei (CCN) made during the CRYSTAL-FACE (Cirrus Regional Study of Tropical Anvils and Cirrus Layers - Florida Area Cirrus Experiment) field campaign. Observations were made with two CCN instruments operating at different supersaturations; these measurements are summarized to characterize the average conditions over southwest Florida in the summertime, adding to the extensive global database of CCN information. Additionally, Chapter 2 presents a so-called closure analysis, whereby the observed CCN concentrations are compared to predictions on activation theory and the measured aerosol size distribution. Despite the use of a simplistic assumptions for the aerosol chemical composition, the analysis confirms that it is possible in some cases to predict atmospheric CCN concentrations from other measured aerosol properties. This is the first time such an analysis has demonstrated this successfully using airborne measurements.

Chapter 2 also describes a case where the CCN in the boundary layer, near the base of a convective cloud, exhibited strong spatial inhomogeneities. This occurrence is examined in detail in Chapter 3. The case study in that chapter characterizes the background boundary layer aerosol around that cloud, and describes the aerosol plume that was encountered several times along the northern side of the base of a mixed-phase convective cloud. The available evidence suggests

that the plume was emitted by an oil-burning power plant near the city of Miami, raising the possibility that such anthropogenic emissions could significantly affect the development of the deep convective systems common over the southeastern United States. While the data collected near the top of the cloud is inconclusive in this case, further analysis in ongoing using available ground-based radar data and computer simulations. In any event, the plume encountered serendipitously during CRYSTAL-FACE raises questions that will likely be explored further in future field campaigns.

The fact that new questions as to the relationship between aerosols and clouds continue to be raised is an indication that improvements in instrumentation would likely significantly enhance our ability to understand the complexity of atmospheric processes. Chapter 4 of this thesis details a proposed improvement to the design of the Fukuta-Saxena CCN Spectrometer. By changing the shape of the growth chamber from a rectangle to a trapezoid and orienting the chamber vertically, the resolvable range of the instrument could be significantly increased. Importantly, the resolution of the proposed design is less susceptible to droplet growth kinetics than currently available instruments, and therefore would provide more reliable data for conditions where the mechanisms of growth are understood the least, i.e., when there is a significant organic component to the aerosol population. Such an instrument, when constructed, will likely prove to be an invaluable tool for better understanding the nature of CCN activity in a wide variety of conditions.

It is clear from the research presented in the previous chapters that field measurements and instrument development play an important role in advancing atmospheric science, particularly with respect to the relationship between aerosols and clouds. The work presented herein add to the extensive information already available, and provide a basis for continued work. While the field has advanced considerably in the last few decades, there is still many large gaps in understanding, a plenty of work still to be done. This thesis is a small step in that direction.

References

Ackerman, A. S., O. B. Toon, and P. V. Hobbs, Numerical modeling of ship tracks produced by injections of cloud condensation nuclei into marine stratiform clouds, *J. Geophys. Res., 100,* 7121-7133, 1995.

Albrecht, B., Aerosols, cloud microphysics and fractional cloudiness, *Science, 245*, 1227-1230, 1989.

Bigg, E. K., Discrepancy between observation and prediction of concentrations of cloud condensation nuclei, *Atmos. Res., 20*, 82-86, 1986.

Bird, R. B., W. E. Stewart, and E. N. Lightfoot, *Transport Phenomena*, 780 pp., John Wiley & Sons, New York, 1960.

Brock, C. A., R. A. Washenfelder, M. Trainer, T. B. Ryerson, J. C. Wilson, J. M. Reeves, L. G. Huey, J. S. Holloway, D. D. Parrish, G. Hübler, and F. C. Fehsenfeld, Particle growth in the plumes of coal-fired power plants, *J. Geophys. Res., 107*(D12), doi:10.1029/2001JD001062, 2002.

Brock, C. A., M. Trainer, T. B. Ryerson, J. A. Neuman, D. D. Parrish, J. S. Holloway, K. K. Nicks Jr., G. J. Frost, G. Hübler, F. C. Fehsenfeld, J. C. Wilson, J. M. Reeves, B. G. Lafleur, H. Hilbers, E. L. Atlas, S. G. Donnelly, S. M. Schauffler, V. R. Stroud, and C. Wiedinmeyer, Particle growth in urban and industrial plumes in Texas, *J. Geophys. Res., 108*(D3), doi:10.1029/2002JD002746, 2003.

Cantrell, W., G. Shaw, C. Leck, L. Granat, and H. Cachier, Relationships between cloud condensation nuclei spectra and aerosol particles on a south-north transect of the Indian Ocean, *J. Geophys. Res., 105*, 15313-15320, 2000.

Cantrell, W., G. Shaw, G. R. Cass, Z. Chowdhury, L. S. Hughes, K. A. Prather, S. A. Guazzotti, and K. R. Coffee, Closure between aerosol particles and cloud condensation nuclei at Kaashidhoo Climate Observatory, *J. Geophys. Res., 106*, 28711-28718, 2001.

Changnon, S. A., Midwestern sunshine and temperature trends since 1901: possible evidence of jet contrail effects, *J. Appl. Met., 20,* 496-508, 1981.

Charlson, R. J., J. H. Seinfeld, A. Nenes, M. Kulmala, A. Laaksonen, and M. C. Facchini, Reshaping the theory of cloud formation, *Science, 292*, 2025-2026, 2001.

Chodes, N., J. Warner, and A. Gagin, A determination of the condensation coefficient of water from the growth rate of small cloud droplets, *J. Atmos. Sci., 31*, 1351-1357, 1974.

Chuang, P. Y. , Measurement of the timescale of hygroscopic growth for atmospheric aerosols, *J. Geophys. Res., 108*(D9), 4282, doi:10.1029/2002JD002757, 2003.

Chuang, P.Y., D. R. Collins, H. Pawlowska, J. R. Snider, H. H. Jonsson, J.-L. Brenguier, R. C. Flagan, and J. H. Seinfeld, CCN measurements during ACE-2 and their relationship to cloud microphysical properties, *Tellus Ser. B, 52*, 843-867, 2000a.

Chuang, P. Y., A. Nenes, J. N. Smith, R. C. Flagan, and J. H. Seinfeld, Design of a CCN instrument for airborne measurement, *J. Atmos. Oceanic Technol., 17*, 1005-1019, 2000b.

Clarke, A. D., J. L. Varner, F. Eisele, R. L. Mauldin, D. Tanner, and M. Litchy, Particle production in the remote marine atmosphere: cloud outflow and subsidence during ACE 1, *J. Geophys. Res., 103,* 16397-16409, 1998.

Clarke, A. D., F. Eisele, V. N. Kapustin, K. Moore, D. Tanner, L. Mauldin, M. Litchy, B. Lienert, M. A. Carroll, and G. Albercook, Nucleation in the equatorial free troposphere: favorable environments during PEM-Tropics, *J. Geophys. Res., 104,* 5735-5744, 1999.

Covert, D. S., J. L. Gras, A. Wiedensohler, and F. Stratmann, Comparison of directly measured CCN with CCN modeled from the number-size distribution in the marine boundary layer during ACE 1 at Cape Grim, Tasmania, *J. Geophys. Res., 103*, 16597-16608, 1998.

Cruz, C.N., and S.N. Pandis, The effect of organic coatings on the cloud condensation nuclei activity of inorganic atmospheric aerosol, *J. Geophys. Res., 103*, 13111-13123, 1998.

DeFelice, T. P., and V. K. Saxena, On the variation of cloud condensation nuclei in association with cloud systems at a mountain-top location, *Atmos. Res., 31*, 13-39, 1994.

Durkee, P. A., K. J. Noone, R. J. Ferek, D. W. Johnson, J. P. Taylor, T. J. Garrett, P. V. Hobbs, J. G. Hudson, C. S. Bretherton, G. Innis, G. M. Frick, W. A. Hoppel, C. D. O'Dowd, L. M. Russell, R. Gasparovic, K. E. Nielson, S. A. Tessmer, E. Öström, S. R. Osborne, R. C. Flagan, J. H. Seinfeld, and H. Rand, The impact of ship-produced aerosols on the microstructure and albedo of warm marine stratocumulus clouds: a test of MAST hypotheses 1i and 1ii, *J. Atmos. Sci., 57*, 2554-2569, 2000.

Environmental Protection Agency (EPA), AIRS user's guide, *Rep. EPA-454/B-94-005*, Washington, D.C., 1994.

Ferek, R. J., D. A. Hegg, P. V. Hobbs, P. A. Durkee, and K. E. Nielsen, Measurements of ship-induced cloud tracks off the Washington coast, *J. Geophys. Res., 103*, 23199-23206, 1998.

Field, P. R., R. Wood, P. R. A. Brown, P. H. Kaye, E. Hirst, R. Greenaway, and J. A. Smith, Ice particle interarrival times measured with a fast FSSP, *J. Atmos. Oceanic Technol., 20*, 249-261, 2003.

Fukuta, N. and V. K. Saxena, A horizontal thermal gradient cloud condensation nucleus spectrometer, *J. Appl. Meteor., 18*, 1352-1362, 1979a.

Fukuta, N. and V. K. Saxena, The principle of a new horizontal thermal gradient cloud condensation nucleus ppectrometer, *J. Rech. Atmos., 13*, 169-188, 1979b.

Garrett, T. J., L. F. Radke, and P. V. Hobbs, Aerosol effects on cloud emissivity and surface longwave hearing in the arctic, *J. Atmos. Sci., 59*, 769-778, 2002.

Gayet, J., G. Febvre, and H. Larsen, The reliability of the PMS FSSP in the presence of small ice crystals, *J. Atmos. Oceanic Technol., 13*, 1300-1310, 1996.

Hegg, D. A., L. F. Radke, and P. V. Hobbs, Measurements of Aitken nuclei and cloud condensation nuclei in the marine atmosphere and their relation to the DMS-cloud-climate hypothesis, *J. Geophys. Res., 96*, 18727-18733, 1991.

Hegg, D. A., R. J. Ferek, and P. V. Hobbs, Cloud condensation nuclei over the Arctic Ocean in early spring, *J. Appl. Meteor., 34*, 2076-2082, 1995.

Hegg, D. A., S. Gao, W. Hoppel, G. Frick, P. Caffrey, W.R. Leaitch, N. Shantz, J. Ambrusko, and T. Albrechcinski, Laboratory studies of the efficiency of selected organic aerosols as CCN, *Atmos. Res., 58*, 155-166, 2001.

Heymsfield, A. H. and G. M. McFarquhar, Microphysics of INDOEX clean and polluted trade cumulus clouds, *J. Geophys. Res., 106*, 28563-28673, 2001.

Hitzenberger, R., A. Berner, H. Giebl, R. Kromp, S. M. Larson, A. Rouc, A. Koch, S. Marischka, and H. Puxbaum, Contribution of carbonaceous material to cloud condensation nuclei concentrations in European background (Mt. Sonnblick) and urban (Vienna) aerosols, *Atmos. Environ., 33*, 2647-2659, 1999.

Hudson, J. G., An instantaneous CCN spectrometer, *J. Atmos. Oceanic Technol., 6*, 1055-1065, 1989.

Hudson, J. G., Cloud condensation nuclei near marine cumulus, *J. Geophys. Res., 98*, 2693-2702, 1993.

Hudson, J. G., and P. R. Frisbie, Surface cloud condensation nuclei and condensation nuclei measurements at Reno, Nevada, *Atmos. Environ., 25*, 2285-2299, 1991.

Hudson, J. G., and S. S. Yum, Maritime-continental drizzle contrasts in small cumuli, *J. Atmos. Sci., 58*, 915-926, 2001.

HYSPLIT4 (HYbrid Single-Particle Lagrangian Integrated Trajectory) Model, 1997. Web address: http://www.arl.noaa.gov/ready/hysplit4.html, NOAA Air Resources Laboratory, Silver Spring, MD.

Intergovernmental Panel on Climate Change (IPCC), *Climate Change 2001: The Scientific Basis*, edited by J.T. Houghton *et al.*, Cambridge Univ. Press, New York, 2001.

Jayne, J. T., D. C. Leard, X. Zhang, P. Davidovits, K. A. Smith, C. E. Kolb, and D. Worsnop, Development of and aerosol mass spectrometer for size and composition analysis of submicron particles, *Aerosol Sci. Technol., 33*, 49– 70, 2000.

Ji, Q., G. E. Shaw, and W. Cantrell, A new instrument for measuring cloud condensation nuclei: cloud condensation nucleus "remover," *J. Geophys. Res., 103*, 28013-28019, 1998.

Jimenez, J. L., et al., Ambient aerosol sampling using the Aerodyne Aerosol Mass Spectrometer, *J. Geophys. Res.*, *108*(D7), 8425, doi:10.1029/2001JD001213, 2003.

Johnson, D. W., S. R. Osborne, and J. P. Taylor, The effects of a localized aerosol perturbation on the microphysics of a stratocumulus cloud layer, in *Nucleation and Atmospheric Aerosols 1996*, edited by M. Kulmala and P.E. Wagner, Elsevier, Oxford, 1996.

Kaufman, Y. J. and R. S. Fraser, The effect of smoke particles on clouds and climate forcing, *Science, 277*, 1636-1638, 1997.

Kaufman, Y. J. and T. Nakajima, Effect of Amazon smoke on could microphysics and albedo-analysis from satellite imagery, *J. Appl. Meteorol., 32*, 719-744, 1993.

Keil, A., M. Wendisch, and J. Heitzenberg, A case study on microphysical and radiative properties of power-plant-originated clouds, *Atmos. Res., 63*, 291-301, 2002.

Li, Y. Q., P. Davidovits, Q. Shi, J. T. Jayne, C. E. Kolb, and D. R. Worsnop, Mass and thermal accommodation of H_2O(g) on liquid water as a function of temperature, *J. Phys. Chem. A., 105*, 10627-10634, 2001.

Liu, P. S. K., W. R. Leaitch, C. M. Banic, S.-M. Li, D. Ngo, and W. J. Megaw, Aerosol observations at Chebogue Point during the 1993 North Atlantic Regional Experiment: relationships among cloud condensation nuclei, size distribution, and chemistry, *J. Geophys. Res., 101*, 28971-28990, 1996.

Martin, G. M., D. W. Johnson, and A. Spice, The measurement and parameterization of effective radius of droplets in warm stratocumulus clouds, *J. Atmos. Sci., 51*, 1823-1842, 1994.

Nenes, A., P.Y. Chuang, R.C. Flagan, and J.H. Seinfeld, A theoretical analysis of cloud condensation nucleus (CCN) instruments, *J. Geophys. Res., 106*, 3449-3474, 2001a.

Nenes, A., S. Ghan, H. Abdul-Razzak, P. Y. Chuang, and J. H. Seinfeld, Kinetic limitations on cloud droplet formation and impact on cloud albedo, *Tellus Ser. B, 53*, 133-149, 2001b.

Nenes, A., R. J. Charlson, M. C. Facchini, M. Kulmala, A. Laaksonen, and J. H. Seinfeld, Can chemical effects on cloud droplet number rival the first indirect effect? *Geophys. Res. Lett., 29*(17), 1848, doi:10.1029/2002GL015295, 2002.

Phillips, V. J., T. W. Choularton, A. M. Blyth, and J. Latham, The influence of aerosol concentration on the glaciation and precipitation of a cumulus cloud, *Q. J. R. Metereol. Soc., 128*, 951-971, 2002.

Prospero, J. M., Long-term measurements of the transport of African mineral dust to the southeastern United States: implications for regional air quality, *J. Geophys. Res., 104*, 15917-15927, 1999.

Pruppacher, H. R. and J. D. Klett, *Microphysics of Clouds and Precipitation*, 976 pp., Kluwer Academic Publishers, Dordrecht, The Netherlands, 1996.

Ramanathan, V., R. D. Cess, E. F. Harrison, P. Minnis, B. R. Barkstrom, E. Ahmad and D. Hartmann, Cloud-radiative forcing and climate: Results from the Earth Radiation Budget Experiment, *Science, 243*, 57-63, 1989.

Raymond, T. M., and S. N. Pandis, Cloud activation of single-component orgarnic aerosol particles, *J. Geophys. Res., 107*(D24), 4787, doi:10.1029/2002JD002159, 2002.

Roberts, G. C. and A. Nenes, A continuous-flow longitudinal thermal-gradient CCN chamber for airborne measurements, manuscript in preparation, 2003.

Roberts, G. C., P. Artaxo, J. Zhou, E. Swietlicki, and M. O. Andreae, Sensitivity of CCN spectra on chemical and physical properties of aerosol: A case study from the Amazon Basin, *J. Geophys. Res., 107*(D20), 8070, doi:10.1029/2001JD00583, 2002.

Roberts, G. C., A. Nenes, M. O. Andreae, and J. H. Seinfeld, Impact of biomass burning on cloud properties in the amazon basin, *J. Geophys. Res., 108*(D2), doi: 10.1029/2001JD000985, 2003.

Rogers, C. F. and P. Squires, A new device for studies of cloud condensation nuclei active at low supersaturations, in *Atmospheric Aerosols and Nuclei: Proceedings of the Ninth International Conference on Atmospheric Aerosols, Condensation, and Ice Nuclei held at University College, Galway, Ireland, 21-27 September, 1977*, edited by A. F. Roddy and T. C. O'Connor, Galway University Press, 1981.

Rosenfeld, D., TRMM observed first direct evidence of smoke from forest fires inhibiting rainfall, *Geophys. Res. Lett., 26*, 3105-3108, 1999.

Rosenfeld, D., Suppression of rain and snow by urban and industrial air pollution, *Science, 287*, 1793-1796, 2000.

Sax, R. I., and J. G. Hudson, Continentality of the south Florida summertime CCN aerosol, *J. Atmos. Sci., 38*, 1467-1479, 1981.

Saxena, V. K., Bursts of cloud condensation nuclei (CCN) by dissipating clouds at Palmer Station, Antarctica, *Geophys. Res. Lett., 23*, 69-72, 1996.

Seinfeld, J. H. and S. N. Pandis, *Atmospheric Chemistry and Physics: From Air Pollution to Climate Change*, 1326 pp., John Wiley, New York, 1998.

Shaw, R. A., and D. Lamb, D., Experimental determination of the thermal accommodation and condensation coefficients of water, *J. Chem. Phys., 111*, 10659-10663, 1999.

Sherwood, S. C., Aerosols and ice particle size in tropical cumulonimbus, *J. Climate, 15*, 1051-1063, 2002.

Silverman, B. A., A critical assessment of glaciogenic seeding of convective clouds for rainfall enhancement, *B. Am. Meteorol. Soc., 82*, 903-924, 2001.

Sinnarwala, A. M. and D. J. Alofs, A cloud nucleus counter with long available growth time, *J. Appl. Meteorol., 12*, 831-835, 1973.

Snider, J. R. and J.-L. Brenguier, Cloud condensation nuclei and cloud droplet measurements during ACE-2, *Tellus Ser. B, 52*, 828-842, 2000.

Twohy, C. H., A. J. Schanot, and W. A. Cooper, Measurement of condensed water content in liquid and ice clouds using an airborne counterflow virtual impactor, *J. Atmos. Oceanic Technol., 14*, 197-202, 1997.

Twomey, S., Measurements of natural cloud nuclei, *J. Rech. Atmos., 1*, 101-105, 1963.

Twomey, S., The composition of cloud nuclei, *J. Atmos. Sci., 28*, 377-381, 1971.

Twomey, S., Influence of pollution on the short-wave albedo of clouds, *J. Atmos. Sci., 34*, 1149-1152, 1977.

VanReken, T. M., T. A. Rissman, G. C. Roberts, V. Varutbangkul, H. H. Jonsson, R. C. Flagan, and J. H. Seinfeld, Toward aerosol/cloud condensation nuclei (CCN) closure during CRYSTAL-FACE, *J. Geophys. Res., 108*(D20), 4633, doi:10.1029/2003JD003582, 2003.

Wang, J., R. C. Flagan, and J. H. Seinfeld, A differential mobility analyzer (DMA) system for submicron aerosol measurements at ambient relative humidity, *Aerosol Sci. Tech., 37*, 46-52, 2003.

Wood, R., D. Johnson, S. Osborne, M. O. Andreae, B. Bandy, T. S. Bates, C. O'Dowd, P. Glantz, K. Noone, P. K. Quinn, J. Rudolph, and K. Suhre, Boundary layer and aerosol evolution during the 3rd Lagrangian experiment of ACE-2, *Tellus Ser. B, 52*, 401-422, 2000.

Zhou, J. C., E. Swietlicki, O. H. Berg, P. P. Aalto, K. Hameri, E. D. Nilsson, and C. Leck, Hygroscopic properties of aerosol particles over the central Arctic Ocean during summer, *J. Geophys. Res., 106*, 32111-32123, 2001.